Contribution to the high temperature thermodynamics of OPC clinker phases

Chancel Mawalala Moundounga

THÈSE

Pour obtenir le grade de

DOCTEUR DE L'UNIVERSITÉ GRENOBLE ALPES

École doctorale : I-MEP2 - Ingénierie - Matériaux, Mécanique, Environnement Energétique, Procédés, Production

Spécialité : 2MGE : Matériaux, Mécanique, Génie civil, Electrochimie Unité de recherche : Science et Ingénierie des Matériaux et Procédés

Contribution à la thermodynamique à haute température des phases d'un clinker OPC

Contribution to the high temperature thermodynamics of OPC clinker phases

Présentée par :

Chancel MAWALALA MOUNDOUNGA

Direction de thèse :

Alexander PISCH CHARGE DE RECHERCHE, CNRS délégation Alpes	Directeur de thèse
Marcus Campbell Bannerman University of Aberdeen	Co-Directeur de thèse

Rapporteurs :

MARC LOMELLO-TAFIN
PROFESSEUR DES UNIVERSITES, Université de Chambéry
THOMAS MATSCHEI
PROFESSEUR, Technical University Aachen

Thèse soutenue publiquement le **16 décembre 2022**, devant le jury composé de :

Alexander PISCH CHARGE DE RECHERCHE HDR, CNRS délégation Alpes	Directeur de thèse
Marc LOMELLO-TAFIN PROFESSEUR DES UNIVERSITES, Université de Chambéry	Rapporteur
Céline DARIE PROFESSEUR DES UNIVERSITES, Université Grenoble Alpes	Présidente
Thomas MATSCHEI PROFESSEUR, Technical University Aachen	Rapporteur
	Rapporteur

DEDICATION

To Solange

ACKNOWLEDGMENTS

I would like to thank Dr. Alexander Pisch in particular for giving me this opportunity to work with him and sharing his experience with me. This work has been a portal of knowledge and opening to other future possibilities for me. I wanted to renew my gratitude to this great man through these few words. I would like to thank Dr. Marcus Campbell Bannerman, my co-supervisor, for his help, his analysis, his scientific contribution and his good mood, this trip to Scotland left me with only positive memories. I have an extremely positive thought for Wahab Abdul and I am extremely grateful to him for his scientific participation and hospitality in Aberdeen. I thank Dr. Iona Nuta for her valuable advice and availability. A special thanks to Laurent Artaud for his help on the synthesis devices and also his kindness and patience. I would like to express my gratitude to Thierry Encinas for his explanations on crystallography. I would like to thank Dr. Yannick Champion, director of the SIMAP laboratory, and all the TOP team for the last three years spent working in a good mood. A thought full of sweetness and love to you Angel, thank you for having supported me and believed in me during these important moments in my life. There are so many people to thank that it would take more than one page to list them. But I would like to finish by thanking my large family whose list of names could constitute a book, but if I had to mention only one I would say thank you Mom, the driving force of my life, it is with tears in my eyes that I write these few letters, reminding me that it will be seven years to the day that we have not seen each other, but I remain hopeful that the universe is conspiring to allow us to meet again.

ABSTRACT

The materials produced by the cement industry have a significant role in daily life, notably cement and concrete which form the basis of modern buildings, bridges and monuments. Portland cement or OPC (Ordinary Portland cement) is made from a mixture of natural materials such as limestone and clay, which are ground and fired at high temperatures (~1450°C) to form clinker, which has strong binding properties. As the global population has grown, demands for cement production have multiplied considerably, driving manufacturers to increase their production. This flourishing industrial growth is not without environmental consequences. Indeed, the production of Portland clinker requires the decarbonation of limestone, which is the source of 50 percent of the CO_2 emissions from the cement manufacturing process. In addition, the fuel used to power the kilns also emits 40 percent of the polluting gases during the cement manufacturing process (Lehne & Preston, 2018).

One of the ways in which the industry is looking to produce cements with a lower clinker content is to optimize the clinker reactivity by adding minor elements. To optimize this process, a thorough knowledge of the thermodynamic properties of the main mineralogical clinker phases is necessary to understand the underlying formation processes and the needed energies. During these last three years of the thesis, our aim was to make an experimental contribution through the study of the thermodynamic properties of some of the key oxides constituting OPC (Ordinary Portland Cement). This work is based on two approaches; the first one being experimental, consists in studying in the laboratory the relative enthalpies, enthalpies of formation and phase transition temperatures of calcium silicates such as Belite (Ca_2SiO_4), Rankinite ($Ca_3Si_2O_7$), Aluminates ($Ca_5Al_6O_{14}$; $CaAl_{12}O_{19}$) and Brownmillerite ($Ca_2Fe_{2-x}Al_xO_5$). The second approach consists of modelling the thermodynamic properties of the binary CaO-Al_2O_3 section to be able to calculate the phase diagram.

This work is part of a joint project called Nanocem CP17 involving a consortium of industry and university researchers. In the framework of this project, a strong collaboration with the University of Aberdeen was implemented; our experimental contribution to the re-modeling of the phase diagram of the CaO-SiO_2 system was recently submitted. One of the particularities of this study is that it provides new experimental thermodynamic data that has never been measured on the oxides investigated. Thus, it constitutes an interesting contribution to the research community.

CONTENTS

GENERAL INTRODUCTION

Cement has been used for thousands of years by various groups of people throughout history. In ancient times, the Egyptians already made mortars from gypsum to bind rocks together. On the other side of the earth, Mayans were building with mortars based on lime from firing limestone rocks. As time went on and knowledge improved, cement-manufacturing processes were perfected. Thus, Romans developed a process allowing constructions to be built in wet environments. The process consisted of blending lime with volcanic ash such as pozzolan. Over time, with the advent of industrialization, cement use and production increased considerably. The industrial revolution played a major role in the development of cement production technology. In 1824, the Scotsman Joseph Aspdin introduced an improved the cement manufacturing process and developed Portland cement, a reference to the limestone mined on the island of Portland, hence the common name OPC (Ordinary Portland Cement). Nevertheless, the discovery of modern cement is credited to Louis Vicat (1818). In recognition of his academic and scientific achievements, Louis Vicat (1818) refused to register a patent on the laws of hydraulicity of cements and limes. One of the advantages of cement manufacture is the fact that it is easy to obtain and the products are readily available, making it an inexpensive and widely used material in construction.

The growth of the global population in recent years required the construction of new buildings for housing, hospitals and various other constructions necessary for human life. To satisfy this demand, cement production is increasing continuously. Since 2015, cement manufacturing has been steadily climbing at a rate of 1.5% per year (Hodgson et *al,* 2022) which has a damaging impact on the environment. Indeed, cement production necessitates using limestone ($CaCO_3$) and its calcination at high temperature contributes to the emission of greenhouse gases. Limestone constitutes about 80% of the raw materials used in the manufacture of cement and is the major source of CO_2 emissions. The chemical CO_2 from the $CaCO_3$ calcination corresponds to roughly 60% of the total emissions. The other 40% are due to the use of carbon bearing fossil fuels that are used for clinkering (Lehne & Preston, 2018). Cement industry pollution accounts for about 8% of the world's CO_2 emissions (Scrivener, 2014). If the use of cement-based concrete were compared to a country, it would

represent the third largest greenhouse gas pollutant in the world behind China and the United States. As it is currently not feasible to substitute limestone, a key issue for the cement sector is to identify alternative ways of reducing limestone input into cement production. To achieve this, the main approaches planned to reduce the carbon impact throughout the cement manufacturing process are as follows: the use of low-carbon fuels, the use of non-polluting raw materials and the development of low-emission or even near-zero emission production processes (Hodgson et *al,* 2022). To reach these targets, manufacturers are investing more and more in research and development to better understand the physiochemical processes involved in clinkerization. This is where chemical thermodynamics intervenes, which is the subject of this manuscript. Indeed, the properties and the stability of the major phases constituting the cement clinker can be strongly affected by the insertion of minor elements and modify not only the chemistry but also the quality of the resulting clinker. However, in order to be able to model the insertion of these minor elements, high quality thermodynamic data is needed for the pure mineralogical phases of a clinker.

Clinker is the main constituent of Portland cement with a global chemical composition of 67wt.% CaO, 22wt.% SiO_2, 5wt.% Al_2O_3, 3wt.% Fe_2O_3 and 3wt.% minor elements (MgO, Na_2O, K_2O, SO_3, TiO_2) (Taylor H. , 1990). Most of the raw materials in the cement clinker manufacturing process are of natural origin. The CaO source is natural limestone. Alumina, iron oxide and silica are mainly from natural clay minerals together with some of the alkalis and magnesium oxide. Iron oxide is sometimes added as hematite. A mixture of these raw materials prior to the burning is called raw mix. This raw mix is burned at temperatures close to 1450°C to transform the raw materials into the reactive phases of the clinker. The major mineralogical phases of an Ordinary Portland clinker are Alite (Ca_3SiO_5 with insertion of minor elements) which forms 50-70 wt% of the final clinker, Belite (Ca_2SiO_4 with minor elements), generally present as a β- Ca_2SiO_4 polymorph and an amount ranging from 15-30 wt. %, the calcium aluminate phase $Ca_3Al_2O_6$ estimated to 5-10wt.% and finally the ferrite phase, the $Ca_2(Al,Fe)_2O_5$ solid solution with an amount varying between 5 and 15 wt.% (Taylor H. , 1990).

In recent years, researchers in thermodynamics developed a computational procedure for studying the thermodynamic properties of multi-component systems. This approach is called CALPHAD (Spencer, 2008) (Calculation of Phase Diagrams)

and consists of first modelling the thermodynamic properties of a unary and then binary, ternary and more complex multi-component systems in order to obtain a coherent Gibbs energy dataset which can be used for phase diagram calculations. The key to this method lies in the quality of the underlying thermodynamic data of the constituents of the system studied. As the major phases of clinker belong to the binary systems $CaO\text{-}SiO_2$, $CaO\text{-}Al_2O_3$ and the ternary $CaO\text{-}Al_2O_3\text{-}Fe_2O_3$, high quality experimental data is necessary to better describe the thermodynamic reactions governing clinker formation. These data will contribute to a better simulation tools to control the manufacturing process and optimize the clinker properties. In order to build up a coherent database, the experimental contribution is therefore essential, and it is this point that motivates the work that is reported in this manuscript.

The main aim of this research is to review and to study experimentally the thermodynamic properties of the compounds and solid solutions of the main mineralogical phases of an OPC "Ordinary Portland Cement" clinker: the various polymorphs of Ca_2SiO_4, Rankinite ($Ca_3Si_2O_7$), different Ca-aluminates ($Ca_5Al_6O_{14}$ and $CaAl_{12}O_{19}$) and the solid solution calcium alumino-ferrite ($Ca_2Al_xFe_{2-x}O_5$). For all compounds and the solution phase, the focus lies on the indirect determination of the heat capacity at high temperature through a series of heat content measurements. In addition, the standard heats of formation were determined with a newly developed solution calorimetric method using a $CaO\text{-}Al_2O_3$ rich based solvent. All the measurements were performed on carefully synthesized and characterized samples. The samples are produced using conventional techniques: powder mixing, grinding, pelletizing, high-temperature sintering and air-cooling. The purity of all samples was checked by X-ray diffraction. The newly generated data was used, together with the critically reviewed data from the literature, to derive new sets of Gibbs energy functions, which can be used in equilibrium calculations.

Throughout this thesis, we will study different multicomponent oxides that constitute a Portland clinker. This research work is divided into four parts, each of which constitutes a chapter:

- The first chapter describes the experimental methods used in the thesis for the synthesis of the silicate, aluminates and the alumino-ferrite solid solution as well as the structural analysis techniques and the methods for the determination of the thermodynamic properties.

- The second chapter focuses on the study of the thermodynamic properties of two calcium silicates: belite (Ca_2SiO_4) and rankinite ($Ca_3Si_2O_7$). In this chapter, we will discuss the parameters of the syntheses that allowed us to obtain these compounds; the thermodynamic properties will also be measured and discussed. We will then finish by presenting the results of a collaborative work carried out with the University of Aberdeen on the phase diagram modelling of the $CaO\text{-}SiO_2$ binary base system for cement clinker production.
- The third chapter deals with the study of the thermodynamic properties of the $Ca_2(Al_x,Fe_{1-x})_2O_5$ solid solution as a function Al/Fe variation.
- The fourth chapter will deal with the study of the binary $CaO\text{-}Al_2O_3$ system. The solids $Ca_5Al_6O_{14}$ and $CaAl_{12}O_{19}$ will be synthesized and their thermodynamic properties will be measured and discussed. The Gibbs energy as a function of temperature for all compounds was generated using the so-called third generation Calphad approach in which the heat capacity of a compound is described by a Plank-Einstein type function. Based on these new Gibbs energies, a full re-modelling of the quasi-binary $CaO\text{-}Al_2O_3$ was performed and will be presented.

Finally, this thesis manuscript will be terminated by a general conclusion in which I will review the important results of my work as well as possible perspectives of this study.

1 CHAPTER 1: EXPERIMENTAL METHODOLOGIES AND MODELLING APPROACH.

1 EXPERIMENTAL METHODOLOGIES

1.1 RAW MIX PREPARATION FOR SYNTHESIS

The syntheses of all compounds performed in the laboratory during our work were done by solid state reaction. The precursor powders ($CaCO_3$, SiO_2, Al_2O_3, Fe_2O_3, MgO) with a purity ≥99.0%, are weighed by using a precision balance (±0.01g), dried for 24 hours at 500°C into a muffle furnace in air to remove any trace of moisture, then mixed by a mechanical mixer. To avoid any foreign incorporation, alumina powders are dried in alumina crucibles while calcium carbonate and silicon oxide in a platinum crucible, iron oxide and magnesium oxide in porcelain bowls. Subsequently, mixed powders are pressed into pellets to increase their reaction rate. Two alternative sets of tools were used for this task.

1. An automatic press: for sample amounts greater than 3 g, 25 tons of pressure is applied for 5 minutes.
2. A manual hydraulic press: an average pressure of 4 tons is applied to a 3g quantity of raw materials.

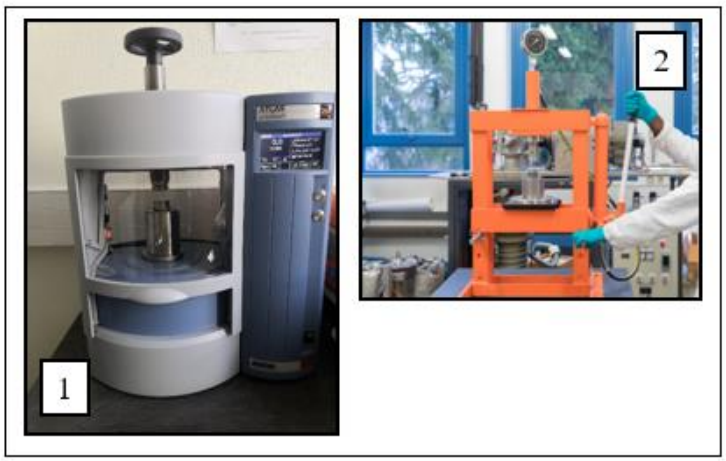

Fig. 1 : Automatic hydraulic work press on the left (1). Manual press on the right (2).

The manual press is used by default for synthesis and for sample processing for calorimetry. The automatic press is mainly employed for high volume synthesis.

1.2 HEAT TREATMENTS OF RAW MATERIALS

Sintering of the raw mix is performed at high temperatures in various furnaces and crucibles based on the chemical elements contained in the mixed powder. Heat treatment is done in two steps:

1. The calcination of $CaCO_3$: this step is carried out at 1000°C during 1 hour; it consists in decarbonizing the $CaCO_3$ according to the following equation : $CaCO_3\,(s) \rightarrow CaO\,(s) + CO_2\,(g)$. Calcium oxide is very reactive to humidity; therefore, it is advisable to keep it as carbonate for longer storage periods to avoid any calcium hydroxide build-up.

2. The second step is the thermal reaction of CaO + additive pure raw materials (SiO_2, Al_2O_3 and Fe_2O_3).

1.2.1 SILICATE SYNTHESIS

Calcium silicates ($CaO\text{-}SiO_2$) are synthesized in a furnace with air atmosphere, since these oxides are stable under oxygen, no inert gas is required for proper completion of the process. Synthesis is carried out in a platinum crucible at a temperature below the melting point of the constituents and the final product. The duration of the synthesis t_1, and the temperature of synthesis T_1 vary with the materials being synthesized, and will be discussed in detail in each case. The heating rate of temperature ramp-up was 200K/h.

Fig. 2: Silicate synthesis in a platinum crucible under air.

Each synthesis is followed by a quenching step, which can be done in air, or water. Quenching is used to cool the sample quickly to avoid any decomposition

reactions on cooling. A water quench being much faster than a quench in air. Rapid cooling allows avoiding phase transformations. In Fig 3, we have an example of water quenching carried out in the laboratory; the process consists in immersing the external walls of the crucible in a container containing water until complete cooling to room temperature. For air quenching, the crucible containing the synthesized sample is taken out of the furnace at high temperature and left in the air until cooling. Throughout our work, we have attempted various methodologies for synthesis, but we will discuss only those results with positive outcome. The phase purity of the samples was checked by X-ray diffraction.

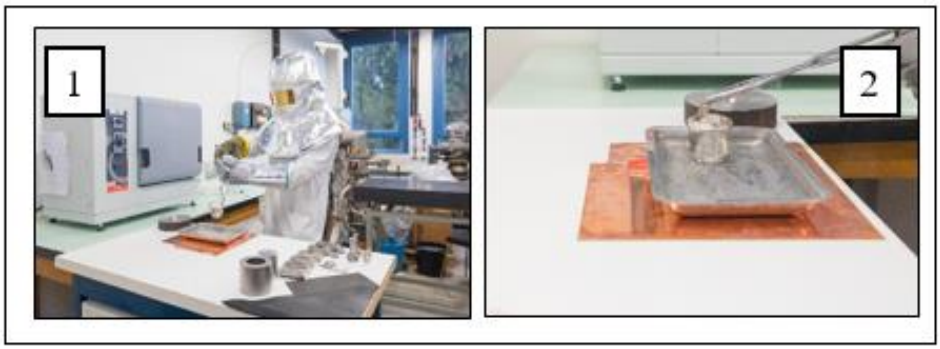

Fig. 3 : Example of quenching the samples in water.

1.2.2 Calcium Aluminates and Ferrites synthesis

Calcium aluminates and ferrites ($CaO\text{-}Fe_2O_3\text{-}Al_2O_3$) are synthesized in a muffle furnace (Fig. 4) under argon flow (30L/1h, purity: H_2O (5 bar) < 3 ppm; C_nH_m < 0.5 ppm; O_2 < 2 ppm). Alumina crucibles are used instead of platinum ones. The heat treatment temperatures were all below 1300°C (1200°C & 1250°C), while the minimum synthesis time t_1 was 12h. The temperature-heating rate in this particular case was 250K/h. The results of the synthesis are characterized by X-ray diffraction.

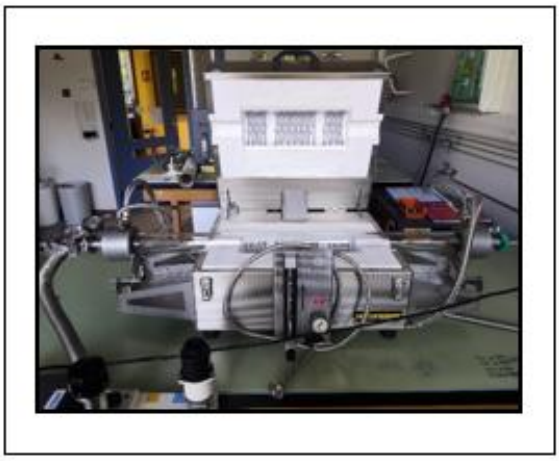

Fig. 4 : Heat treatment in muffle furnace under argon gas.

1.3 PHASE CHARACTERIZATION METHOD

To ensure that the previously synthesized sample contains only the expected phase, X-ray diffraction measurements were carried out. The X-ray diffraction study is performed on samples that were ground into a fine, homogeneous powder. This step enables not only the indexing of the diffraction peaks of the phase present in the sample, but also access to the crystalline structure as well as to the lattice parameters of the sought phase. The diffraction peaks of the raw diagram, obtained after acquisition, can be indexed using a database containing crystallographic information on the phase studied.

1.3.1 SAMPLE PREPARATION FOR CHARACTERIZATION

Samples from the syntheses are characterized by X-ray diffraction in order to identify the expected phase. The pellets are ground into a fine powder, and put into a sample holder. Powder amounts used for X-ray diffraction measurements was less than 2 g. Differential Scanning Calorimetry (DSC) measurements are performed on powders of amount ≤ 200 mg. For the drop calorimetric measurements (heat content; dissolution), pellets were produced with masses ranging from 15 mg up to 150 mg.

1.3.2 PRINCIPLE OF X-RAY

X-rays diffraction is a technique for characterizing solids to determine the phases present in a material. The principle is to subject the sample to a monochromatic beam of X-rays and to collect the diffraction spectrum emitted by the sample. The X-

ray diffraction peaks are produced by constructive interference of the diffracted beam on condition that the difference in path travelled by the beam between two planes is δ=nλ. Bragg's law gives the conditions for diffraction:

$$2d_{hkl}sin\Theta = n.\lambda \qquad [1]$$

Where d_{hkl} corresponds to the distance between two crystallographic planes

Θ: Bragg angle.

n : Step.

λ: x-ray wavelength.

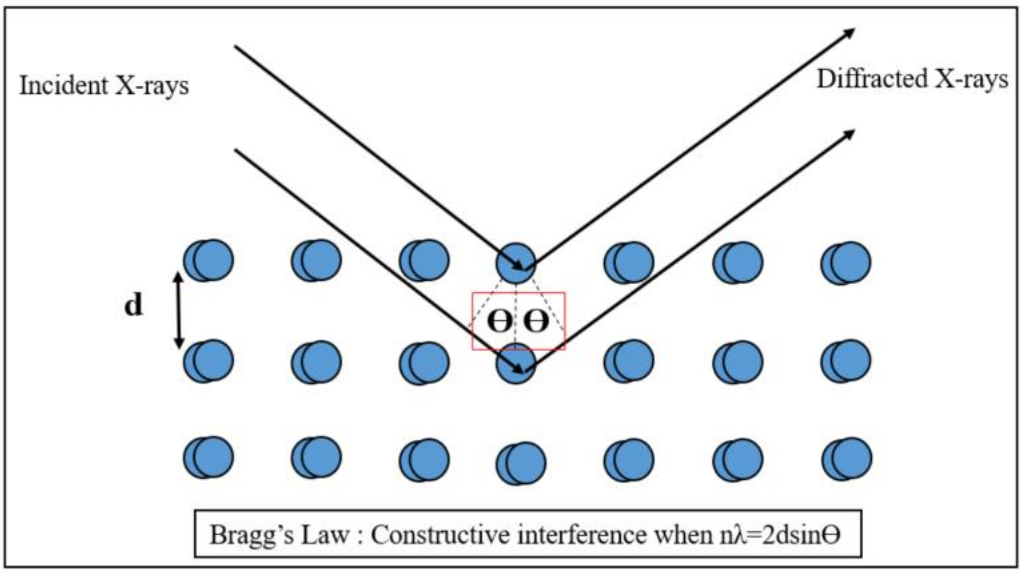

Fig. 5 : Principle of X-ray diffraction.

By varying the orientation of the beam with respect to crystal, several d_{hkl} can be measured. The position of each peak and their relative intensity can be traced back to the nature of the crystal using databases. The X-rays diffraction apparatus used is a X'Pert Pro MPD from PANalytical with CuKα radiation of wavelength λ= 1.5419 Å. The measurements are made in reflection, on a Bragg Brentano configuration. The data processing is done with the Diffract.EVA software and the database we use as a priority is PDF4+2022. This database is oriented towards inorganic materials (about 450,000 records: 90% inorganic and 10% organic or polymers).

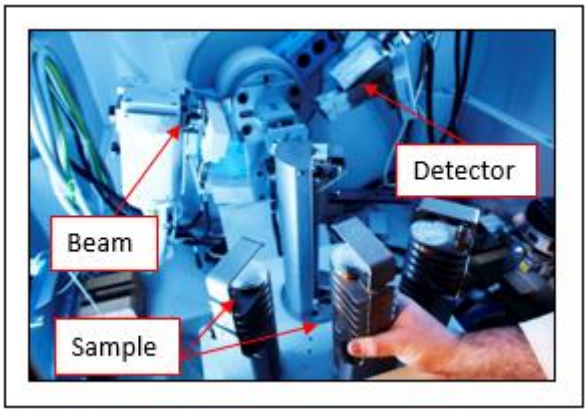

Fig. 6 : PANalytical's X'Pert Pro MPD for X-ray diffraction measurements.

1.4 DROP CALORIMETER

A MHTC96 calorimeter from SETARAM with two different drop measuring heads (Type S thermopile, 1300°C max, Type B thermopile, 1500°C max) equipped with thermo-cell, furnace and a multi-sample introducer that can hold up to 23 samples were used for the heat content and the drop dissolution measurements. The thermo-cell, composed of 16 thermocouples distributed on the bottom and on the entire lateral surface of the crucible, offers a good sensitivity. The multi-sample introducer is connected to a vertical tube, which guides the sample during the drop and acts and an exhaust for any vapours potentially given off by the sample. The furnace is connected to a closed water system, which circulates continuously and cools the external and junction of the calorimeter. An acquisition system linked to a computer enables the data collected from the measurements to be processed.

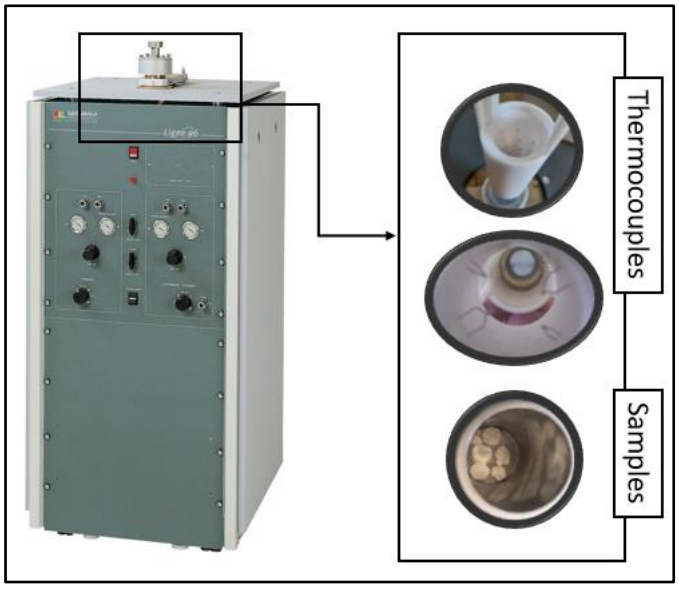

Fig. 7 : Drop Calorimeter MHTC96 from SETARAM used for heat content measurements.

1.4.1 THE CRUCIBLES

The measurements are carried out in an alumina with a platinum inlay crucible (diameter 13 mm and weight 46 mm). The crucible is introduced into the measuring cell and the temperature evolution of the sample is measured by the thermocouples around. Although the regulation temperature of the furnace is taken below the measurement head, a difference exists between the furnace temperature and the sample temperature. The regulation temperature was adjusted to be as close as possible to the target temperatures of the measurements.

1.4.2 GAS SWEEPING

The calorimeter contains two separate gas circuits, one for the furnace and the other for the experiment chamber. The argon gas circuit protects the graphite resistance against oxidation and reduces residual traces of humidity. All measurements were performed under flowing Ar (argon gas) in the measurement cell.

1.4.3 CALIBRATION

1.4.3.1Calibration process

All measurements are carried in a platinum crucible (diameter 13 mm and weight 46 mm) which is inserted in an Al_2O_3 crucible under flowing Ar atmosphere. The

calorimeter is calibrated using pure alumina (Al_2O_3, 99.95%) pieces, which are dried and calcined at 1400°C for 12h. The pellets have a mass ranging from 15 to 150 mg (uncertainty ±0.02 mg). The crucible is loaded with alumina powder up to 15 mm for better reproducibility of the measurements. Three series of 6 or 7 alumina samples are dropped for each temperature from 600°C to 1480°C and the associated heat effect recorded and integrated using the Calypso software package (SETARAM). The number of drops per measurement series was limited to 6 or 7 to avoid piling up pellets in the crucible. With this number of samples, only one layer is covered in the crucible, which leads to results with better reproducibility and repeatability. The calibration constant at a given temperature is calculated using calculated heat content values for Al_2O_3 using the FTOxid database. The measured surface (in µV.s) for each sample is plotted as a function of heat content of Al_2O_3 (in J). The calibration constant (in µV.s/J) was calculated by performing a linear regression passing through origin. The uncertainty of the calibration constant corresponds to twice the standard variation of the slope. The temperature of the introduction into the calorimeter was measured with a calibrated thermocouple (uncertainty ±0.1K). The variation of the high temperature calorimeter is ±0.4K and a return to the baseline is observed within 25 min.

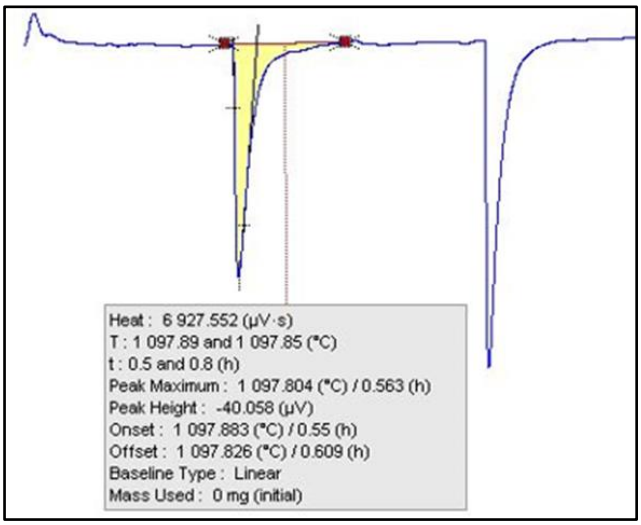

Fig. 8 : Signal obtained after dropping a pellet between the ambient temperature and the measurement temperature.

1.4.3.2Calibration constant

The calibrations of the calorimeters were carried out at different temperatures of measurements varying from 600°C to 1480°C. Fig. 9 shows the evolution of the

calibration constant as a function of the measurement temperature. The uncertainty given is twice the standard deviation of the slope. The calibration constant values obtained as a function of temperature and the uncertainty on the data are shown in Table 1.

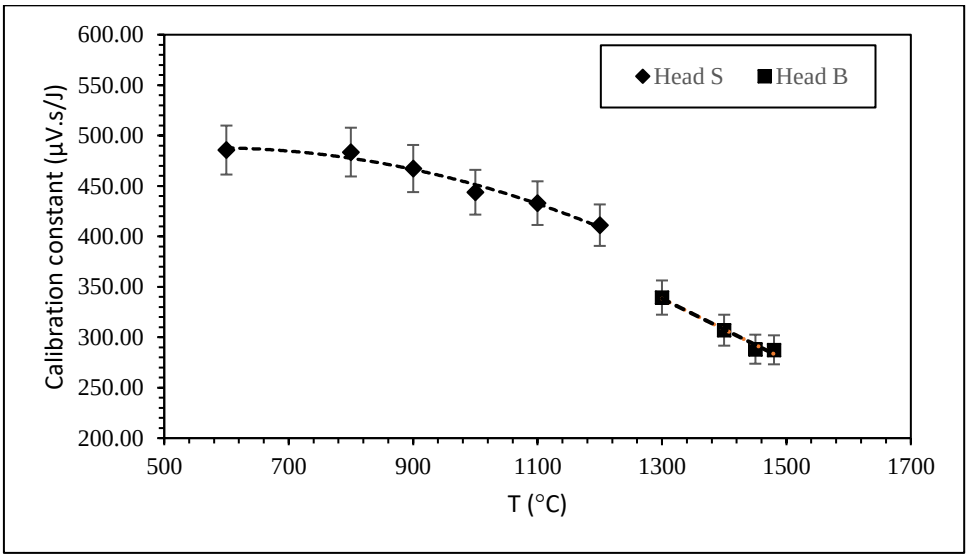

Fig. 9 : Evolution of the calibration constant as a function of the temperature.

T (°C)	Calibration (µV.s/J)	u(constant) (2□)
600	485.63	5.79
800	483.6	5.58
900	467.3	5.26
1000	443.8	5.38
1100	433	5.86
1200	411.15	6.3
1300	339.37	5.34
1400	307.03	2.82
1450	288.18	4.31
1480	287.55	5.49

Table 1 : Calibration constant at different selected temperatures.

1.4.3.3Measurement method overview

For the heat content measurement, pellets were produced with sample weights ranging from 15 to 80 mg (uncertainty ±0.02 mg). Again, two series of 6/7 pellet dropped at each temperature of calibration. The observed integrated heat effects (surface area of peak in µV.s) were plotted as a function of the phase amount introduced into the calorimeter. A linear regression forced passing through the origin was performed to determine the slope. The uncertainty of the measurement corresponds to twice the standard deviation of the slope. The measured heat content corresponds to the slope divided by the calibration constant. The uncertainty of the heat content is the combined uncertainty of the measured surface slope and the uncertainty of the calibration constant using the following formula:

$$\text{For } y = \frac{x_1}{x_2} : u_c(y) = \sqrt{(\frac{1}{x_2})^2 u^2(x_1) + (\frac{x_1}{x_2^2})^2 u^2(x_2)} \qquad [2]$$

In the above formula x_1 (µV.s) is the area of the dropped sample signal x_2 (µV.s.J^{-1}) the calibration constant. Again, the introduction temperature was measured by thermocouple (±0.1K).

1.5 DROP SOLUTION MEASUREMENTS

The standard heat of formation of a compound can be determined using drop solution calorimetry. For any compound, at least two dissolution experiments must be performed. For a fictive compound AB with components A and B, the corresponding dissolution reactions are

- Reference drop: (A+B)(25°C) + solvent (T) = solution (T) Q_{A+B}
- Compound drop: AB (25°C) + solvent (T) = solution (T) Q_{AB}

In both cases, the final state is the same, i.e. a solution at the temperature of dissolution with identical composition. The standard heat of formation becomes then:

$\Delta_f H = Q_{A+B} - Q_{AB}$

If the concentration of A, B and AB in the solvent is small, it is possible, to separate the contribution from A and B. This means, a universal value for pure A and B are measured and can be used.

Separate reference:

- A (25°C + solvent (T) = solution (A)(T) Q_A
- B (25°C) + solvent (T) = solution (B)(T) Q_B

In this case, the standard heat of formation can be determined by:

$\Delta_f H = Q_A + Q_B - Q_{AB}$

In general, for small dilutions, the measured heat is independent of temperature. In this case, a mean value is calculated from a series of dissolution experiments. The uncertainty is then calculated from the standard deviation in a classical way. In case of an obvious composition dependence, the value at infinite dilution is calculated by linear extrapolation to zero concentration.

In the case of oxides, there are two types of solvents used in the literature: aqueous acids or bases and salt mixtures (Navrotsky, 1977). Typical solvents for CaO and Al_2O_3 based systems are hydrofluoric acid (Coughlin,1956) or Hydrochloric acid (Koehler et al, 1961), lead borate $PbO.B_2O_3$ (Navrotsky, 1977) (Trofymluk et *al*, 2005) or eutectic $(Li,Na)_2O.B_2O_3$ (Geiger et al, 1988). More recently, a pure oxide-based solvent was used by Koryttseva and Navrotsky, (2017). The authors used the mixture CaO (45.9 mol%), SiO_2 (35.1 mol%), Al_2O_3 (8.3 mol%), MgO (10.7mol%) in analogy to an Asian blast furnace slag. Due to the high SiO_2 content, this solvent has an acidic nature. The evolution as a function of temperature for this composition was calculated using Factsage and the FTOxid database and is plotted in Fig. 10.

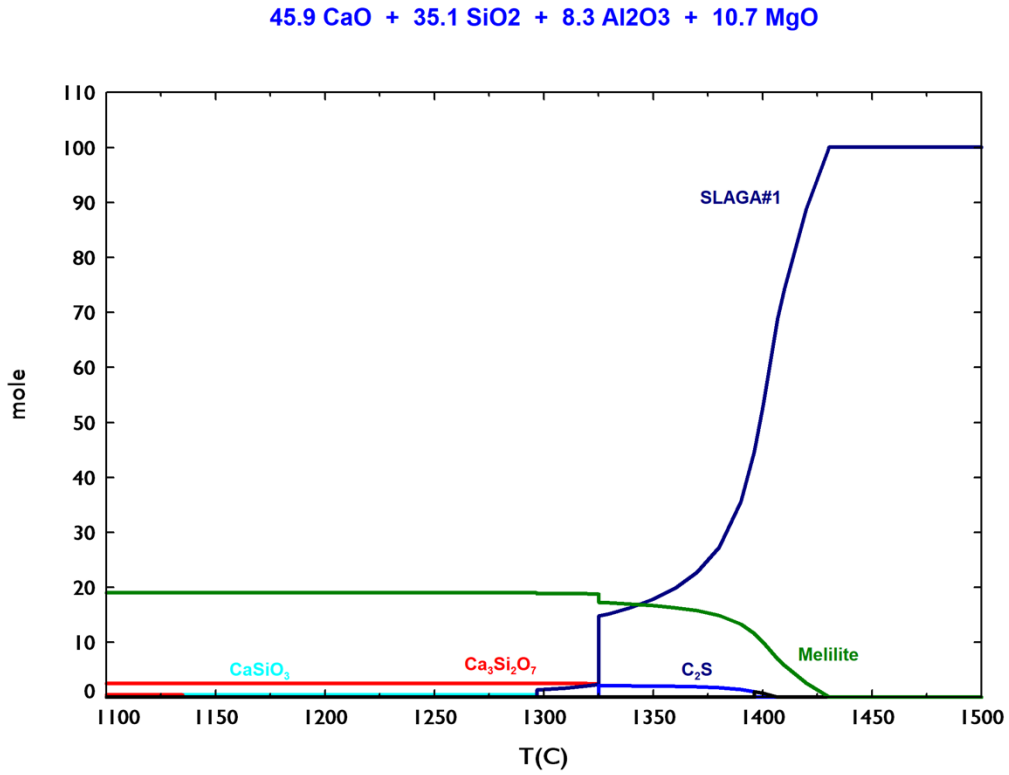

Fig. 10 : Phase evolution as a function of temperature for the Asian slag solvent used by (Koryttseva & Navrotsky, 2017)

In mass fraction, the solvent composition is : CaO 43.183 wt.%, SiO_2 35.383 wt%, Al_2O_3 14.198 wt.% and MgO 7.235 wt.%.

In our work, the idea was to test a different solvent as we did not have the constraint to work in the acidic region of the C-S-A-M system. For practical reasons (easier cleaning of the Pt crucible), a solvent rich in C-A was chosen owing a more basic behaviour. The composition is: CaO 48.0 wt.% (59.20 mol%), SiO_2 2.9 wt.% (3.34 mol%), Al_2O_3 45.1 wt.% (30.60 mol%), MgO 4.0 wt.% (6.86 mol%). The calculated phase evolution for this alternative solvent as a function of temperature is reproduced in Fig. 11. It has been checked by thermodynamic calculations that the solubility range of the liquid phase is sufficient for the dissolution of the main oxides (CaO, Al_2O_3, SiO_2, Fe_2O_3) targeted in our study. The calculated melting point of this alternative liquid composition is 1340°C. The measured melting point is 1310 $\pm$ 5°C which is lower than the modelled one by FactSage.

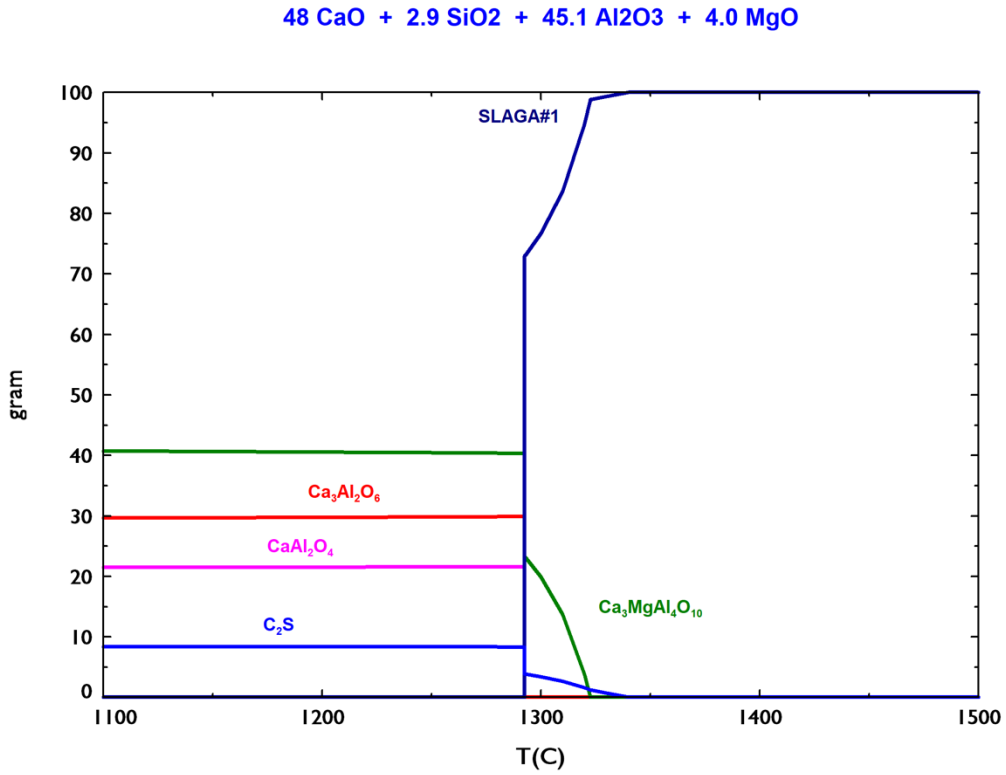

Fig. 11 : Phase evolution as a function of temperature for the novel basic solvent used in this work.

The isothermal temperature of the calorimeter was set to 1450°C. Pellets of each sample (pure oxide or compound) with typical weight ranging from 5 to 15 mg were dropped into the solvent from room temperature. Again, the exact introduction temperature was recorded with a uncertainty of +/- 0.1K. Dissolution time for the dissolved sample, i.e. return to the baseline, was achieved within 30min for all samples. The measurements were performed in flowing argon atmosphere. The calibration constant at 1450°C was again determined by dropping pure Alumina pellets into a crucible filled with Al_2O_3 powder up to 1.5 cm. The calibration constant is 296.115 $\pm$ 5.703 µV.s/J for the drop solution measurements.

The measured heat of dissolution for the pure components are summed up in Table 2. The heat content data for the pure compounds were calculated using Factsage and the FTOxid database.

The measurement gave reliable results for CaO, Al_2O_3 and Fe_2O_3. In the case of SiO_2, an exothermic reaction takes place as shown in Fig.12. For kinetic reasons, a solid silicate forms in the melt which is then very slow to dissolve. A reliable measurement is therefore not possible for silica.

Oxide	Hdiss (kJ/mol)	H(1450°C) - H(25°C) (kJ/mol)	Hsol (1450°C) (kJ/mol)
CaO	77.6 ± 2.7	74.7	-3.1± 2.7
Al_2O_3	148.6± 2.7	173.3	-24.7± 2.7
Fe_2O_3	352.5± 7.4	202.0	149.5± 7.4

Table 2 : The heat of solution of CaO and Al_2O_3 at 1450°C in the basic solvent is exothermic. For Fe_2O_3, the heat value is endothermic.

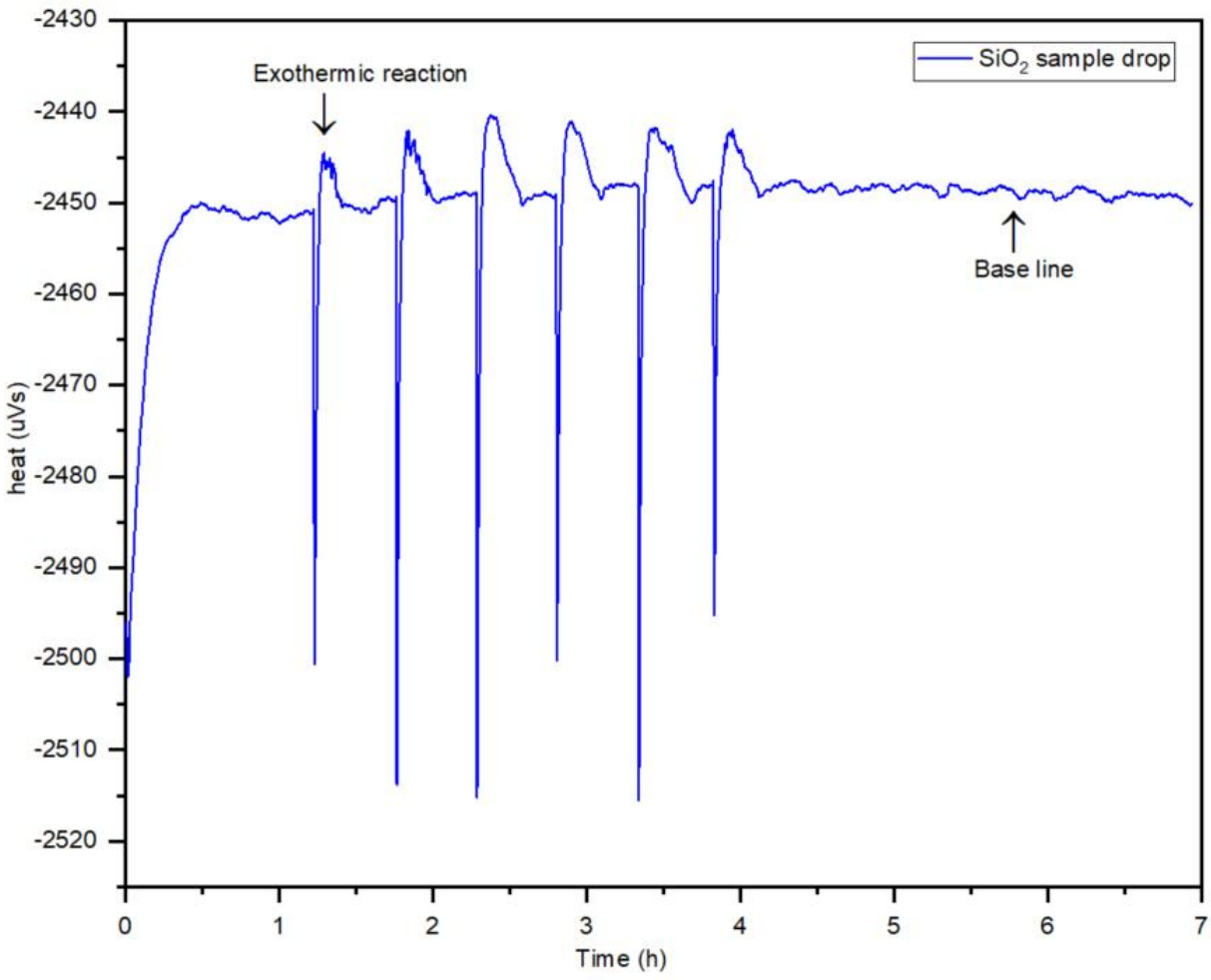

Fig. 12 : Dissolution of SiO_2 with an exothermic reaction overlapping the dissolution.

The experimental heat of dissolution for pure CaO is presented in Fig.13, for pure Al_2O_3 in Fig.14 and for pure Fe_2O_3 in Fig. 15.

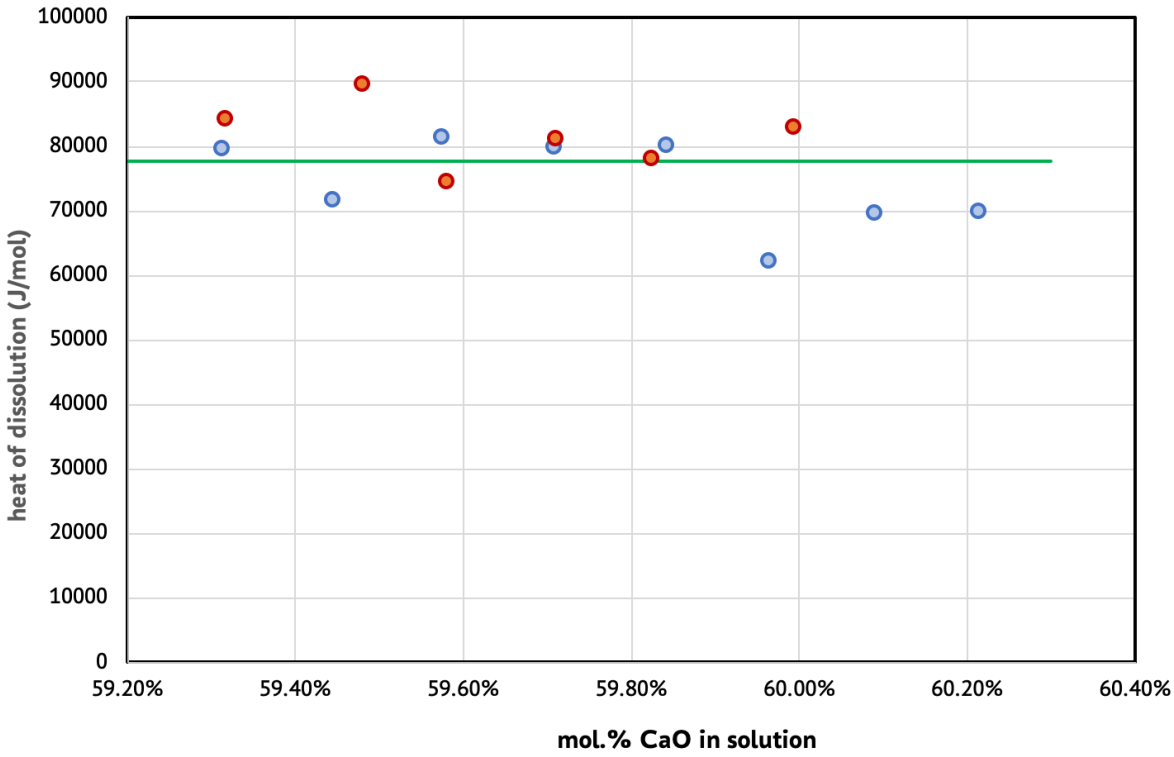

Fig. 13 : Heat of dissolution as a function of CaO content.

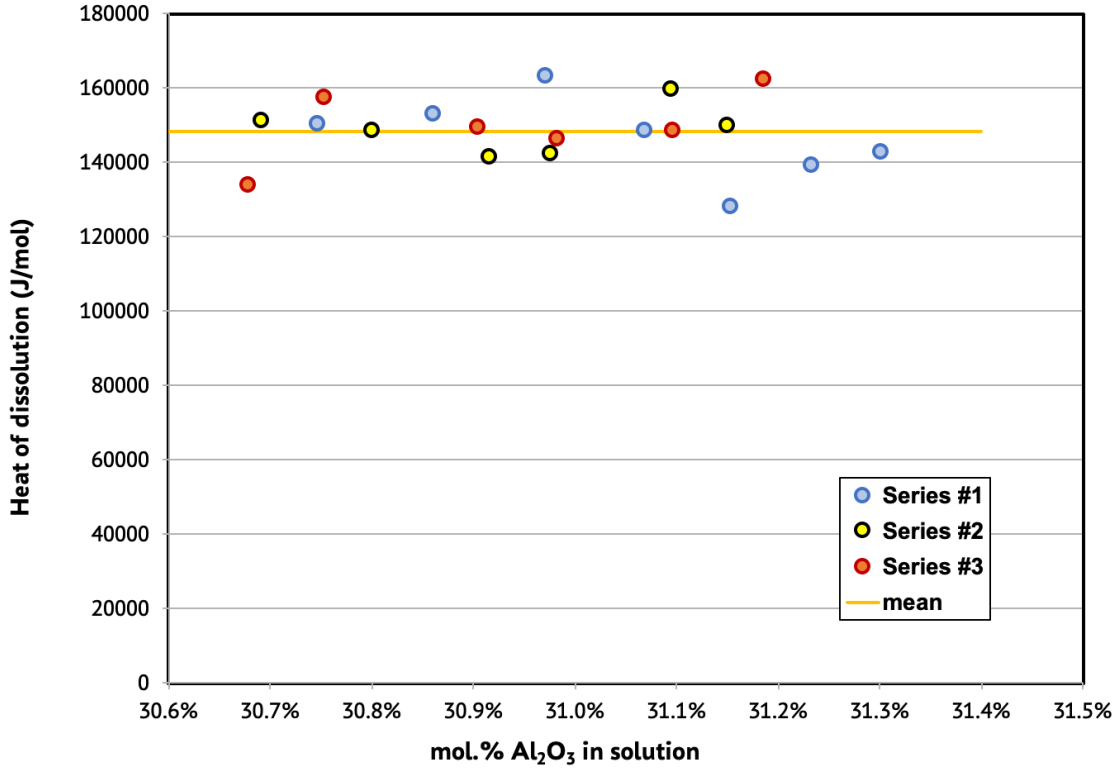

Fig. 14 : Heat of dissolution as a function of Al_2O_3 content.

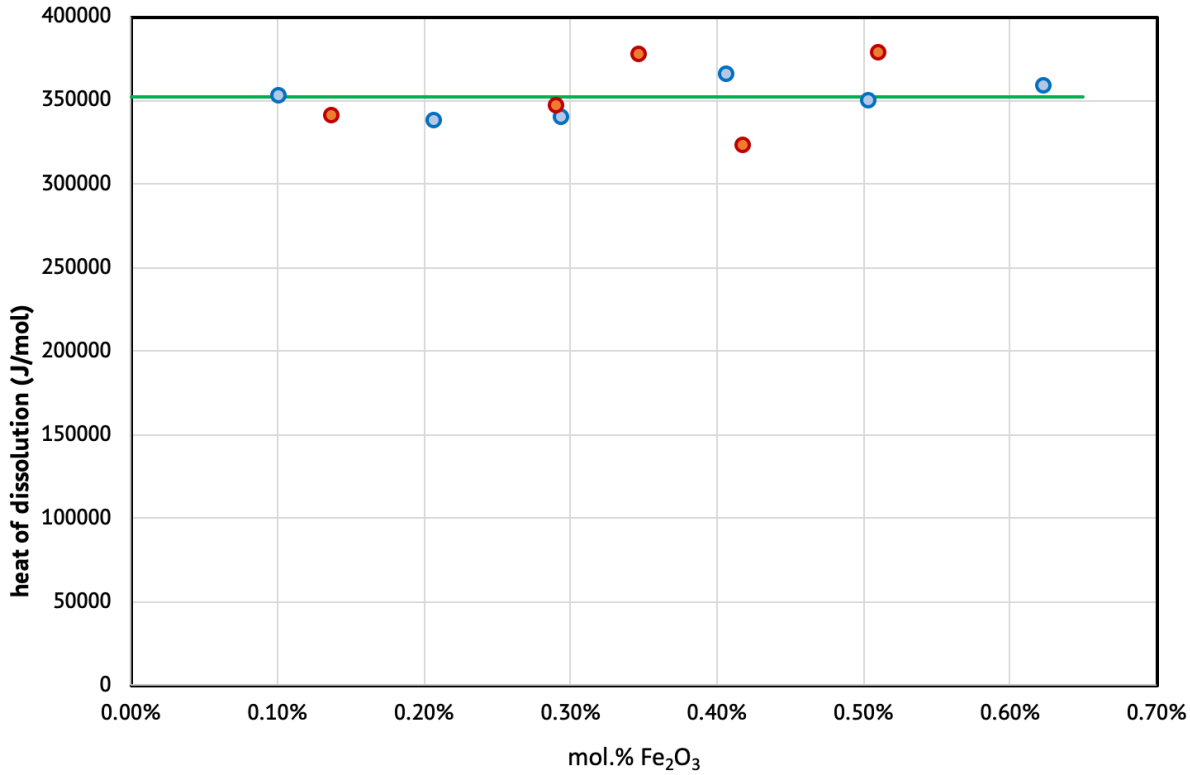

Fig. 15 : Heat of dissolution as a function of Fe_2O_3 content.

1.6 Differential Scanning Calorimetry

1.6.1 General overview

Differential Scanning Calorimetry is a thermal analysis technique that allows the characterization of temperature and enthalpy of phase transitions in the studied material. This technique can be used to measure the transition temperature, enthalpies of transition reactions and heat capacity (Cp).

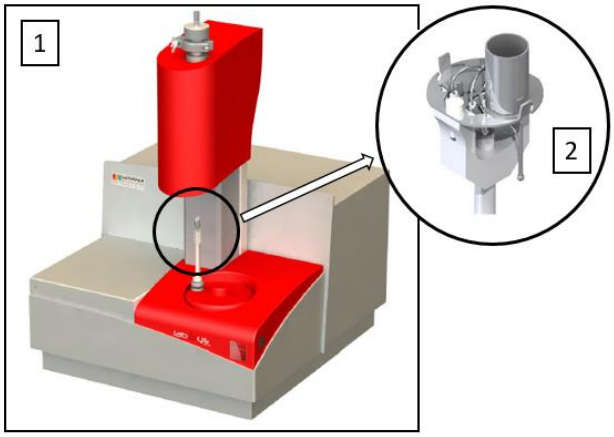

Fig. 16 : Labsys^{TM} Evo used in the laboratory for sample measurements.

The apparatus used in the laboratory for DSC is the Labsys^{TM} Evo designed by SETERAM. It is composed of a TG balance connected to the DSC sensors, a metal resistor furnace with a maximum temperature of 1600°C, a gas circuit (Ar: H_2O (5 bar) < 3 ppm; C_nH_m < 0.5 ppm; O2 < 2 ppm) and a cooling water circuit. Gas circuit protects the crucible and sample from oxidation and the sensors when working temperature is above 500°C. Pure platinum crucibles are used for all measurements in this work.

1.6.2 Calibration method

Calibration was performed with NaCl and K_2SO_4 as reference samples. The measured temperatures of the reference samples are used to determine the temperature difference between the DSC signal and the actual reference value from the databases. The calibration equation given in Fig. 19 was chosen to correct our experiment values. The signals results are plotted in Fig. 17 and 18. K_2SO_4 has two transition points, a first solid-solid transition and a second solid-liquid one, while NaCl has only one transition point. Measurements are performed at different rate to improve accuracy.

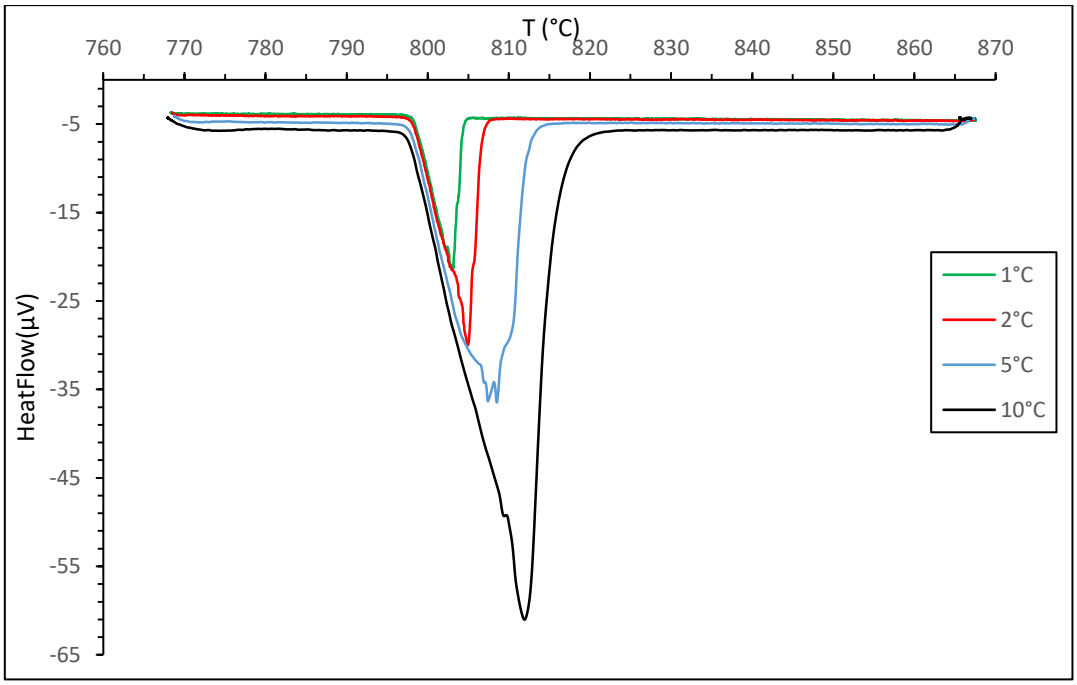

Fig. 17 : DSC signal for NaCl reference sample.

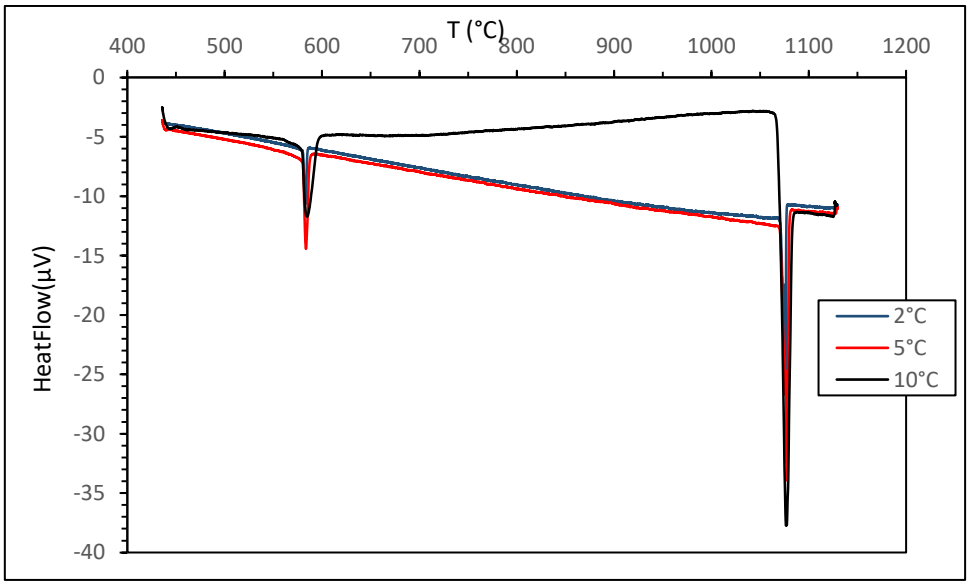

Fig. 18 : DSC signal for K_2SO_4 reference sample.

In order to establish the calibration equation, we have plotted in Fig 19 the mean values of the melting temperatures measured at 5K/min and 10K/min as a function of the literature data. The linear regression described by equation [3] is used to correct the experimental values.

T, 5K/min (±5K)	T, 10K/min (±5K)	FTPS	Chemistry
579	575	583.85	K_2SO_4
795	796	800.65	NaCl
1068	1065	1068.85	K_2SO_4

Table 3 : Melting temperature from reference compound.

In order to establish the calibration equation, we have plotted in Fig. 19 the mean values of the melting temperatures measured at 5K/min and 10K/min as a function of the literature data. The linear regression described by equation [3] is used to correct the experimental values.

$$T_{real} = aT_{meas} + b \quad [3]$$

T_{meas} and T_{real} are respectively the measured and corrected values, the coefficient *a* and constant *b* come from the linear regression given in Fig. 19.

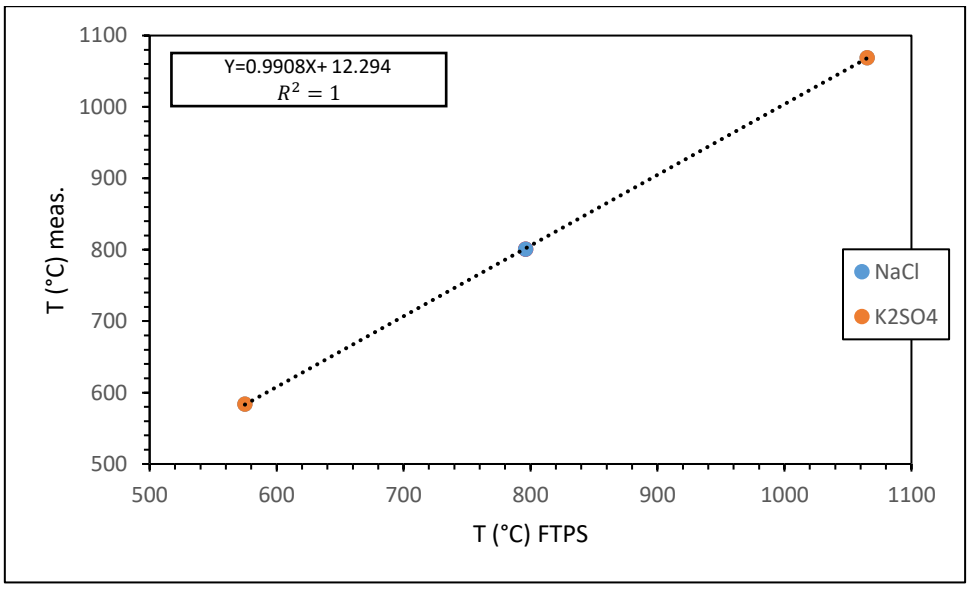

Fig. 19 : Temperature calibration curve.

1.7 SCANNING ELECTRON MICROSCOPY (SEM)

Scanning electron microscopy is a sample analysis technique frequently used in solid-state chemistry. This technique is mainly based on electron-matter interactions. An electron beam scans the surface of the sample and then transmits the information

to a detector. The shock between the primary electrons of the beam and the atoms generates secondary electrons by ionization. These low energy electrons are ejected at the surface of the sample. Other information from the interactions can also take place, including electron scattering, absorption, Auger electron emission, electron scattering, X-rays or light. Each of these phenomena can be used with an adapted detection technique.

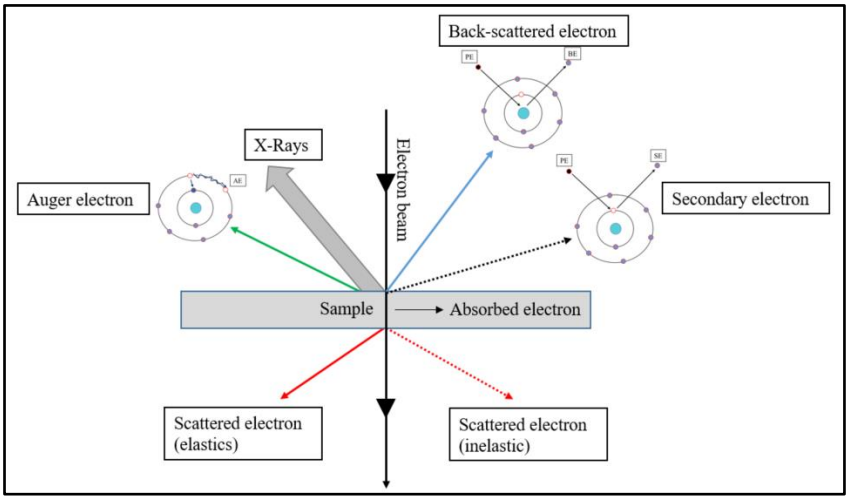

Fig. 20 : Representation of the different interactions between the material and the electron beam during a SEM measurement.

1.8 MODELLING APPROACH

1.8.1 THE MODEL FOR THE SOLID PHASES

The Ringberg seminar (Chase, et al., 1995), a meeting of specialist in numerical modelling of thermodynamic properties, aimed at choosing and adopting more universal models to represent and describe the heat capacity as a function of temperature of an element or compounds in its crystalline, liquid or gaseous state. The goal of this conference was to invent a mathematical model that does not necessarily have a physical significance but could be handled with more ease numerically. The heat capacity at constant pressure Cp is considered as the most important property for thermodynamic modeling, as it translates the evolution of the thermodynamic potentials (G, H and S) as a function of temperature. Thus, two models describing the heat capacity have been chosen in order to manipulate the thermodynamic properties with confidence.

$$C_{fit,Debye}=C_{Debye} + aT + bT^2 \qquad [4]$$

The Debye model is given ($C_{fit,Debye}$) by the equation 4 and C_{Debye} is described by the expression in equation 5.

$$C_{fit,Debye} = 9R + (\frac{T}{\Theta_D})^3 \int_0^{\frac{\Theta_D}{T}} \frac{e^x x^4}{(e^x-1)^2} dx \qquad [5]$$

$$C_{fit,Einstein} = C_{Einstein} + aT + bT^2 \qquad [6]$$

The $C_{Einstein}$ is described by the expression in equation 7.

$$C_{Einstein} = 3R + (\frac{\Theta_E}{T})^2 \frac{e^x x^4}{(e^{\Theta_{E/T}}-1)^2} \qquad [7]$$

According to the conclusions of the Ringberg seminar (Chase, et al., 1995), the Debye model is accurate in the case of describing experimental heat capacities at low temperatures (<250K) but it is not easy to be handled to calculate G, H and S as there is no analytical solution to the function described in equation [5]. The Einstein model gives excellent results especially for T>250K and the function can easily be integrated. Where Θ_D and Θ_E describe the Debye and Einstein temperatures respectively, R is the universal gas constant, aT and bT^2 are the adjustable parameters that ensure the continuity of the function describing the thermodynamic properties of the crystalline solid up to the melting point. This term of $aT+bT^2$ is also called anharmonic contribution. The low-order anharmonic corrections are described by the term aT, while bT^2 contains the higher-order anharmonic. Although the Debye model correctly describes the Cp at low temperature, it is advisable to use the Einstein model, which has been used recently by Bajenova et *al* (2020) but also by Deffrennes et *al* (2020). In our study, the following equation with 3 temperatures of Einstein was used to describe the heat capacity as a function of temperature of the solid phases.

$$Cp = 3R\left(\sum_i^n \alpha^i (\frac{\Theta_E^i}{T})^2 \frac{\exp\left(\frac{\Theta_E^i}{T}\right)}{(\exp\left(\frac{\Theta_E^i}{T}\right)-1)^2}\right) + a_1 T + a_2 T^2 \qquad [8]$$

$$G = E_0 + \frac{3}{2} R \sum_i^n \Theta^i \alpha^i - 3RT\left(\sum_i^n \alpha^i \ln(\exp(\frac{\Theta^i}{T}) - 1)\right) + \frac{a_1}{2} T^2 - \frac{a_2}{6} T^3 \qquad [9]$$

T(K) for the absolute temperature and α^i is the weights of the input of each Einstein temperature contribution. For example, for the compounds $Ca_3Al_2O_6$ the sum

of α^i should ideally be equal to the number of atoms in the phase stoichiometry, i.e. 11. The thermodynamic description of the heat capacities of all aluminates was performed using a 3-term Einstein function from 0K to the melting point, the anharmonic adjustment at high temperature was done with two terms $a_1T+a_2T^2$ as suggested by the Ringberg seminar. Bajenova et *al* (2020) successfully used this model in the case of thermodynamic description of pure SiO_2 at 1 atm and Defrennes et *al* (2020) for the modelling of the thermodynamic properties of pure lime CaO.

1.8.2 THE MODEL FOR THE LIQUID PHASES

The thermodynamic description of the liquid phase is done using the associates model . This model is particularly used when short-range order is observed in the liquid phase, which is the case in metal-oxygen systems but also in some oxide-oxide system with strong interaction. The concept is based on the one hand on the description of oxygen atoms bound to two Al (in the case of a $CaO-Al_2O_3$ binary liquid) in this case called “Bridging Oxygen” (BO) and on the other hand on an oxygen-Aluminium-calcium alternation called “Non bridging Oxygen” (NBO). Introduction of Ca^+ stabilizes AlO_4^- (Neuville et *al*, 2010) and forms fictitious Q^n species (where Q refers to tetrahedral site AlO_4, n corresponds to the number of bridging oxygen per tetrahedron). There are different configurations Q^n species of aluminium in the $CaO-Al_2O_3$ system. Q^4 for pure liquid Al_2O_3; Q^3 corresponds to a fictitious $Ca_2Al_2O_5$ liquid species; Q^2 describes $Ca_3Al_2O_6$ liquid species; Q^1 and Q^0 respectively for $Ca_4Al_2O_7$ and $Ca_5Al_2O_8$. Both Q^4 and Q^2 have been observed by spectroscopic measurements, Q^1 and Q^0 are associated with very high calcium compounds and are difficult to confirm experimentally due to the high melting temperature and Q^3 remains a subject of debate. Regarding the stoichiometry of these species there is no general rule fixed on basic oxides. In the $CaO-Al_2O_3$ system, $Ca_3Al_2O_6$ melt will directly describe the associate Q^2.

Gibbs energy of the solution is therefore expressed with the Gibbs energies of the species in the solution.

$$G_m^{liq} = \sum_k x_k G_k^{liq} + RT \sum_k x_k \ln(x_k) + \sum_i x_i \sum_j x_j \sum_v (x_i - x_j)^v L_{i,j}^{liq} \qquad [10]$$

- $\sum_k x_k G_k^{liq}$: this term is called reference term and describes the mechanical mixture of the species without interaction. In the case for the CaO-Al_2O_3 system, the species are liquid CaO, Al_2O_3 (Q^4) and $Ca_3Al_2O_6$ (Q^2)
- $RT\sum_k x_k ln(x_k)$: the ideal entropy with *R* ideal gas constant and *T* temperature.
- $x_i x_j \sum_v (x_i - x_j)^v L_{i,j,k}^{liq}$: corresponds to the binary interaction terms between the different species.

$L_{i,j}^{liq}$ are the temperature dependent binary interaction parameters, which are optimized using experimental data available such as activities as function of composition and temperature, phase diagram and heat of mixing.

$$L_{i,j}^{liq} = a_{i,j}^{liq} + b_{i,j}^{liq} \qquad [11]$$

The associates model was selected for our work since it is implemented in all Gibbs energy minimization codes of various software such as Pandat, ThermoCalc, FactSage or OpenCalphad. The phase diagram modelling and calculations were performed using the Pandat software.

2 CHAPTER 2: THERMODYNAMIC STUDIES OF SELECTED COMPOUNDS IN THE SYSTEM C-S: BELITE & RANKINITE.

2.1 INTRODUCTION

Knowledge of the thermodynamic behaviour of the major constituents of cement is necessary to understand the factors that govern the formation and stability of Portland clinker compounds and phases. This chapter deals with the thermodynamic properties of belite (Ca_2SiO_4) and rankinite ($Ca_3Si_2O_7$). These two compounds are important constituents of Portland type and carbonatable clinkers. The measurements carried out in this chapter are complementary to those existing in the literature. All results will constitute an important addition to a better description of the CaO-SiO_2 binary system. This work will provide new data that was never measured before, especially on pure rankinte and belite. This chapter is divided into two main parts. The first part will focus on the study of belite, including a review of the literature and our experimental measurements, which will be compared with thermodynamic models. The second part will be focused on the study of rankinite.

2.2 Ca_2SiO_4 AND $Ca_3Si_2O_7$ IN CaO-SiO_2 SYSTEM

The CaO-SiO_2 quasi-binary phase diagram is one of the most studied in the field of oxide chemistry. Rankin and Wright (1915) carried out an early investigation on this system. Subsequently, additional experimental and assessed studies have complemented the previous cited work. Notably Philips and Muan (1959), Greig (1927) and Roy (1958) for experiments contribution. Then, Pelton and Blender (1986) , Taylor and Dinsdale (1987) or Hillert et *al* (1990) for the assessed phase diagram. Four solid compounds occur in this binary system, including Ca_3SiO_5, Ca_2SiO_4, $Ca_3Si_2O_7$ and $CaSiO_3$ at atmospheric pressures. Among them, two compounds melt congruently ($CaSiO_3$ and Ca_2SiO_4) while the others melt incongruently ($Ca_3Si_2O_7$ and Ca_3SiO_5). Building up a thermodynamically accurate database on oxides requires a consistent experimental contribution. Regarding rankinite and belite, the higher temperatures at which both oxides exist have been a limitation in the recent past. A major step in the thermodynamic study of high melting point oxides was the successful development of the calorimetric method. This method will be a starting point for the belite and rankinite research. The experiments carried out in this chapter will provide a substantial complement to the existing data and will be our experimental contribution to a joint project to reassess the CaO-SiO_2 phase diagram. Fig. 21 shows the first phase

diagram studied and reported by Rankin and Wright (1915). Fig. 22 is the SiO_2-$2CaO.SiO_2$ section from the experimental work of Greig (1927). In Fig. 23, we have shown the diagram currently used by ceramists and drew by Philips and Muan (1959), whose research is based on data from Rankin and Wright, Greig (1927) and Roy (1958).

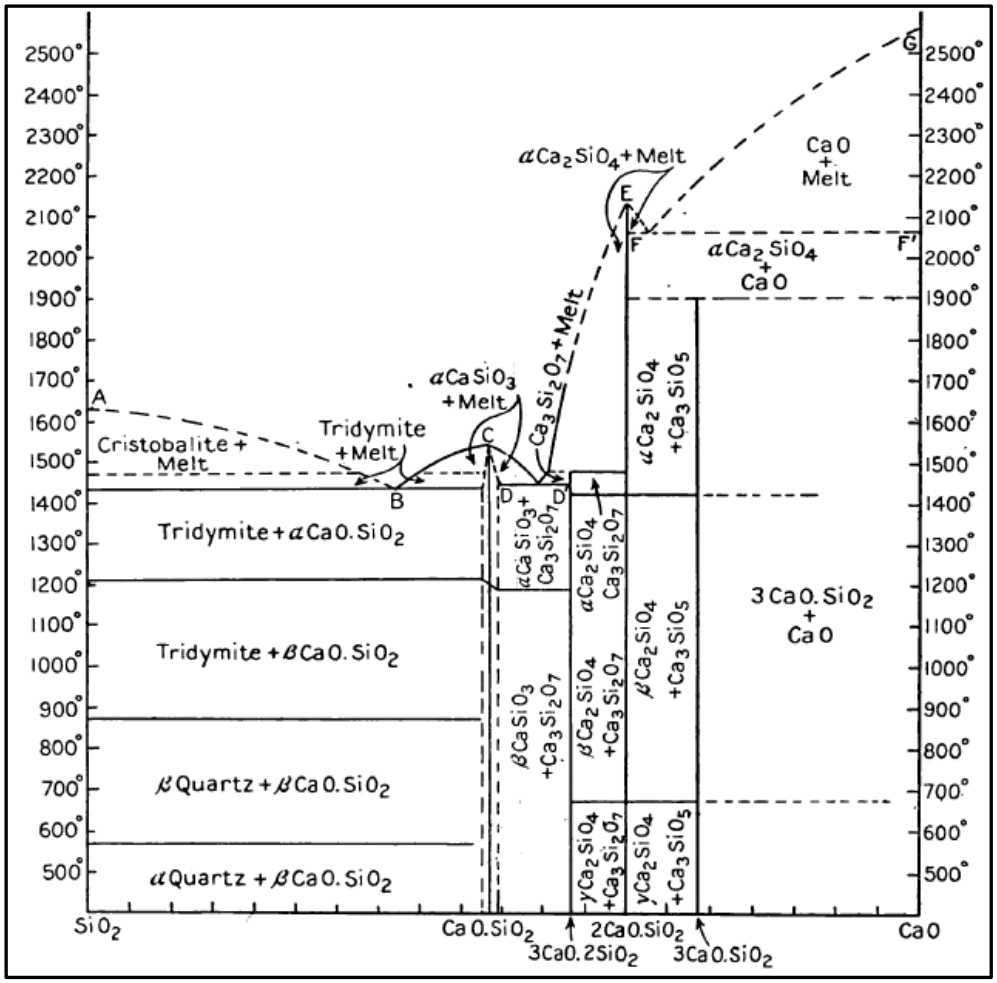

Fig. 21 : CaO-SiO_2 first phase diagram from Rankin and Wright (1915).

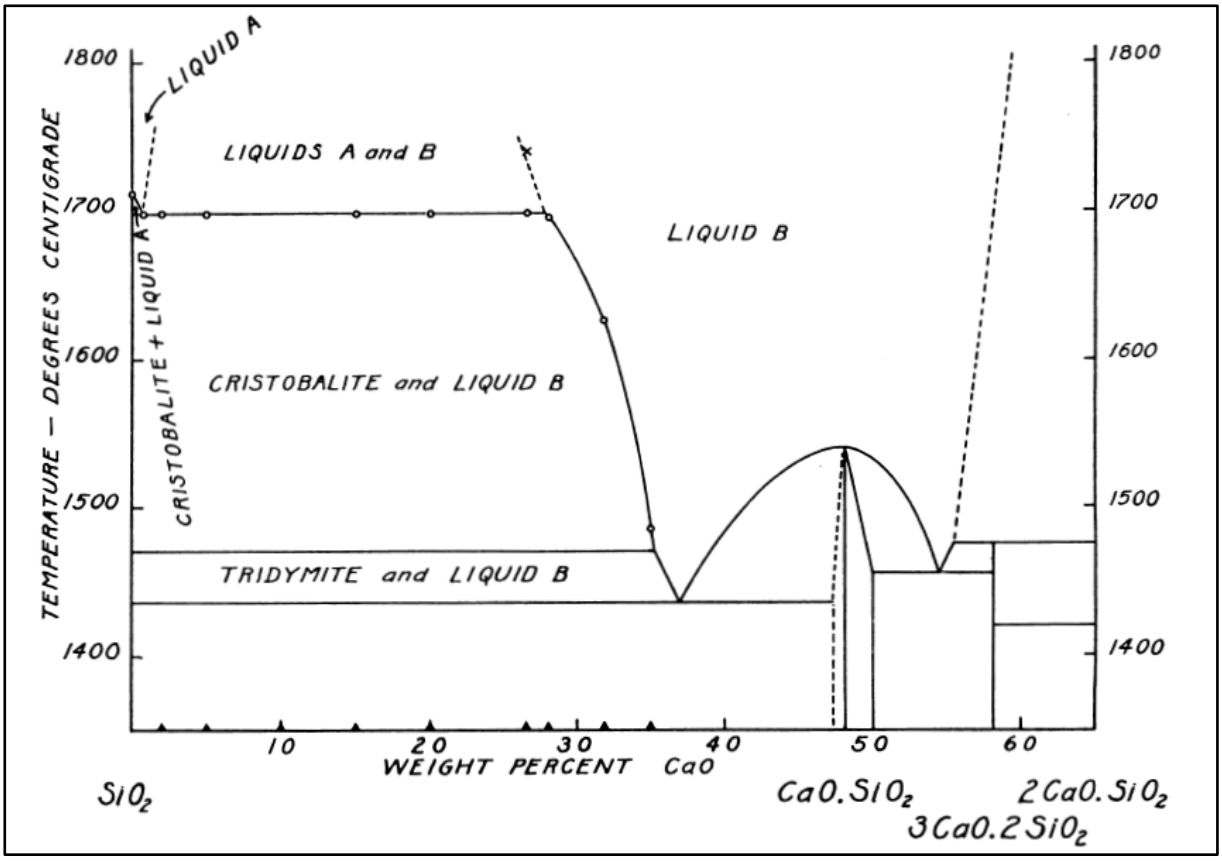

Fig. 22 : Lime-silica (SiO_2-$2CaO.SiO_2$) phase diagram reported by Greig (1927).

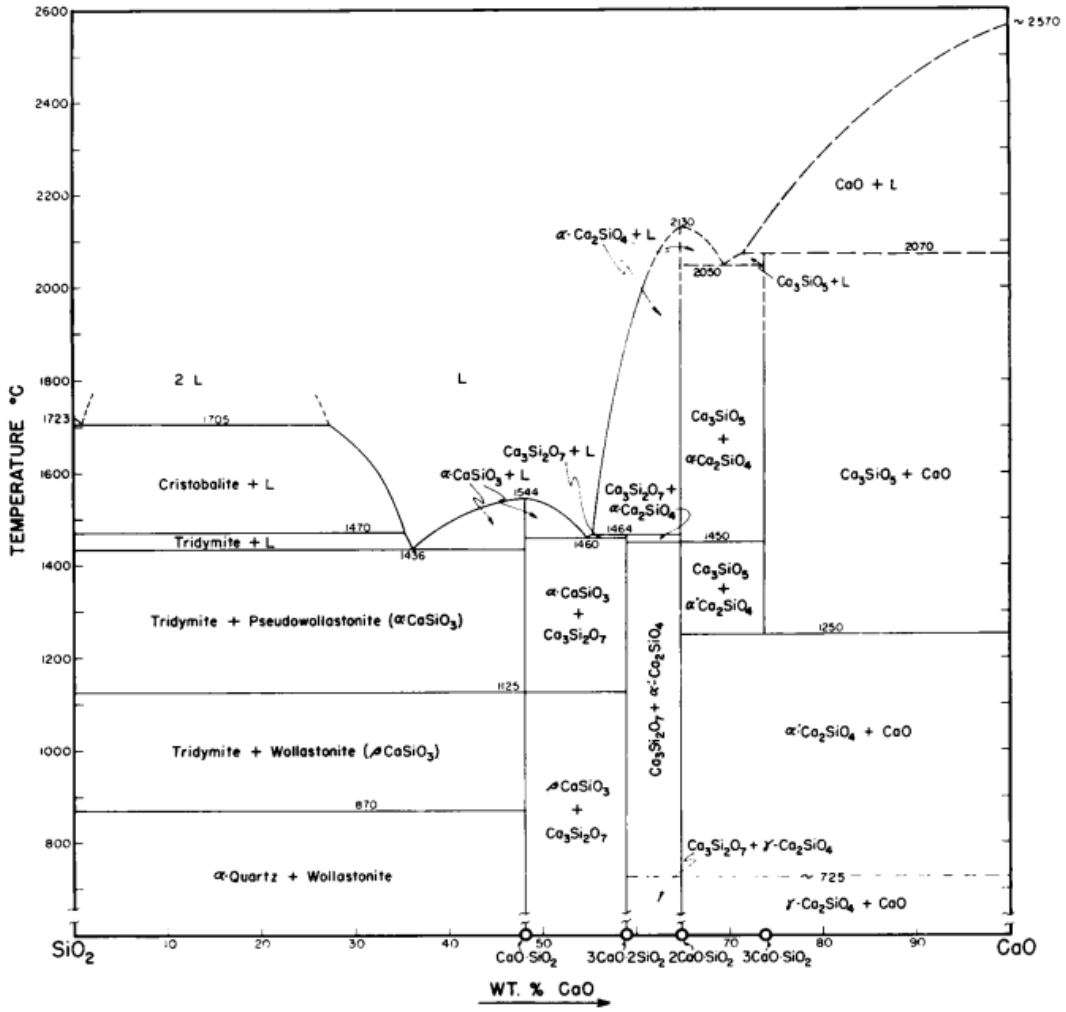

Fig. 23 : Phillips and Muan *(1959)* CaO-SiO_2 phase diagram based on data of Rankin and Wright *(1915)* and Greig *(1927)*. Significant changes with respect to stability relations dicalcium and dicalcium silicates, based on Roy *(1958)*.

2.3 LITERATURE REVIEW ON Ca_2SiO_4

2.3.1 GENERAL ASPECT OF Ca_2SiO_4 POLYMORPHISM

The structural properties of calcium orthosilicate were the subject of several studies due to their interest in the cement industry. Since 1915, Rankin and Wright (1915) had already reported the polymorphic character of calcium orthosilicate. Bredig (1950) confirmed the results of this first study decades later. Calcium orthosilicate exists in five polymorphic forms named α, α' (α'_H and α'_L), β and γ. The range of existence and stability of each polymorph is temperature dependent and in some cases, the stabilization of the polymorph after quench at room temperature requires the insertion of foreign ions also known as stabilizers. The α-Ca_2SiO_4 polymorph is

stable above 1450°C and melts at 2130°C (Eysel and Hahn, 1970). On cooling α- Ca_2SiO_4 transforms into α'- Ca_2SiO_4, this polymorph exists in two intermediate phases α'_H and α'_L of close crystallographic structure, the range of existence of α'- Ca_2SiO_4 is between 850°C and 1400°C (Smith, 1962). The γ- Ca_2SiO_4 polymorph is the most stable at room temperature, its formation is the product of the transformation of the metastable β- Ca_2SiO_4 form upon cooling. The phase transition temperatures of calcium orthosilicate are closely related to the composition, indeed, the purity of the precursors or the presence of foreign ions can influence the transition temperature. The insertion of iron oxide (FeO) into the calcium orthosilicate favors the increase of the β- Ca_2SiO_4 →γ- Ca_2SiO_4 transition temperature. The γ- Ca_2SiO_4 → α'- Ca_2SiO_4 transition occurs at 847°C (Coughlin & O'Brien, 1957), this transformation is irreversible, similarly the β- Ca_2SiO_4→γ- Ca_2SiO_4 transition is also irreversible and occurs below 500°C (Eysel and Hahn, 1970), apart from these two mentioned transitions, the other phase transitions are reversible. It is common to find transition temperature values slightly different from those given in Fig. 24 depending on the actual composition of the polymorph: presence of impurity or stoichiometric imbalance due to an excess of one of the precursors. Influence of the composition on the transition temperatures was studied by Forest (1971). In their work, the authors showed that the composition plays a major role on the value of the transition temperature of calcium orthosilicate polymorphs. This particularity explains the differences between the transition temperature values given in the literature by different authors (Smith, 1962) (Forest, 1971) (Coughlin & O'Brien, 1957). Fig. 24 is a polymorphic transformation scheme for calcium orthosilicate, based on the work of Eysel and Hahn (1970).

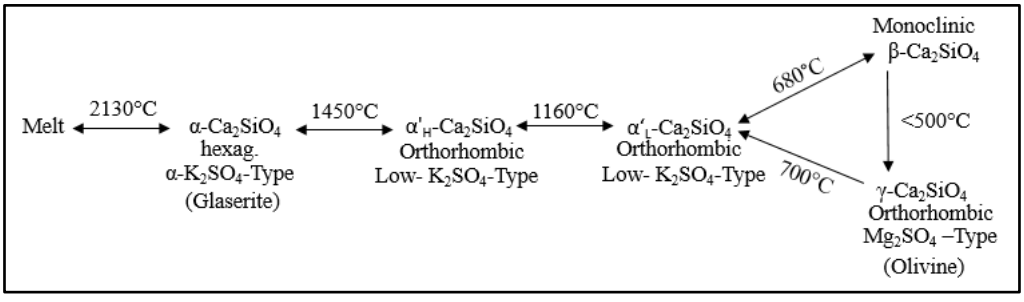

Fig. 24 : Polymorphic transformation of Ca_2SiO_4 as a function of temperature evolution by Eysel and Hahn (1970).

The β-Ca_2SiO_4 phase is metastable and undergoes structural rearrangements on cooling and then stabilizes in the γ-Ca_2SiO_4 phase, this reaction is called displacive. The β-Ca_2SiO_4 →γ-Ca_2SiO_4 transition is slow at atmospheric pressure and induces a 12% increase in crystal volume at room temperature; this phenomenon is called dusting and was observed in the laboratory during the synthesis of γ-Ca_2SiO_4. The γ→α'$_L$ transformation occurs only on heating, the phase transition is slow due to the low transition temperature and the large structural rearrangement. This transformation is called semi-reconstructive because it induces a change in the coordination of the Ca atoms as well as a rotation of the tetrahedron (Forest, 1971). It has been shown that the transformations from α'$_H$ to α'$_L$ and α'$_L$ to β are reversible (Smith, 1962) (Eysel & Hahn, 1970) (Saalfeld, 1975). Nevertheless, the α'$_H$ and α'$_L$ forms have similar structures and are therefore difficult to dissociate and distinguish. Since both polymorphic forms exist at probably identical free energies, transformation from α'$_H$ to α'$_L$ does not cause any consequent crystallographic cell deformation as is a continuous phase transitions.

2.3.2 Ca_2SiO_4 Crystallographic structures

The growing interest in the crystallographic study of calcium orthosilicate polymorphs dates back to the previous century. Indeed, one of the first structural studies of the γ- Ca_2SiO_4 polymorph was done by analogy with the structure of the olivine Mg_2SiO_4 (O'Daniel and Tscheischwili, 1942) (Smith et *al,* 1965). The γ- Ca_2SiO_4 crystallizes in an orthorhombic lattice and all these symmetries belong to the space group Pbmn. All calcium ions (Ca) are octahedrally configured, but the Si-O interatomic distances in the SiO_4 tetrahedron are irregular. As shown in figure 19, the polymorph β-Ca_2SiO_4 crystallizes on cooling and is in metastable equilibrium with α'$_L$- Ca_2SiO_4, unlike γ- Ca_2SiO_4, pure β- Ca_2SiO_4 is difficult to stabilize at room temperature, in cement clinkers it is stabilized by other oxides such as K_2O, Al_2O_3, $Ca_3(PO_4)_2$, B_2O_3 or at high pressure. Different studies have reported the importance of minor elements in the stability of β- Ca_2SiO_4 (Chan et *al*, 1988) (Cuesta et *al*, 2014), β- Ca_2SiO_4 has a crystallographic structure similar to that of β-K_2SO_4 in which Ca replaces K and Si at the S position. The polymorphs α'$_L$- Ca_2SiO_4 and α'$_H$- Ca_2SiO_4 have very similar structures and are difficult to distinguish. Both polymorphs crystallize in an orthorhombic lattice and differ only in their symmetry group. Finally, the α-Ca_2SiO_4 polymorph crystallizes in a hexagonal lattice and is stabilized after quench $CaNaPO_4$

and P_2O_5 (Ghosh et *al* 1979). The crystallographic parameters of the calcium orthosilicate polymorphs are summarized in Table 4. The α,α',β-Ca_2SiO_4 polymorphs are shown in Fig. 25, the γ-Ca_2SiO_4 variety will be synthesized and represented in the experimental part of our investigation.

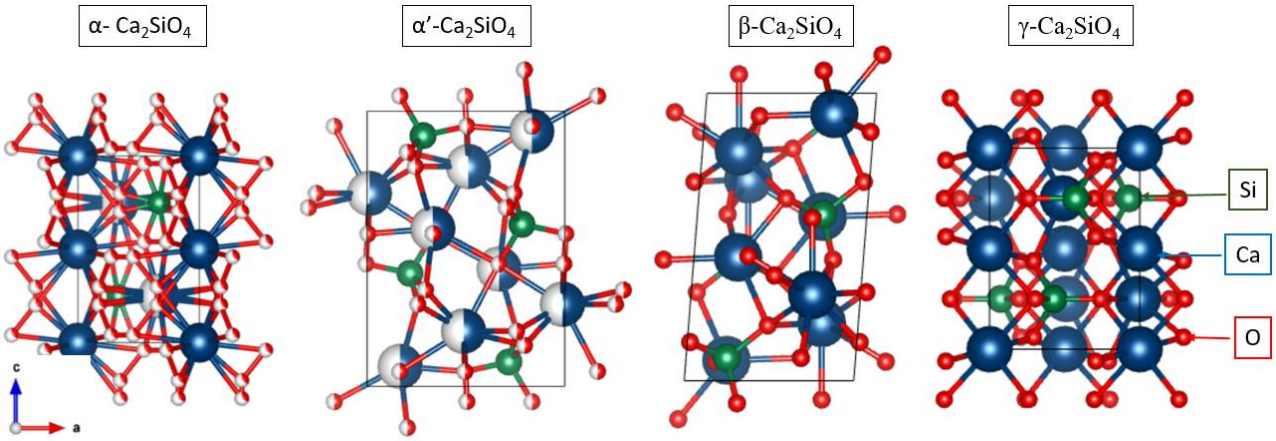

Fig. 25 : Crystallographic representation of Ca_2SiO_4 polymorphs.

Polymorph	Structure type	Symmetry & Space group	Cell content	Ca coordination	Lattice parameter (Å)	Sources
γ	Olivine type	Orthorhombic Pbnm	Z=4	Ca(1)= 6 Ca(2)= 6	a= 5.091±0.010 b=6.782±0.020 c=11.371±0.010 a=5.081 b=6.778 c=11.224 a=5.06±0.02 b=6.78±0.04 c=11.28±0.06 a=5.0778	Smith et *al* (1965) Udagawa et *al* (1980) O'Daniel and Tscheischwili (1942)

					b=11.2154 c=6.7574	Mumme et *al* (1996)
β	Strongly deformed low-K_2SO_4 type	Monoclinic $P2_1/n$	Z=4	Ca(1) = 6+6 Ca(2)= 8	a=5.48±0.02 b= 6.76±0.02 c= 9.28±0.02 β= 94.33° Stabilized with B_2O_3	Midgley (1952)
					a=9.34 b=5.51 c= 6.76 Y=94.3° at 293K Stabilized with $Ca_3(PO_4)_2$	Saalfeld (1975)
					a=5.502±0.001 b=6.745±0.001 c=9.297±0.001 β=94.59±0.02° at 25°C Without stabilizing reagents	Jost et *al* (1977)
					a=5.5319 b=6.7572 c=9.2805 β=94.569°	Mumme et *al* (1996)

α'_L	Slightly deformed low-K_2SO_4 type	Orthorhombic Ccm21(Several other space group possible) Pcmn	Z=16	Ca(1) = 10 Ca(2)= 9 (Subcell)	a=18.80 b=11.07 c=6.85 a=9.49 a=9.48 b=5.59 b=5.59 c=6.85 c=6.83*3 at 1200°C 1000°C a=9.41 b=5.53 c=6.81*3 1073K	Suzuki and Yamaguchi (1968) Saalfeld (1975)
α'_H	low-K_2SO_4 type	Orthorhombic $P2_1/cmn$ Pnma	Z=4	Ca(1 = 10 Ca(2)= 9	a= 5.450 b= 5.573 c= 6.860 a=6.7673 b=5.5191 c=9.3031	Regourd et *al* (1968) Mumme et *al* (1996)
α	Glaserite type	Hexagonal P3m1	Z=2	Ca(1)= 10 Ca(2)= 6 Ca(3)= 6+6	a= 5.45 c= 7.19	Bredig (1950)

Table 4 : Crystallographic data of Ca_2SiO_4 polymorphs according to different studies from the literature.

2.4 Ca_2SiO_4 THERMODYNAMICS DATA REVIEW

One of the crucial points of this work is to fill the gap in terms of experimental thermodynamic data. The critical review of the literature has allowed us to highlight a number of gaps in the thermodynamic data for calcium orthosilicate varieties, in particular relative enthalpy. As early as 1951, the enthalpy of formation of β-Ca_2SiO_4 was already known thanks to the work of Elsner et *al* (1935), Johannson and Thorvaldson (1934), Ayed et *al* (1993) and King (1951). Later, Coughlin (1957) measured relative enthalpy of β,α',α- Ca_2SiO_4 from 25°C to 1543°C and of the γ-Ca_2SiO_4 variety up to the inversion temperature γ-Ca_2SiO_4→α'- Ca_2SiO_4. The γ-Ca_2SiO_4→α'-Ca_2SiO_4 heat of transition was evaluated by Coughlin and later by Forest (1971) but remains a subject of discussion. In this manuscript, the experimental work, especially the heat content measurements will cover a wider temperature range from the γ-Ca_2SiO_4 polymorph existence domain to α-Ca_2SiO_4. King (1957) and Todd (1951) have also measured the low temperature heat capacities of γ-Ca_2SiO_4 and β-Ca_2SiO_4 respectively and various thermodynamic databases implemented Ca_2SiO_4 heat of transition data by critical assessment of the available literature data (Haas (1981) and FactSage software).

2.4.1 HEAT OF TRANSITION

There are some discrepancies between the experimental values and some data calculated from FactSage software and its thermodynamic databases. Using commercial data outside of experiments induces errors in calculations of further thermodynamic properties. In fact, an excessively high heat of transition with respect to the measurements leads to an overestimation of the relative enthalpies. Although modelling is useful because it allows us to explore properties not accessed through experiments, one of the benefits of doing experiments is that it allows us to validate a model. Thus, unlike FTPS data from FactSage software, Haas (1981) model provides a heat of transition more consistent with Coughlin and O'Brien (1957) and Forest (1971) experiment. In Table 5, we gathered polymorph Ca_2SiO_4 heat of transition data from various sources.

Chemistry	Transition	$T_{Transition}$ (°C)	$\Delta H_{Transition}$ KJ.mole^{-1}	Method	Sources
Ca_2SiO_4	$\gamma \rightarrow \alpha'_L$	880 847	14.1	Differential thermal analysis (French paper).	Forest (1971)
			14.4	Inverse drop Calorimeter: sample kept in platinum-rhodium capsules.	Coughlin and O'Brien (1957)
			36.75	Calculated value from FTPS database	FactSage software
			13.70±2.46	Calculated value	Haas (1981)
		711	13.0	Differential thermal analysis at 0.34GPa	Hanic et *al* (1987)
	$\beta \rightarrow \alpha'_L$	680 697	1.4	Differential thermal analysis (French paper).	Forest (1971)
			1.8	Inverse drop Calorimeter: sample kept in platinum-rhodium capsules.	Coughlin and O'Brien (1957)
	$\beta \rightarrow \gamma$		6.11	Differential thermal analysis (French paper).	Forest (1971)
	$\alpha'_H \rightarrow \alpha$	1437	13.5	Differential thermal analysis (French paper).	Forest (1971)
			14.2	Inverse drop Calorimeter: sample kept in platinum-rhodium capsules.	Coughlin and O'Brien (1957)
			4.28	Calculated value from FTPS database	FactSage software
			14.39±3.39	Calculated value	Haas (1981)

Table 5 : Enthalpy and temperature of polymorphic transition of Ca_2SiO_4.

2.4.2 HEAT OF FORMATION

Research in the literature on direct measurements of standard enthalpies of formation is gathered in Table 6. In addition, there are databases listing enthalpies of formation of Ca_2SiO_4 for the different polymorphs based on thermodynamic calculations or models. For example, to deduce α'- Ca_2SiO_4 standard enthalpy of formation, Haas et *al* (1981) used the heat of decomposition of Ca_3SiO_5 to β- Ca_2SiO_4, measured by Benz and Wagner (1961) via E.M.F. Similarly, for β- Ca_2SiO_4 value was derived from the enthalpy of reaction $Ca_3SiO_5 \leftrightarrow$ β- Ca_2SiO_4 + CaO reported by Brunauer et *al* (1956) in solution calorimetry in HNO_3 acid. Methods used to obtain these values do not imply the validity of data; we aimed to report only experimental values whose measurement methods are explicitly described in the papers.

Chemistry	$\Delta H°_f$(KJ/mole)		Method of investigation	Sources
	from oxides	from elements		
β- Ca_2SiO_4	-126.31 ±0.96	-2256.85	Hydrofluoric Acid solution calorimeter.	King (1951)
	-139	-	Calorimeter Richards adiabatic type: heat of solution in HCl-200H_2O at 20°C	Johannson and Thorvaldson (1934)
	-116.36	-	Reported by Materials Project	(MaterialsProject, s.d.)
	-125.	-	Dissolution calorimetry in HCl+20H_2O and HCl+200 H_2O	Eitel and Richter (1942)
	-123.2	-	Dissolution calorimetry in HNO_3+HF acid bath	Elsner et *al* (1935)
	-	-2306.77±4.44	High-temperature drop-solution calorimetry at 700°C using a custom-built Tian-Calvet-type twin-	Grevel (2022)
γ- Ca_2SiO_4	-	-2315.98±4.47		

			microcalorimeter with $2PbO.B_2O_3$.	
	-143	-	Calorimeter Richards adiabatic type: heat of solution in HCl-$200H_2O$ at 20°C	Johannson and Thorvaldson (1934)
	-119±1	-	Calorimeter of dissolution in PbO-B_2O_3 at 900°C	Ayed et *al* (1993)
	-126.49	-	Reported by Materials Project	(MaterialsProject, s.d.)

Table 6 : Heat of formation reported in various published paper.

2.5 EXPERIMENTAL STUDY OF BELITE

2.5.1 SYNTHESIS PROCEDURE

The previous section discussed the data available in the literature for the solid phases. There are several key measurements, which should be repeated or missing data that must be ascertained to complete a thermodynamic assessment targeted at modelling cement clinker formulation. This section details the experimental methods and preparation used to obtain these measurements. The starting materials are $CaCO_3$ (Alpha Aesar, 99.5%) and SiO_2 (Sibelco, 99%) which are dried in a muffle furnace at 500°C in air for 24h. The mixture is homogenized in a mechanical mixer for 24h and pelletized using a hydraulic workshop press (4.5 tons on 3g of powder). For Ca_2SiO_4, a powder mixture of $CaCO_3$ (6.97±0.01g) and SiO_2 (2.09±0.01g) is calcined at 1000°C for 1h and annealed at 1550°C for 8h followed by slow cooling to room temperature. A loss on ignition of 34.08% (in agreement with theoretical value) is recorded. Fig. 26 is the reagent mixture pelleted by press before heat treatment. After the heat treatment, the bright colour of the mix remains unchanged. Dust build-up after cooling is an indication that a γ- Ca_2SiO_4 phase is occurring. Structural analysis will provide a purity assessment on the phase from the reaction proceeds.

Fig. 26 : Sample in a platinum crucible for heat treatment. For Ca_2SiO_4, heat treatment in pellet form is not required as the pellets change to powder at low temperatures. Nevertheless, the specific reaction area is greater and heat transfer is more homogeneous.

2.5.2 Ca_2SiO_4 X-RAY PHASE ANALYSIS

Samples mineralogical composition identification was carried out using X-ray diffraction (X'Pert Pro MPD, PANalytical), with CuKα radiation of λ= 1.5419 Å. Crystallographic study by X-ray diffraction confirmed a single polycrystalline phase and all peaks identified as belonging to γ-Ca_2SiO_4 olivine crystallizing in an orthorhombic symmetry lattice. Cell parameters adjustment was done with DIFFRAC.EVA5.2 from Brucker AXS based on PDF4+ 2022 database. X-rays recording has carried out over a period of 1h 59 min on a 2Θ angular range from 10° to 120°. Ca_2SiO_4 X-rays diffraction pattern is plotted in Fig. 27. Regarding the lattice parameters, results gathered in Table 7 agree with published literature. Discrepancies between our crystallographic data and literature are mainly related to the type and purity of starting material as well as synthesis procedure. For instance, we used 99.5% $CaCO_3$ to produce CaO while Smith et *al* (1965) employed $Ca(NO_3)_2$ as a raw material but did not specify purity. Although Udagawa et *al* (1980) started experiment with $CaCO_3$ as a CaO precursor; the author synthesized γ-Ca_2SiO_4 by flux method in presence of $CaCl_2$ as flux in an electric furnace.

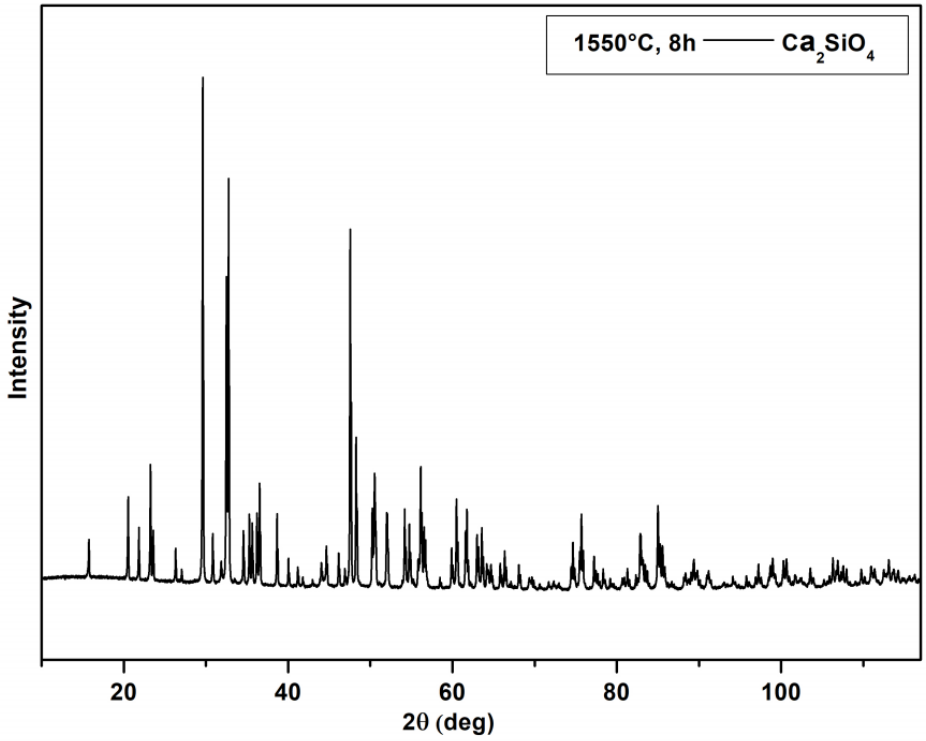

Fig. 27 : X-ray diffraction pattern over an angular range from 10 to 120°.

pace group	Pbnm
Lattice parameter a	5.078 Å
Lattice parameter b	6.760 Å
Lattice parameter c	11.225 Å
α=β=Ɣ	90.000°
Unit cell Volume	385.324 $Å^3$

Table 7 : γ-Ca_2SiO_4 crystallographic data calculated from X-ray pattern after synthesis.

From the crystallographic data, we have reproduced the crystallographic structure on VESTA software. The layout of the oxygen atoms around the cations can be illustrated.

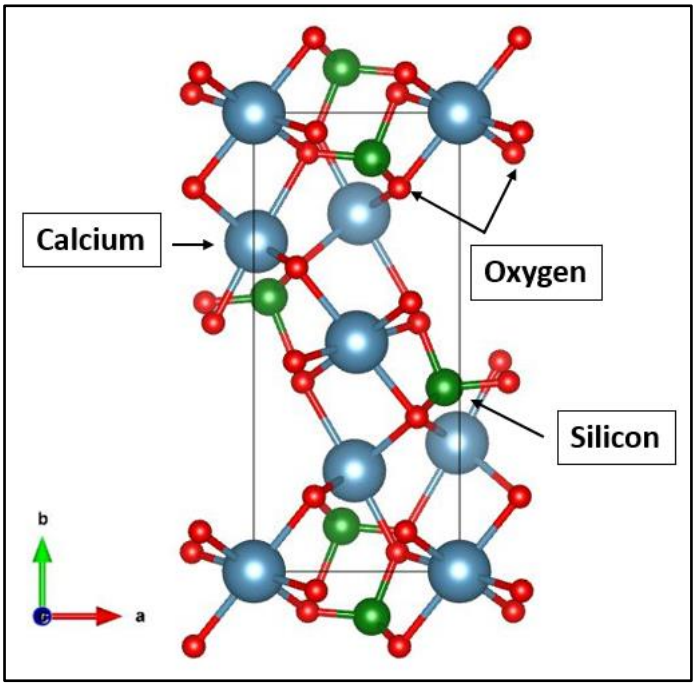

Fig. 28 : Crystallographic structure of Ca_2SiO_4 obtained after X-rays measurement on the synthesized sample.

2.5.3 DIFFERENTIAL SCANNING CALORIMETRY: CA_2SIO_4

We measured the transition temperature of Ca_2SiO_4 by DSC Labsys^{TM} Evo. On heating, the powder in the platinum crucible sintered at high temperature, and then on cooling, the sintered powder gained volume, reflecting the transformation of α'-Ca_2SiO_4 to γ- Ca_2SiO_4 (with an intermediate metastable β- Ca_2SiO_4 as stated Eysel and Hahn, 1970).

Fig. 29 : Ca_2SiO_4 dusting after DSC measurement.

2.5.3.1Heating

The first peak (a) on the DSC curve is the transition from γ- Ca_2SiO_4 to α'-Ca_2SiO_4, the signal is not well characterized and the temperature of this transition

cannot be precisely defined. But, this signal lies between 800°C and 900°C, which is in agreement with the transition temperature of γ- Ca_2SiO_4 → α'- Ca_2SiO_4 847°C reported by Coughlin and O'Brien (1957) and . For the second (b), the start of the curve deviates from its baseline at 1413°C forming a more defined peak than the previous one, the minimum of the peak is at 1430°C whereas the return from the baseline is at 1447°C. Although it is not clear exactly which transition temperature values should be used for the ascent, it can be seen that the interval of existence of the transition peak is in agreement with the literature value. Furthermore, it was found that the baseline increases with temperature when acquiring this particular compound.

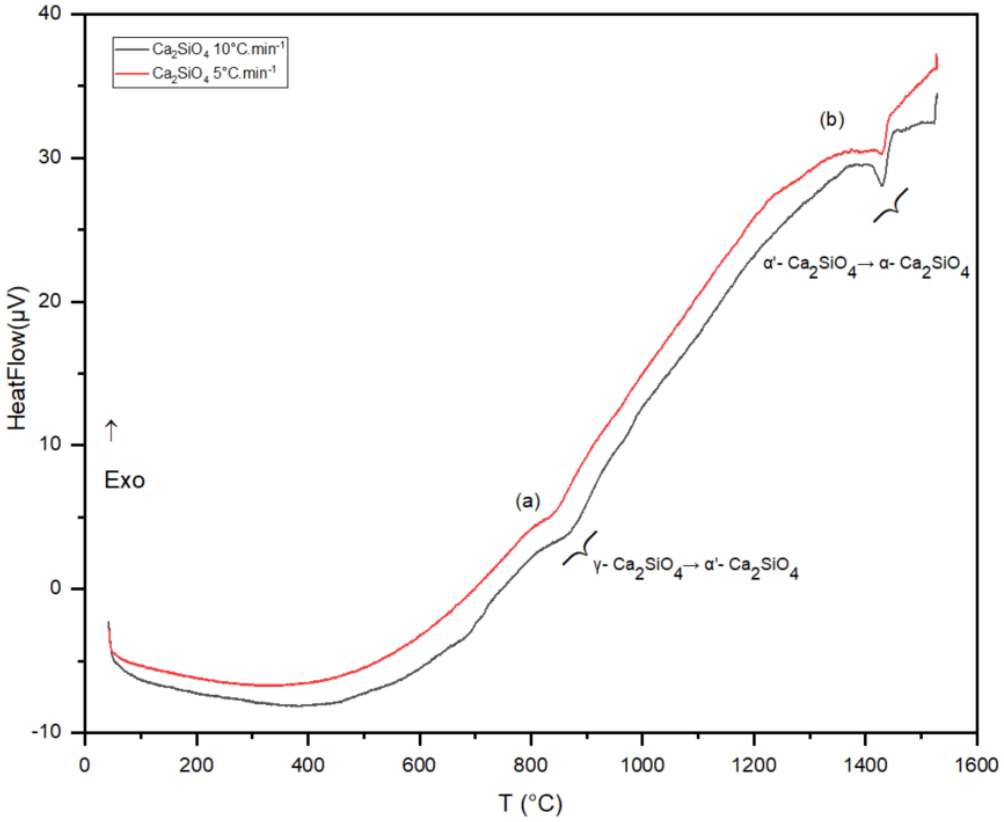

Fig. 30 : DSC Labsys^{TM} Evo signal of the Ca_2SiO_4 variety obtained after two runs at 5°C and 10°C on heating.

2.5.3.2Cooling

In crystalline materials, the exothermic transformation indicating the crystallization of the compound corresponds to the beginning of the deviation of the DSC curve, in contrast to Fig [24], we have quite well differentiated peaks which allow us to more accurately deduce the polymorphic inversion point. Thus, exothermic peaks on cooling correspond to the transformation of Ca_2SiO_4 variety. The α-Ca_2SiO_4 → α'-

Ca_2SiO_4, α'- Ca_2SiO_4 → β- Ca_2SiO_4 and β- Ca_2SiO_4 → α'- Ca_2SiO_4 transitions occur at 1416°C, 667°C and 373°C respectively. We also identified an exothermic peak (i) at 480°C. Regarding this signal (i), it does not correspond to any transition; it is probably related to impurities in the sample that were not detectable by X-rays diffraction. We have plotted in Fig 31, the DSC curve obtained for 5°C and 10°C.min^{-1} rate.

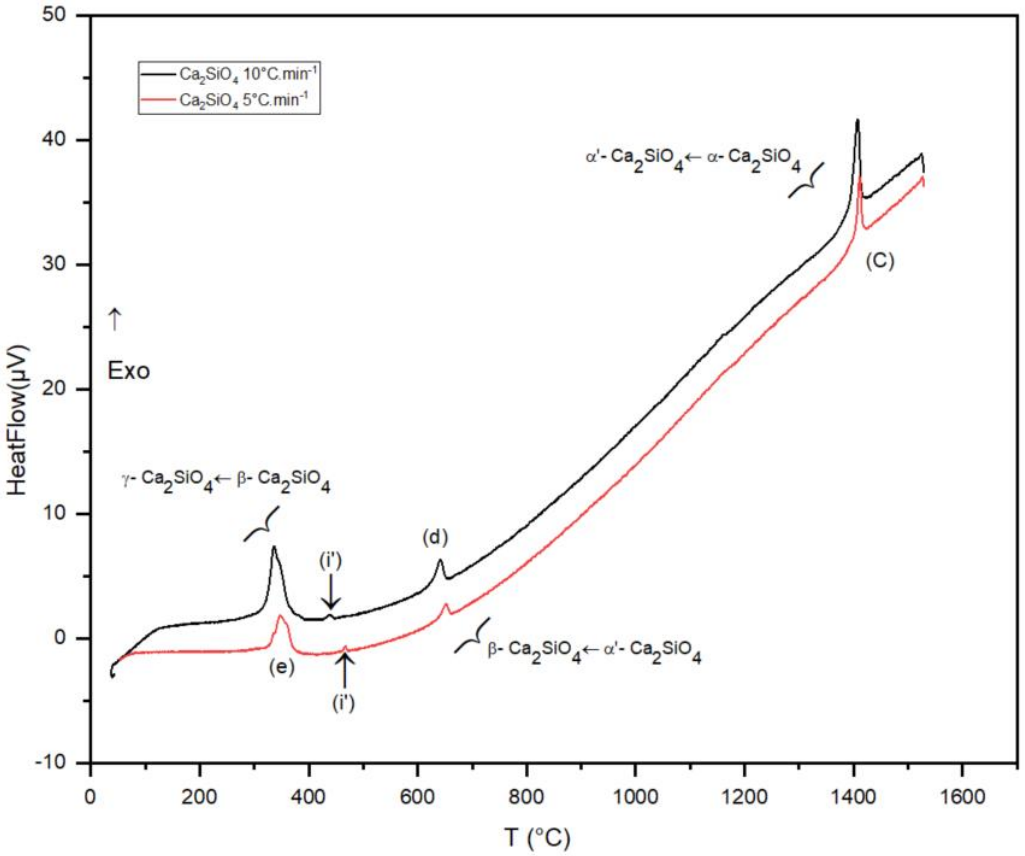

Fig. 31 : DSC Labsys^{TM} Evo signal of the Ca_2SiO_4 variety obtained after two runs at 5°C and 10°C on cooling.

In Table 8, we compared the polymorphic transformation temperatures recorded during the cooling process by Smith et *al* (1961) with our results. As the authors have done, we have also used K_2SO_4 for calibration. For the α-Ca_2SiO_4 → β- Ca_2SiO_4 inversion, we agree with the value from high-temperature X-ray powder diffraction while DTA reports a higher value. For α-Ca_2SiO_4 → α'- Ca_2SiO_4, our values are lower than those in the literature. Similar to our study, Smith et *al* (1961) identified two unexplained peaks, but we disagree on the β-α' transition point. Raw materials purity and method of analysis influence the quality of the measurements, which partly explains discrepancies in Table 8.

Transition type	Temperature (°C)	Method of investigation	Sources
α-Ca_2SiO_4 → α'-Ca_2SiO_4	1416±5	DSC	This study
	1422	DTA calibrated with K_2SO_4 (583°C) and Diopside (1392°C)	Smith et *al* (1961)
α'- Ca_2SiO_4 → β-Ca_2SiO_4	667.	DSC	This study
	694	DTA calibrated with K_2SO_4 (583°C) and Diopside (1392°C)	Smith et *al* (1961)
	670±5	High-temperature X-ray powder diffraction calibrated with K_2SO_4 (583°C) and melting point K_2SO_4 (1076°C)	Smith et *al* (1961)
β- Ca_2SiO_4 → γ-Ca_2SiO_4	373	DSC	This study
	400	DTA calibrated with K_2SO_4 (583°C) and Diopside (1392°C)	Smith et *al* (1961)

Table 8 : Transition temperature during cooling compared to those reported by Smith et *al* (1961).

2.5.4 Ca_2SiO_4 RELATIVE ENTHALPY MEASUREMENT

Assessment on Ca_2SiO_4 thermodynamic properties reveals a lack of relevant relative enthalpy dataset and inconsistencies between the experimental information and the data stored in thermodynamic databases. Thanks to Coughlin and O'Brien's (1957) important work in providing available values on β-Ca_2SiO_4→α', α-Ca_2SiO_4. In this section new experimental measurements of relative enthalpy of Ca_2SiO_4 polymorphs from γ-Ca_2SiO_4 to α',α-Ca_2SiO_4 will be discussed. Relative enthalpy

measurements were performed after calorimeter calibration with α-Al_2O_3 at Ca_2SiO_4 polymorph existence temperatures. As mentioned previously, starting polymorph for the drop measurements was the most stable form γ-Ca_2SiO_4.

2.5.5 RESULTS AND DISCUSSION

The results of the relative enthalpies measurements are summed up in Table 9. There are no heat content measurements of the γ→α' Ca_2SiO_4 transition in the literature. Coughlin & O'Brien (1957) measured the β, α'-Ca_2SiO_4 relative enthalpy by an inversed drop calorimetric technique. The temperature of transition γ→α' is situated near 847°C. Therefore, in this present work the measured values include the γ-Ca_2SiO_4 to α'- Ca_2SiO_4 in the temperature range 699.7-1482.1°C.

When the temperature is above 847°C, pellets turned into powder after cooling step at low temperature due to the dusting effect to γ-Ca_2SiO_4 on cooling. In contrast to γ-Ca_2SiO_4→α'-Ca_2SiO_4 transition, the α'→γ inversion is not a direct reaction, a metastable intermediate form β-Ca_2SiO_4 bridges α'- Ca_2SiO_4 and γ- Ca_2SiO_4. As a result, a volume expansion occurs in the material due to structural rearrangements, which leads to a pellet dusting. It indicates compound revert to a γ- Ca_2SiO_4 state.

Relative enthalpy				
T	T	H_T-H_{298K}		u(ΔH)
°C	K	J/ mol	J/mol	%
Ca_2SiO_4 (mol. wt. 172.24)				
25	298.15	-	-	-
699.7	972.86	108430.8	3617.9	3.3
798.9	1072.09	123306.7	3251.5	2.6
898.2	1171.39	148801.8	3879.2	2.6
998.5	1271.67	171305.2	4185.5	2.4
1097.9	1371.05	187889.9	4479.1	2.4
1197.9	1471.05	212360.1	6444.6	3
1399.6	1672.77	263620.1	7455.5	2.8
1451.1	1724.25	277736.3	9601.6	3.5
1482.1	1755.25	281175.5	11658.3	4.1

Table 9 : Relative enthalpies data from drop calorimetry for Ca_2SiO_4.

Measured data are plotted in Fig. 32. Our results are compared with those in the literature. Coughlin (1957) carried out thermodynamic measurements by using two distinct polymorphs as reference, namely γ- Ca_2SiO_4, the more stable form, and β- Ca_2SiO_4 containing 0.32% aluminium and iron oxide and 0.14% magnesium oxide. For α'α -Ca_2SiO_4, Coughlin (1957) data have been adjusted with γ- Ca_2SiO_4→ β- Ca_2SiO_4 enthalpy of transition from Forest (1971), in order to have the same reference state. For γ- Ca_2SiO_4→ α'- Ca_2SiO_4, there is good agreement with Coughlin (1957). Similarly, for γ- Ca_2SiO_4→ α- Ca_2SiO_4 we agree with the corrected values from assessment.

Using Coughlin (1957) data (β, α') and our experimental results (γ, α'), we calculated the average value of the γ- Ca_2SiO_4→ β- Ca_2SiO_4 transition and then deduced the β→α' transition: 1812 $J.mole^{-1}$. This result is in agreement with Coughlin (1957) finding: 1841 $J.mole^{-1}$ at 697°C. We were unable to extract usable results for γ- Ca_2SiO_4→ α'- Ca_2SiO_4 transition, but by extending data to the transition temperature (847°C), we estimated the transition enthalpy to be 4722.33 $J.mole^{-1}$, which is questionable as it is much lower than the literature value: ~14 $KJ.mole^{-1}$, (Coughlin & O'Brien, High temperature heat contents of calcium orthosilicate, 1957) and (Forest, 1971).

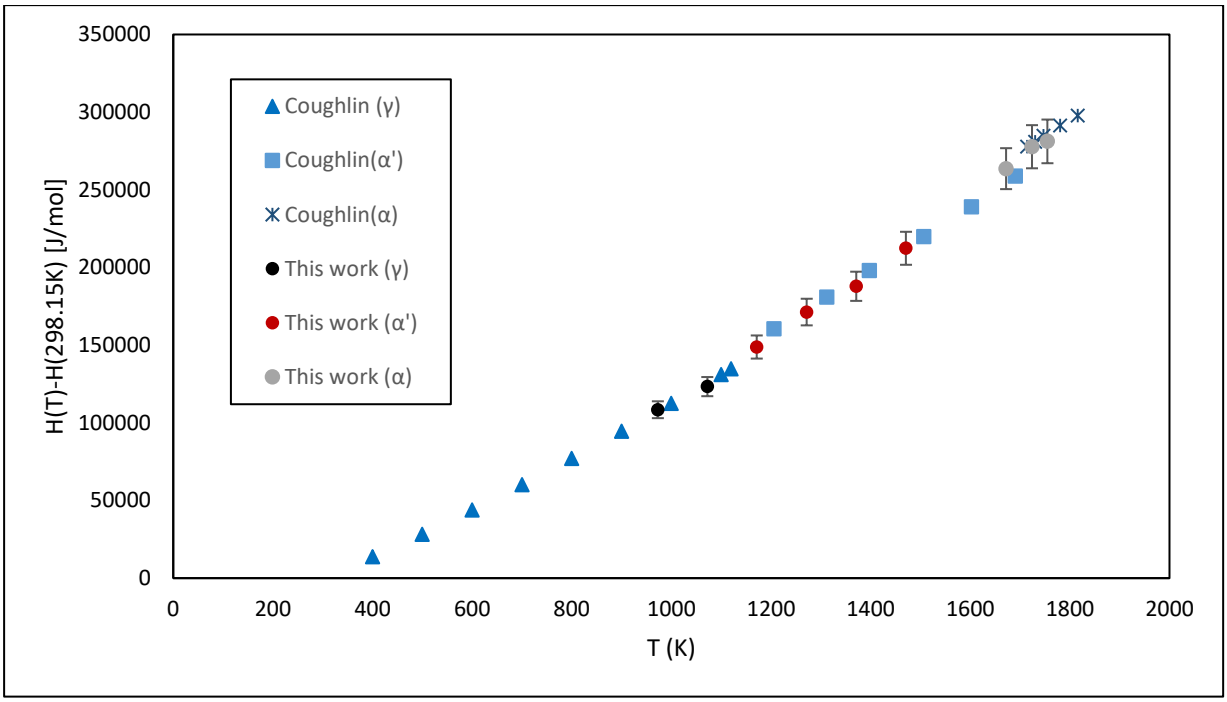

Fig. 32 : Comparison between Coughlin's experimental data and our measurements. Coughlin (1957) data for α'-Ca_2SiO_4 have been corrected with enthalpy of transition γ- Ca_2SiO_4→ β- Ca_2SiO_4 from Forest (1971) to have the same reference state.

Various polynomial models have been proposed to describe Ca_2SiO_4 relative enthalpies from room temperature to melting point. To confirm validity of the theoretical model, we have plotted Haas et *al* (1981) data, FTPs database together with our experimental results. Haas et *al* (1981) model is based on fitting Coughlin's experimental data with an estimated standard error of 274 J.mole^{-1} or about 0.14% of the absorbed value.

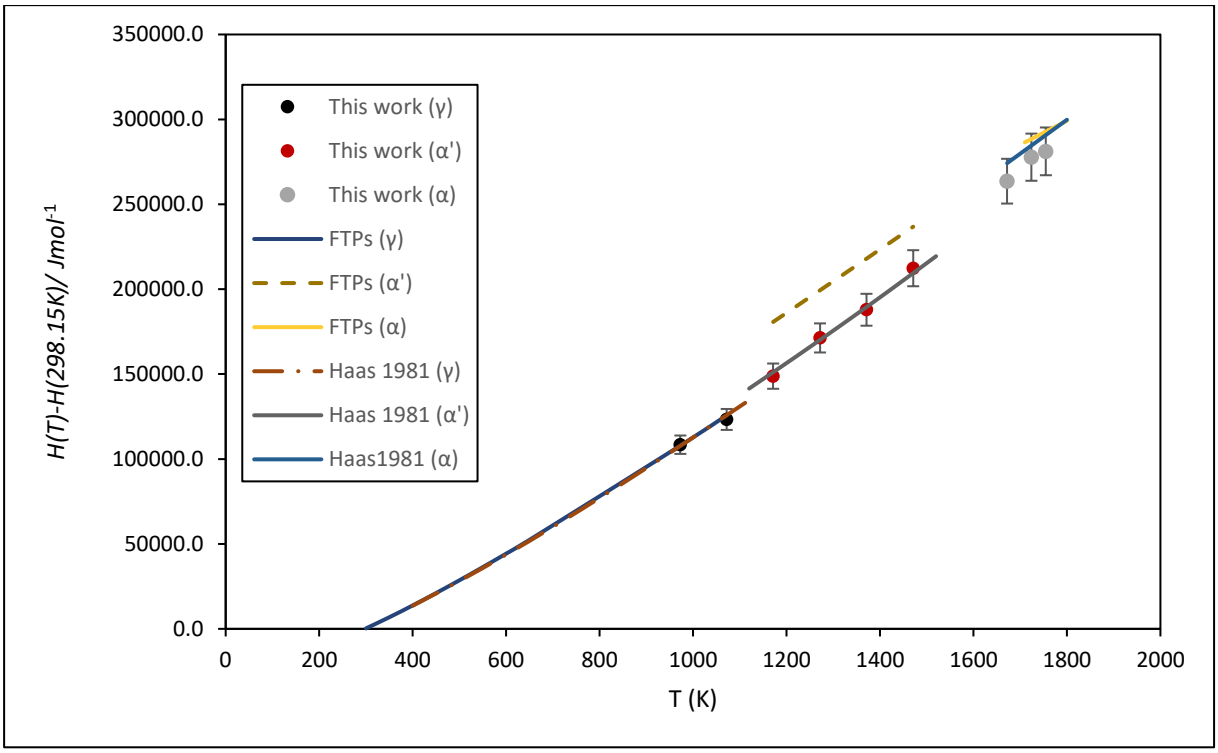

Fig. 33 : Comparison between experimental data and data from theoretical models.

Haas et *al* (1981) model and the FTPs database correctly describe the heat contents of γ-Ca_2SiO_4 in the temperature range 699.86-799.09°C and we infer models are accurate up to the inversion temperature 847°C. The experimental results thus confirm models accuracy. For α'-Ca_2SiO_4, there is an average difference of 26.4KJ.mole^{-1} between experimental values and data from FTPs. However, Haas et *al* (1981) model is in agreement with our experiment. For the polymorph α-Ca_2SiO_4, FTPS and Haas et *al* (1981) data seems to be overestimated. The α'-Ca_2SiO_4 → α-Ca_2SiO_4 transition temperature is reported in the literature to be 1423°C (Smith et al, 1961) and 1416°C in our DSC measurements. The drop measurement was performed at 1400°C, and should correspond to α'-Ca_2SiO_4. However, our value anomalously high and agrees better with α-Ca_2SiO_4. It can be suggested that at this temperature the inversion process may have started.

2.6 LITERATURE REVIEW ON $Ca_3Si_2O_7$

2.6.1 CRYSTALLOGRAPHIC STRUCTURE AND POLYMORPHISM OF $Ca_3Si_2O_7$

$Ca_3Si_2O_7$ is commonly found as a natural mineral in the form of two polymorphs: rankinite and kilchoanite. Roy (1958) first synthesized a Z phase with chemical formula 9CaO. 6SiO_2. H_2O, Kilchoanite is obtained by dihydroxylation of the hydrate without changing the symmetry. Moody first defined lattice parameters of Rankinite but did not determine crystal structure (Moody, 1952). Regarding the structure, Rankinite consists to Si_2O_7 structural units linked tetrahedra parallel to the c-axis and Ca atoms with seven nearest neighbours of oxygen. Kilchoanite is composed of isolated SiO_4 tetrahedra and isolated Si_3O_{10} triple-linked tetrahedra groups; the crystallographic structure is close to that of calcio-olivine (γ-Ca_2SiO_4). There are four types of Ca in kilchoanite; three are octahedrally coordinated while one has eight close oxygen neighbours. Rankinite is a high temperature polymorph of kilchoanite but it is not possible to obtain kilchoanite from rankinite even with slow cooling. It consists of groups of Si_2O_7 tetrahedra bonded together by Ca atoms each having sevens coordinated oxygen.

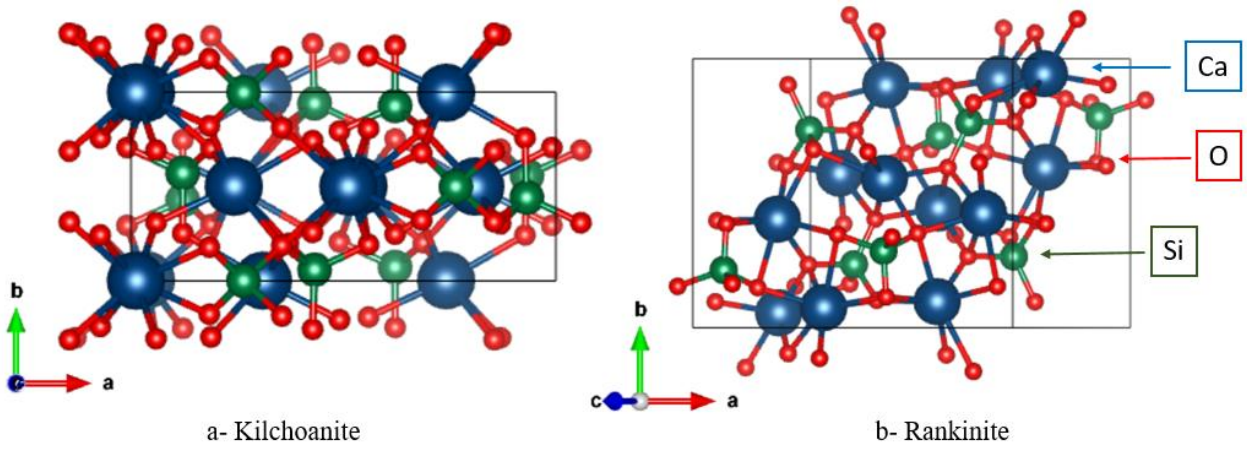

Fig. 34 : Crystallographic representation of the two polymorphs of $Ca_3Si_2O_7$.

Compound	Structure type	Symmetry & Space group	Cell content	Lattice parameter (Å)	Sources
$Ca_3Si_2O_7$	Kilchoanite	Orthorhombic I2cm	Z=8	a=11.42 b=5.09 c=21.95	Taylor (1971)

				α=β=γ=90°	
	Kilchoanite	Orthorhombic I2cm	Z=8	a= 11.4525 b= 5.0867 c=21.9963 α=β=γ=90°	Galuskin, et *al*. (2012)
	Rankinte	Monoclinic $P12_1/a1$	Z=4	a= 10.55 b= 8.88 c= 7.85 β =120.1°±0.5 α=γ=90°	Moody (1953)
				a=10.60±0.02 b=8.92±0.02 c=7.89±0.02 β =119.6°±0.1 α=γ=90°	Kusachi (1975)
				a= 10.557 b= 8.885 c= 7.858 β = 119.586 α=γ=90°	Saburi, et *al.* (1976)

Table 10 : Structural data of the polymorph of $Ca_3Si_2O_7$.

2.6.2 $Ca_3Si_2O_7$ THERMODYNAMIC DATA REVIEW

The name Rankinite was used as a tribute to G. A Rankin (1915), it is a rare and natural mineral found in fused rocks and in carbonatable clinkers. Rankinite is

formed from a mixture of silica and limestone in the ratio 2:3 and can be isolated and synthesized in the laboratory. However, there are very few published studies on the thermodynamics of rankinite; the main data known from the literature are low temperature heat capacities which were measured by King (1957), the standard enthalpy of formation by Weeks (1956) and EMF measurement by Benz and Wagner (1961) in a different temperature range. No data on relative enthalpy are known in the published papers, so it is difficult to have a precise thermodynamic description of the Gibbs energy of rankinite. Table 11 summarizes various data from the literature. This work will provide additional experimental data on rankinite.

Chemistry	Transition type	Transition temperature (°C)	Method of investigation	Sources
$Ca_3Si_2O_7$	Kilchoanite→Rankinite	954-1090	-	Hanic (1987)
		1150	DTA	Mistuda and Fukuo (1969)
Heat of formation referred to oxides component				
Chemistry	Heat of formation (KJ.mole-1)	Uncertainty (±)	Method of investigation	Sources
$Ca_3Si_2O_7$ (rankinite form)	-229.137	2.092	Solution Calorimetry with solvent composition 5%HF and 20%HCl acid at 81°C	Weeks (1953)
	-206	2	Calorimeter of dissolution in PbO-B_2O_3 at 900°C	Ayed et *al* (1993)

Table 11 : Thermodynamic data of Rankinite polymorph.

2.6.3 $Ca_3Si_2O_7$ EXPERIMENTAL STUDY

2.6.3.1Synthesis procedure and technical analysis

After showing the work on rankinite reported in the literature, this part deals with the laboratory experiments carried out to provide consistent thermodynamic data for clinker modelling. Rankinite ($Ca_3Si_2O_7$) is prepared from a dry powder mixture of $CaCO_3$ (6.25 ± 0.01g, Alpha Aesar, 99.5%) and SiO_2 (2.50 ± 0.01g, Sibelco, 99%). Again, the mixture is homogenized in a mechanical mixer for 24 hours and pelletized by hydraulic workshop press (~4.5 tons on 3g of powder). The annealing process is repeated four times at 1420°C/12h with intermediate grinding steps between each thermal treatment. The compositional analysis reveals a loss on ignition of 31.94% in agreement with calculation. The formation of rankinite is governed by the reaction of $CaSiO_3$ and Ca_2SiO_4 according to the following equation: $Ca_2SiO_4 + CaSiO_3 \rightarrow Ca_3Si_2O_7$. As in the case of Ca_2SiO_4, a mineralogical composition was carried out by X-ray diffraction (X'Pert Pro MPD, PANalytical), with CuKα radiation of λ= 1.5419 Å. Additionally, $Ca_3Si_2O_7$ Melting point was measured by differential scanning calorimetry with apparatus Labsys^{TM} Evo designed by SETERAM. We carried out calibration with NaCl and K_2SO_4 as reference sample at 5K and 10K ramp rates.

2.6.3.2$Ca_2Si_3O_7$ X-ray phase analysis

X-ray diffraction after first heat treatment reveals the secondary phases $CaSiO_3$ and Ca_2SiO_4. After grinding and a second heat treatment we found a decrease in the amount of secondary phase quoted above. Intermediate grinding and mixing at each heat treatment allowed a better homogenization of the reaction products. Finally, after 4 series of thermal annealing, the minor phases ($CaSiO_3$ and Ca_2SiO_4) have completely reacted according to the following equation: $CaSiO_3+Ca_2SiO_4 \rightarrow Ca_3Si_2O_7$. All diffraction peaks were identified at the $Ca_3Si_2O_7$ phase. The crystalline solid from the synthesis crystallizes in a monoclinic lattice; the structural parameters are gathered in Table 12.

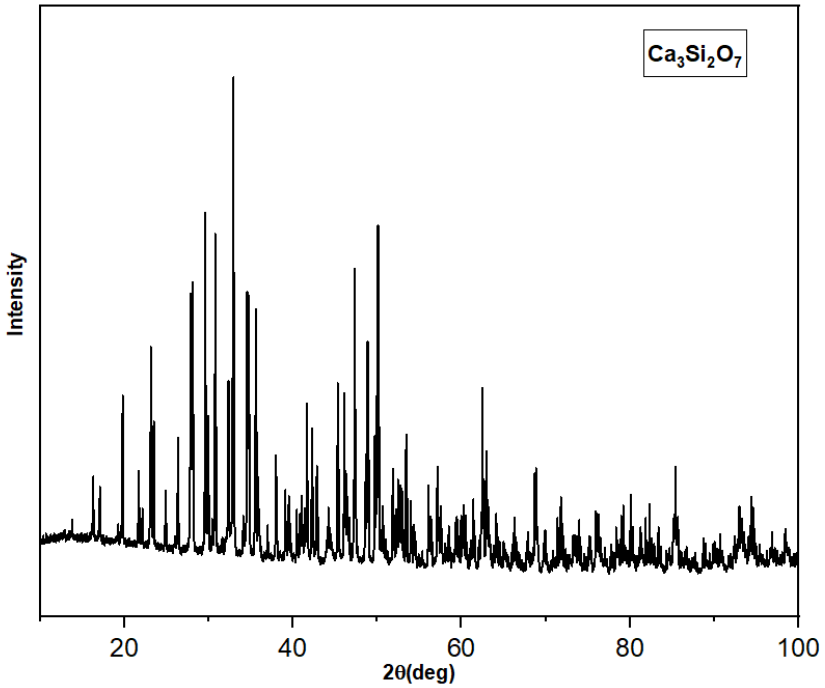

Fig. 35 *:* $Ca_3Si_2O_7$ X-ray diffraction pattern over an angular range from 10 to 120°.

Space group	P121/c1
Lattice parameter a	10.587 Å
Lattice parameter b	8.910 Å
Lattice parameter c	7.882 Å
α =Ƴ	90.000°
β	119.6°

Table 12 : $Ca_3Si_2O_7$ crystallographic data calculated from X-ray pattern.

2.6.4 DIFFERENTIAL SCANNING CALORIMETRY

The melting temperature of rankinite was determined by differential scanning calorimetry. The measurement was performed at a rate of rise of 10K per minute. The first deviation from the baseline curve is related to premelting. This effect has been observed in the past on pseudowallostonite and gehlenite and is associated with the strong dynamics of calcium atoms near the melting point. According to the studies of Richet et *al* (1994), premelting can also be an atomic rearrangement of the solid while keeping a crystalline structural order in the proximity of the real melting point. Premelting has for effect a notable increase of the heat capacities but also of the transport properties of some mineral (Bouhfid et *al*, 2002). Differential scanning

calorimetry measurements indicate that the pre-melting temperature of rankinite is at 1327°C the sample increases in temperature until complete deviation from the baseline: the beginning of melting. Then, the peak decreases until the most negative value of the DSC curve: the end of the melting. The pre-melting and melting temperatures were determined through the DSC plot in Fig. 36 of the rankinite and then corrected using the calibration equation from the standard sample K_2SO_4 and NaCl, whose measurements were made at a rate of 10K/min.

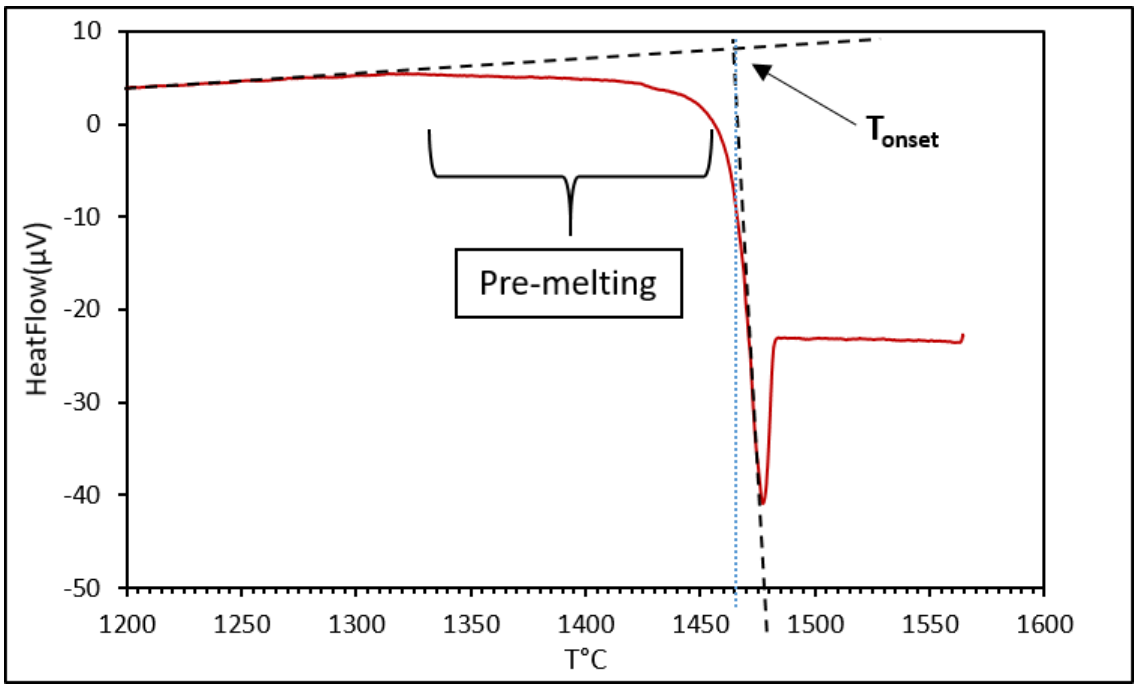

Fig. 36 : DSC Labsys^{TM} Evo signal of the $Ca_3Si_2O_7$ variety obtained after two runs at 5 and 10K/min on heating.

DSC first deviation from the baseline corresponds to the premelting temperature and occurs at 1328°C, the beginning of the melting starts at 1465°C that is in agreement with the temperature of the invariant given by Phillips and Muan (1959) is 1464°C, while the melting ends at 1480°C. In the case of the melting of an invariant, the temperature of the beginning of melting should be equal to the temperature of the end of melting, but in practice, the DSC curve has a slope, which approximates a vertical flow, the variation of this slope depends on the rate of temperature rise set by

the experimenter. In the case of measurement on the rankinite there is a difference of 15.60°C between the beginning and the end of the melting.

In order to illustrate this effect of pre-melting on the heat capacities, we have plotted in Fig. 35 rankinite ($Ca_3Si_2O_7$) relative enthalpy in the form of mean heat capacity, Cm=(HT-H298.15K) / (T-273.15). A significant increase in the mean heat capacities can be clearly observed in the area near the melting point of rankinite. Although no particular study on rankinite in the premelting zone has been carried out, it seems that this behaviour is attributed to a cationic disorder for some oxides (Richet et *al*, 1994 and Bouhfid et *al*, 2002).

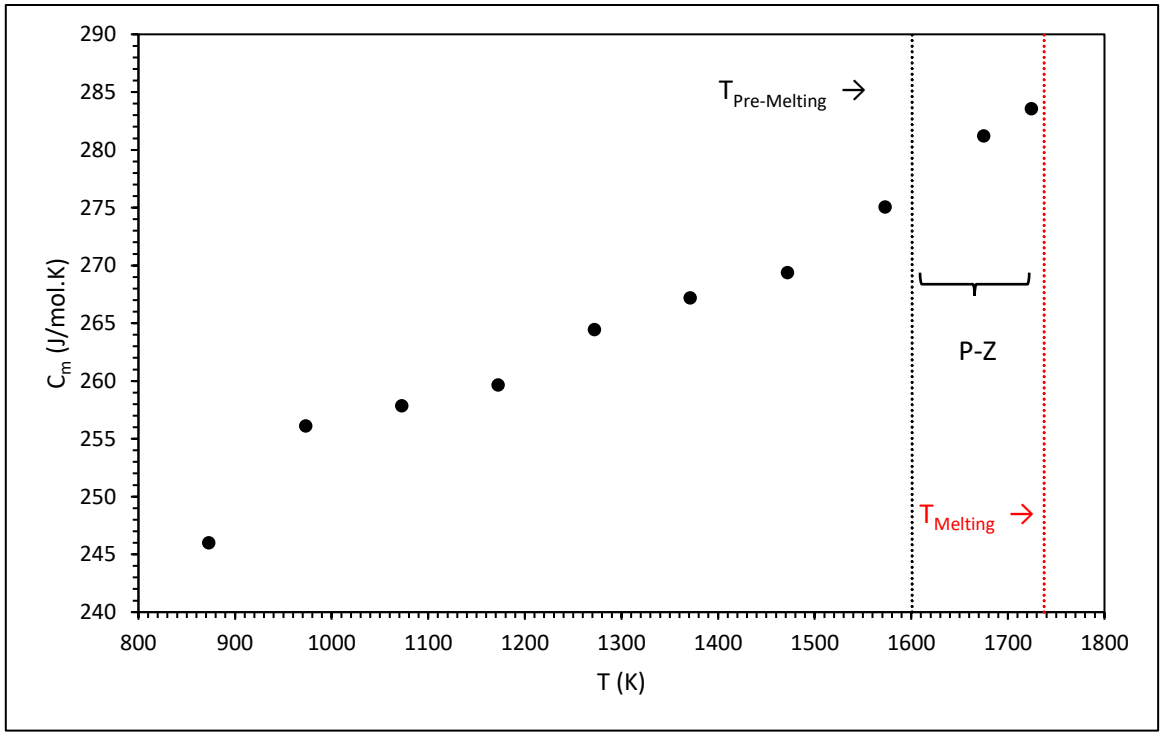

Fig. 37 : Mean heat capacity of Rankinite ($Ca_3Si_2O_7$), P-Z means premelting zone.

2.6.5 RELATIVE ENTHALPY

The results of the heat content measurements for Rankinite are summarized in Table 13. No experimental data exists in the literature on the heat capacity or heat content of Rankinite at these high temperatures.

Relative enthalpy				
T	T	H_T-H_{298K}	u(ΔH)	
°C	K	J/ mol	J/mol	%
$Ca_3Si_2O_7$ (mol. wt. 288.41)				
25	298.15	-	-	-
599.3	872.45	147433.0	3570.3	2.4
699.8	972.95	179222.4	4109.9	2.3
799.2	1072.35	206085.9	5517.3	2.7
899.0	1172.15	233439.6	6032.1	2.6
998.8	1271.95	264146.9	6983.6	2.6
1097.7	1370.85	293304.5	7690.3	2.6
1198.5	1471.65	322841.2	6913.1	2.1
1299.73	1572.88	360589.2	11760.62	3.26

Table 13 : Experimental results of heat content measurements on rankinite.

Haas et *al* (1981) suggested a thermodynamic model describing the evolution of relative enthalpy over the temperature range from room to the melting point. This model is based on Neumann Kopp's additive rule and the authors used the heat capacities measured by King (1957) for the low temperature boundary and estimated high temperature values from CaO and SiO_2 constituents summation. Haas claims that his model applied to $Ca_3Si_2O_7$ is valid over a temperature range from room temperature to 1127°C at a reference pressure of 101.325 kPa. To assess the accuracy of Haas et *al* (1981) and FTPS models with respect to the experimental results, we plotted data in the same Fig. 38.

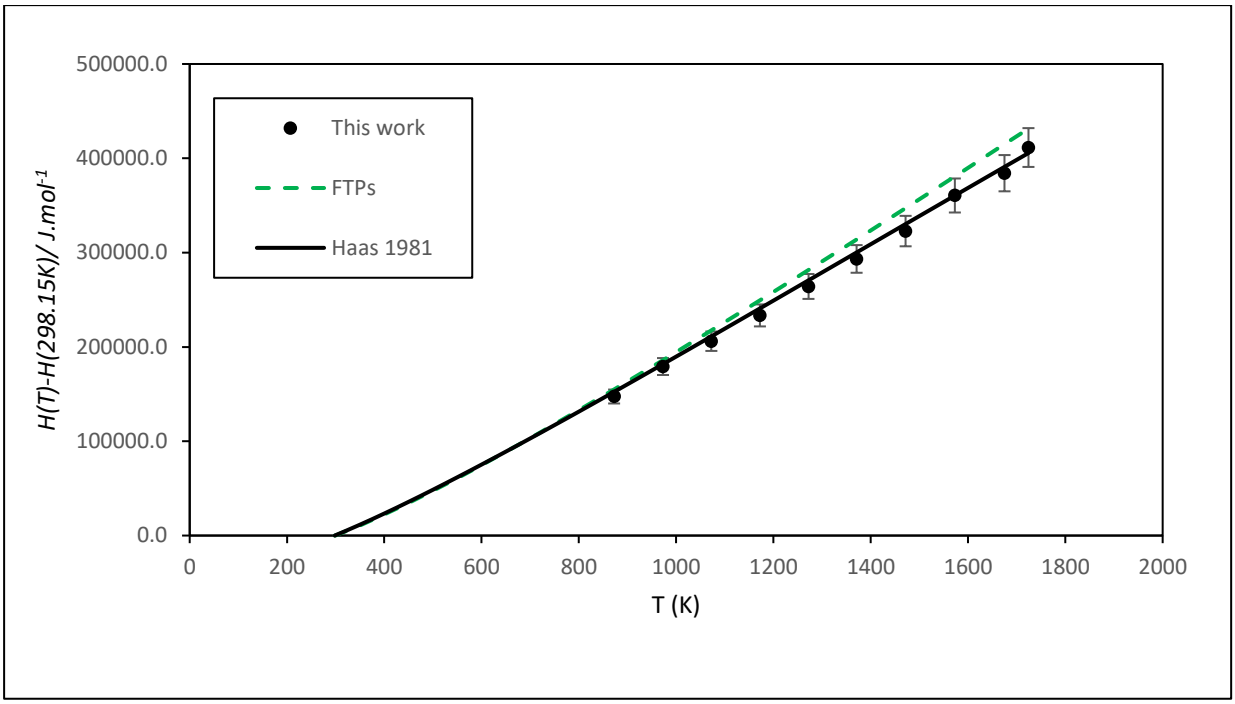

Fig. 38 : Comparison of experimental data and theoretical thermodynamic models.

It is obvious there are a significant discrepancy between the experiment values and those from the commercial FTPS database (from FactSage software). Authors clearly overestimated relative enthalpies above 799°C. However, our values confirm the validity of the Haas et al's estimated model (1981).

Experiments are an important step to not only provide real values but also to validate the models made accessible to customers. Many users rely on the data reported in the FTPS without checking its validity. Which, moreover, are not always describe accurately the thermodynamic and properties of the compounds studied.

2.6.6 ENTHALPY OF FORMATION

Although the enthalpy of dissolution of SiO_2 is not measured directly, it is possible to obtain this value indirectly. By starting from the value of $\Delta_f H$ fixed at -136KJ.mole^{-1} and the enthalpy of dissolution of Ca_2SiO_4, we calculated $\Delta_{diss}H$ of SiO_2 and then determined the corresponding value for the enthalpy of formation of $Ca_3Si_2O_7$. The heat of dissolution is described by linear variation. To calculate the standard heat of formation, we extrapolated the value to infinite dilution in the solvent using a linear regression. The obtained value is:

Q_{diss} (25°C) = 578925.8 ± 14069.0 J.mole^{-1}.

Using the dissolution data for pure CaO from chapter 1 and SiO_2 calculated indirectly, the $Ca_3Si_2O_7$ standard heat of formation is:

$\Delta_f H$(25°C) = -200211.0 ± 25679.2 J.mole^{-1}.

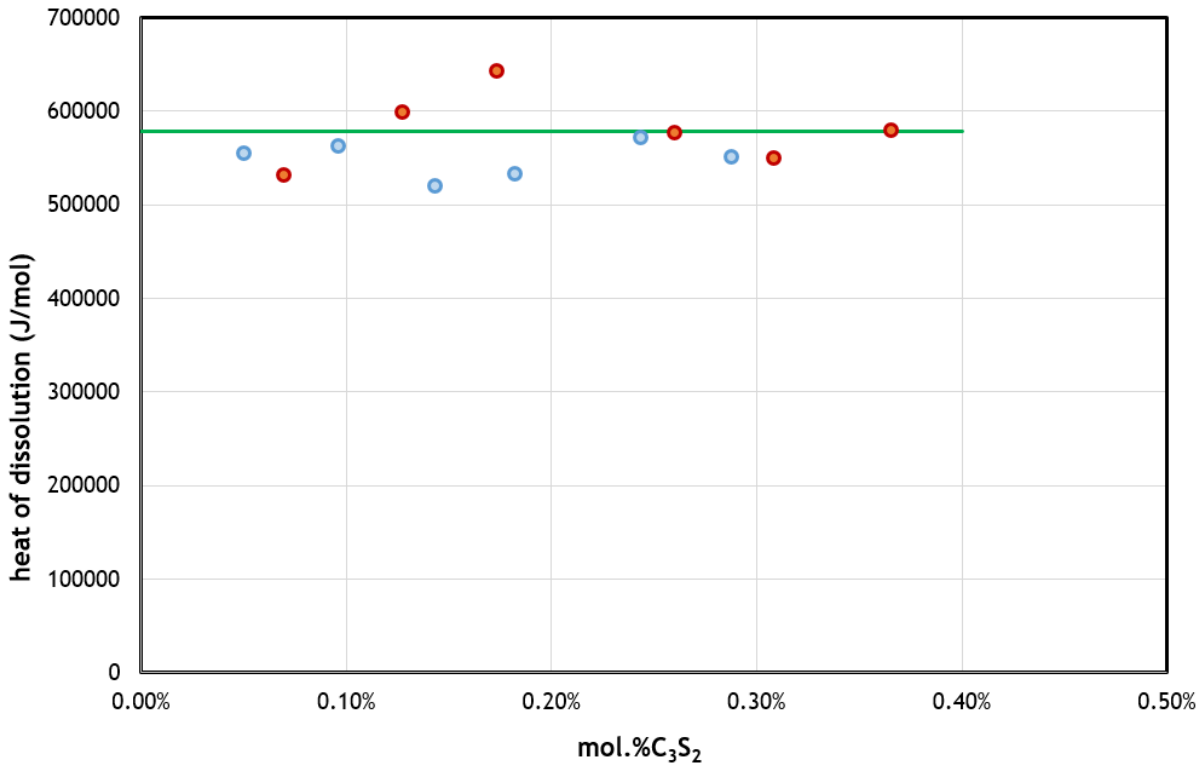

Fig. 39 : Heat of dissolution of $Ca_3Si_2O_7$.

2.6.7 EXPERIMENTAL CONTRIBUTION TO A NEW CaO-SiO$_2$ ASSESSED PHASE DIAGRAM

Rankinite and belite experiments contribution allowed us to provide new complementary data on CaO-SiO_2 section. Relative enthalpies measurements confirmed the validity of Haas (1981) model on the one hand and on the other hand highlighted discrepancies between the measurements and data from FTPS commercial database, in particular for the polymorph α'- Ca_2SiO_4, α- Ca_2SiO_4 and $Ca_3Si_2O_7$. In the framework of a collaboration with the University of Aberdeen, an assessed phase diagram based on a new automatic fitting approach was computed with our new experimental values (Abdul, Mawalala, Pisch, & Bannerman, 2022). The new modelling of the CaO-SiO_2 phase diagram is based on the 3rd generation

CALPHAD approach. Rankinte and belite polymorph (γ- Ca_2SiO_4 and α'- Ca_2SiO_4) low temperature heat capacities from assessment were combined with relative enthalpies measured at high temperature, in order to describe solid thermodynamic proprieties from 0K to melting point for both solid compound. The results of the model obtained locally for the phases we studied reproduce correctly the experimental data. Fig. 40 is the phase diagram obtained and evaluated by including the new thermodynamic data (Abdul, Mawalala, Pisch, & Bannerman, 2022).

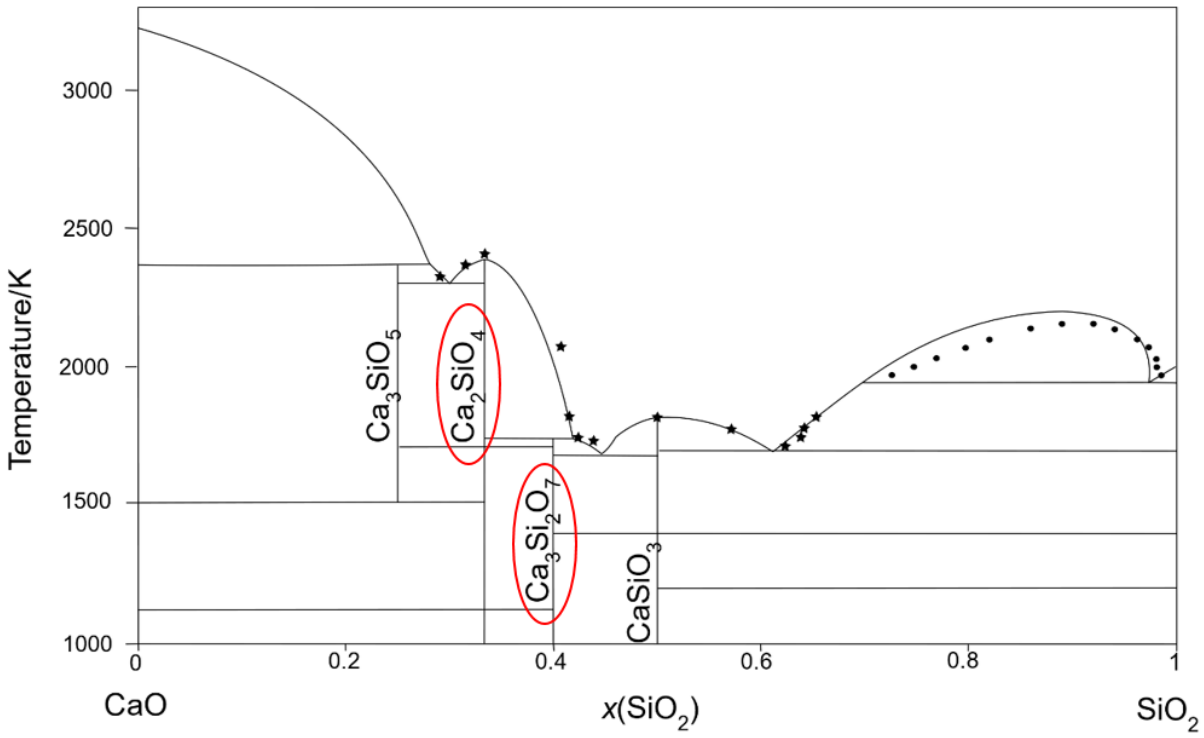

Fig. 40 : New phase diagram assessed including experimental data obtained in this chapter (Abdul, Mawalala, Pisch, & Bannerman, 2022).

We plotted in Fig. 41 experimental results and fits to these data as they were used in the collaborative project. This work has led to the writing of a collaborative paper with the University of Aberdeen (Abdul, Mawalala, Pisch, & Bannerman, 2022).

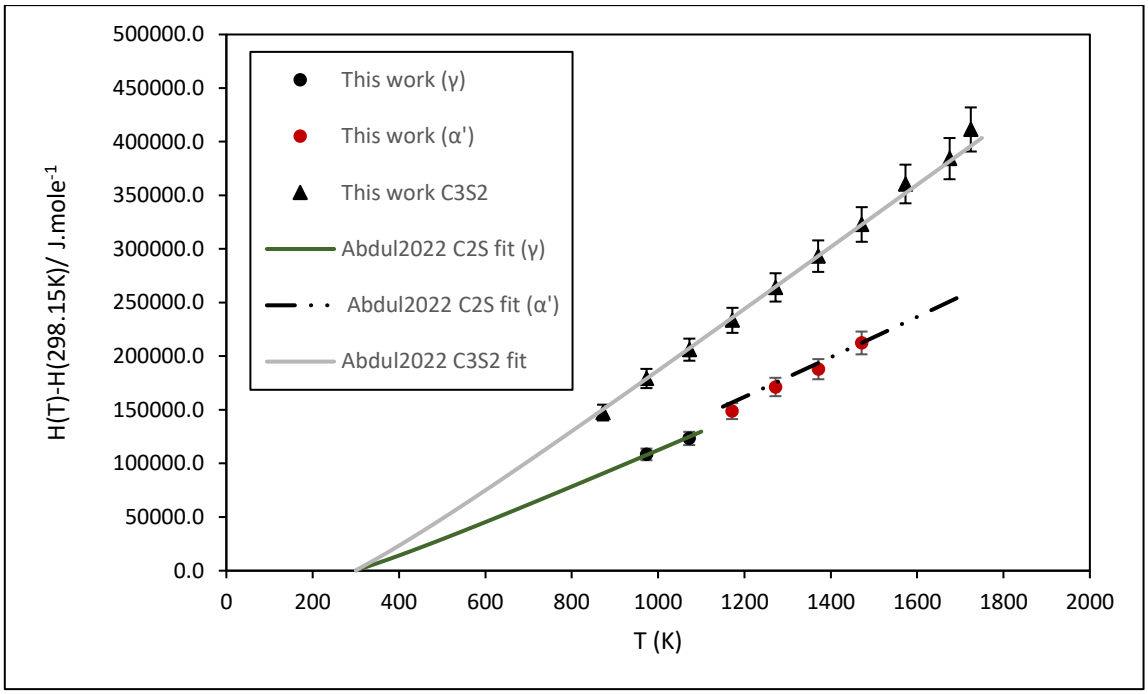

Fig. 41 : Experimental relative enthalpy of $Ca_3Si_2O_7$ and γ,α'-Ca_2SiO_4 and fitting at high temperature.

2.7 CONCLUSION

Understanding the thermodynamic processes that govern thermal properties of Rankinite and Belite is important in Portland cement clinkers. This chapter highlighted a lack of available data for $Ca_3Si_2O_7$ and the Ca_2SiO_4 polymorphs. Rankinite and belite were synthesized by the solid-solid method, the pure phases were identified by X-rays and the relative enthalpies of γ- Ca_2SiO_4→*α'*- Ca_2SiO_4, γ- Ca_2SiO_4→*α*- Ca_2SiO_4 and $Ca_3Si_2O_7$ were measured by drop calorimetry. Regarding the temperature transition, for γ, β, *α', α*- Ca_2SiO_4, inversion was identified in the temperature range in agreement with the value reported in the literature but some discrepancies are reported. Our study of Rankinite has provided new relative enthalpy values never before measured; the peritectic melting point obtained experimentally also corresponds to that quoted in the literature. Additionally, a premelting effect on $Ca_3Si_2O_7$ could be an interesting prospect for further investigation. This work contributed to the re-assessment of the CaO-SiO_2 phase diagram through collaborative work with the University of Aberdeen.

3 CHAPTER 3: THE FERRITE PHASE.

3.1 INTRODUCTION

Brownmillerite, also known as C4AF in cement chemistry nomenclature, is one of the four constituents commonly found in Portland cement. It is known since 1897 through the work of Tornebohm who originally named it celite. An interesting feature of Brownmillerite is its ability to resist sulfates, which is an important property for heavy construction in water contact areas. There are also much wider applications, notably as electrodes for solid oxygen fuel cells, catalysts for hydrogen production or as gas sensors. In this chapter, the available experimental information on the structure and the thermodynamic properties will be reviewed. In addition, new experimental thermodynamic properties were measured to better describe the Gibbs energy of brownmillerite. The main thermodynamic properties studied are heat contents and the standard heat of formation as a function of composition together with the melting points. This chapter consists of a first part reviewing the existing studies on brownmillerite and a second experimental part complementing work already published.

3.2 FERRITE (C4AF) IN THE SYSTEM CaO-Al_2O_3-Fe_2O_3

The ternary phase with the highest concentration of calcium occurring in the CaO-Al_2O_3-Fe_2O_3 system is brownmillerite. This compound is commonly encountered in Ordinary Portland and high alumina cements. Various studies based on methods such as X-ray and neutron diffraction, chemical and thermal analysis highlighted that this compound is in fact a solid solution $Ca_2Fe_{2-x}Al_xO_5$ is present ranging from $Ca_2Fe_2O_5$ to $Ca_2Al_2O_5$. Under normal atmospheric pressure conditions and in absence of other additional oxide compounds such as CaO, Al_2O_3 and Fe_2O_3, the solid solution $Ca_2Fe_{2-x}Al_xO_5$ exists in the composition range x=0 to x=1.4 (Taylor H. W., 1971). Brownmillerite is obtained when x=1 but $Ca_2Al_2O_5$ (x=2) end member composition can only be synthesized at 2.5 GPa pressure (Aggarwal et *al,* 1972).

Newkirk and Thwaite (2002) studied the ternary CaO-Al_2O_3-Fe_2O_3 phase diagrams in the composition range important to cement chemistry Fig. 42. Tie lines were determined by microscopy, X-rays diffraction and differential thermal analysis. At point E1, CaO, $Ca_3Al_2O_6$ and the ferrite phase are in equilibrium at 1389°C. An Eutectic equilibrium E2 between $Ca_3Al_2O_6$, $Ca_{12}Al_{14}O_{33}$ and ferrite occurs at 1336°C while the $Ca_{12}Al_{14}O_{33}$-$CaAl_2O_4$-ferrite invariant is present at 1335°C (Newkirk & Thwaite, 1958)

and melting point of Ca_2FeAlO_5 is reported to be 1415±5 °C (Lea (1935) and Hansen et *al* (1928)).

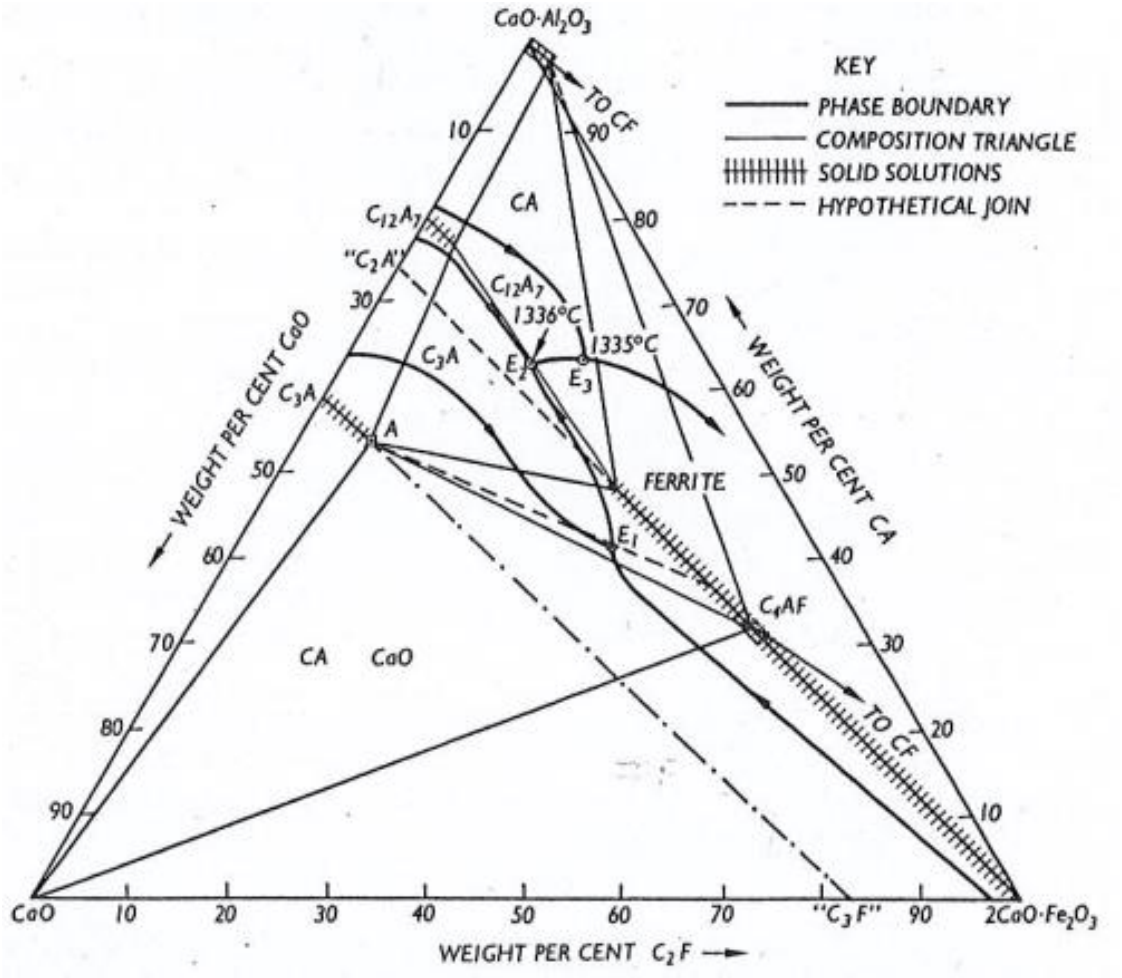

Fig. 42: System CaO-$CaO.Al_2O_3$-$2CaO.Fe_2O_3$, pseudo-ternary (Newkirk & Thwaite, 1958).

3.3 $CA_2FE_{2-x}AL_xO_5$ SOLID SOLUTIONS: CRYSTAL STRUCTURE AND COMPOSITION

Since Hansen et *al's* work (1928), later corroborated by the investigation of Solacolu (1932), it is now known that in dicalcium ferrite ($Ca_2Fe_2O_5$) part of Fe^{3+} can be substituted by Al^{3+} whose solid solution formula is written as $Ca_2Fe_{2-x}Al_xO_5$. Brownmillerite consists of sheets of corner-sharing $(Fe,Al)O_6$ octahedron connected to a single chain of $(Al,Fe)O_4$ tetrahedron parallel to *c* axis, calcium (Ca^{2+}) is located in the interstitial site between alternating layer of octahedral sheet and single tetrahedral chain (Colville & Geller, 1971). Al^{3+} and Fe^{3+} are randomly located on both potential sites.

Pure $Ca_2Fe_2O_5$ belongs to the Pcmn space group but the $Ca_2Fe_{2-x}Al_xO_5$ solid solution is not isostructural throughout its full composition range (Smith, Crystallographic Changes with the Substitution of Aluminum for Iron in Dicalcium Ferrite, 1962). Indeed, the insertion of Al^{3+} ions leads to a first order phase transition from Pcmn to Ibm2. The first observations indicated a structure change from primitive to body centred at x=0.66. It was shown through X-ray diffraction studies that the transition is located within 0.4<x<0.6 [references]. Study of evolution of lattice parameters as a function of Al composition led Fukuda and Ando (2002) located the transition value at x=0.47 while Redhammer et *al* (2004) reported x=0.56. Discrepancies between the transition values are mainly related to the method of synthesis and material purity employed.

Numerous studies reported the change in the lattice parameters with increasing Al^{3+} content. We have calculated the volume of the crystal along the $Ca_2Fe_{2-x}Al_xO_5$ solid solution from the various data collected in the literature. The crystal volume variation of the solid solution as a function of the amount of Al^{3+} is plotted in Fig. 43.

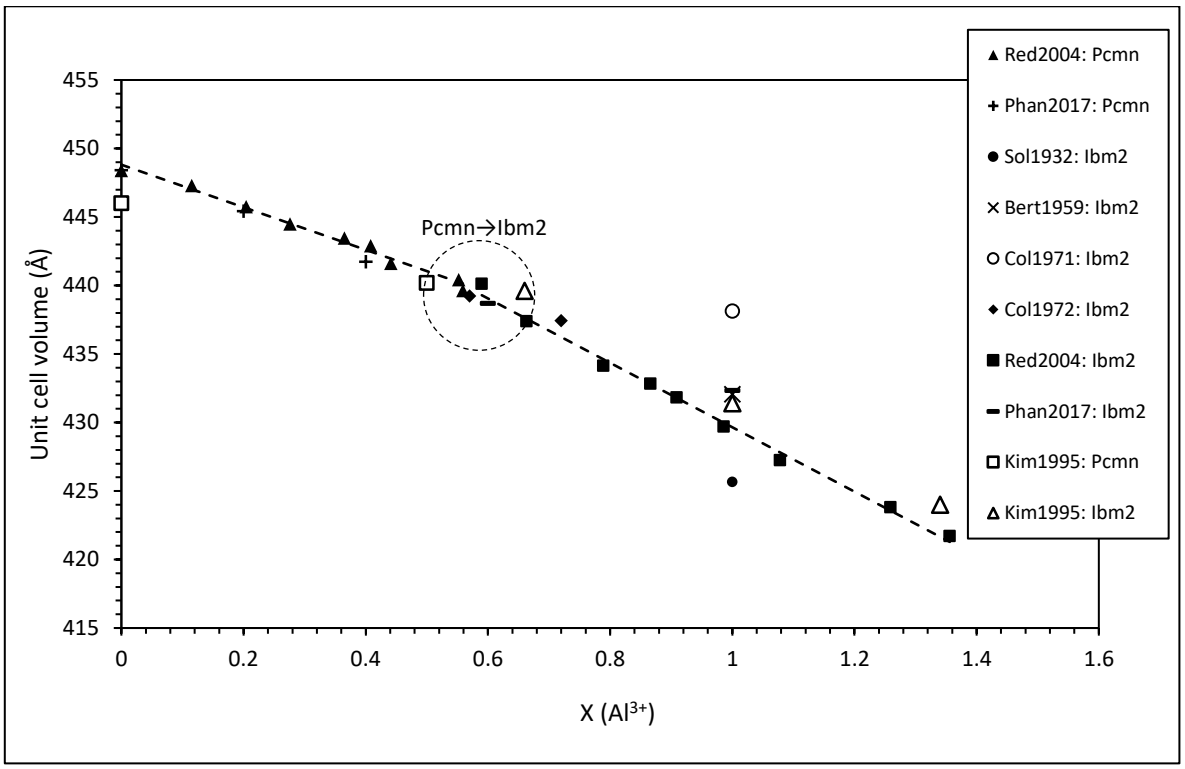

Fig. 43 : Unit cell volume variations in the solid solution $Ca_2Fe_{2-x}Al_xO_5$ at 25°C.

Substitution of Fe^{3+} ions by Al^{3+} induces a decrease of the lattice parameters and therefore the volume of the crystal. Aluminium atoms are smaller (50pm) than iron atoms (64pm) and take up less cell space. Evolution of the volume as a function of the Al^{3+} ions composition Fig. 40 is characterized by a slope shift between $0 \leq x \leq 0.6$ Redhammer et *al* (2004) corresponding to the Pcmn→Ibm2 transition zone. In addition, Al^{3+} insertion in crystal cell affects the mean metal-oxygen bond length (Redhammer et *al*, 2004). For the structural parameters, we have gathered data from two main compositions (x= 0 and x=1) in Table 14. This shows that, the lattice parameter values from the various studies are in the same order of magnitude.

Chemistry	Structure type	Symmetry & Space group	Cell content	Lattice parameter (Å)	Sources
$Ca_2Fe_2O_5$	Perovskite	Pseudo-quadratic Pcmn	Z=4	a=5.64 b=14.68 c=5.39 α=β=γ=90°	Bertaut, Blum, & Sagnières, (1959)
				=5.596 b=14.76 c=5.427 α=β=γ=90°	Redhammer et *al* (2004)
Ca_2FeAlO_5	Perovskite	Orthorhombic Ibm2	Z=2	a=5.58 b=14.50 c=5.34 α=β=γ=90°	Bertaut et *al*, (1959)
			Z=4	a=5.584 b=14.60 c=5.374 α=β=γ=90°	Colville and Geller (1971)
				a=5.52 b=14.44 c=5.34 α=β=γ=90°	Solacolu (1932)

Table 14 : Crystallographic data of $Ca_2Fe_{2-x}Al_xO_5$ solid solution as a function of composition from various sources for two selected compositions.

3.4 MAGNETIC TRANSITION OVERVIEW

At room temperature, the $Ca_2Fe_{2-x}Al_xO_5$ solid solution is antiferromagnetically ordered when the amount of Al ions is between 0 and 1 (Phan et *al*., 2018). Some studies based on Mossbauer spectra established the Neel temperature of pure $Ca_2Fe_2O_5$ and Ca_2FeAlO_5. According to the work of Kim et *al* (1995) the magnetic transition of Ca_2FeAlO_5 occurs at 60±15°C while Grant et al reported 77°C. For $Ca_2Fe_2O_5$ the Neel temperature is reported to be 445°C by Redhammer et *al* (2004) and 452°C (Zhou and Goodenough, 2005).

3.5 FERRITE HEAT OF FORMATION

The standard enthalpy of formation ($\Delta H°_f$) of brownmillerite reported in the literature was mainly measured by calorimetric methods. One of the first published data on ferrite dates from 1956. In their study, the authors, Newman and Hoffman (1956) reported $Ca_6Al_4Fe_2O_{15}$ and $Ca_2Fe_2O_5$ $\Delta H°_f$ at 25°C. In order to investigate the $\Delta H°_f$, Koehler et *al* (1961) established a Hess cycle from the dissolution reactions of $Ca_2Fe_2O_5$ in hydrochloric acid. Furthermore, Prasanna and Navrotsky (1994) calculated $\Delta H°_f$ of $Ca_2Fe_2O_3$ referred to the oxides based on the enthalpies in solution of CaO, Fe_2O_3 and $CaFeO_{2.5}$ and derived the value referred to the elements at 25°C. Regarding Ca_2FeAlO_5, standard enthalpy of formation of this composition has been measured by Ayed et *al* (1993). The only existing data on this component is the energy of formation calculated from the elements normalized per atom in the unit cell. We have gathered in Table 15 the measured values from the constituent oxides and Table 16 calculated data from Materials Project, FactSage database, additionally we added Koehler et *al* (1961) and Prasanna and Navrotsky (1994) results. Although this chapter is particularly focused on the study of Ca_2FeAlO_5, it is important to highlight the work that has been done on the other ferrites coexisting around C4AF according to the ternary phase diagram.

Chemistry	$\Delta H°_f$(kJ/mole)	Uncertainty (±)	Method of investigation	Sources
$Ca_2Fe_2O_5$	-31.13	0.42	Isothermal-jacket calorimeter: heat of solution in HCl, 26.61 H_2O (2.00 N at 25±0.8°C), 1g dissolved in 600g of solvent. Heat of dilution of aqueous $CaCl_2$, $AlCl_3$ and $FeCl_3$ in the same acid.	Newman and Hoffman (1956)
	-44.18	3.01	Hydrochloric acid calorimetry at 30.00°C, 4.0779g of dicalcium ferrite with 1.936.2g of 4.360 molal hydrochloric acid.	Koehler et *al* (1961)
	-45.00[a]	3.80	High temperature Calvet twin Calorimeter at 800°C with $2PbO.B_2O_3$ as solvent (20 mg in 30g of glass-solvent under Ar flow)	Prasanna and Navrotsky (1994)
Ca_2FeAlO_5	-47	2	Dissolution calorimetry in High Temperature Calvet Calorimeter, wih $2PbO\text{-}B_2O_3$ at 1173K	Ayed et *al* (1993)
$Ca_6Al_4Fe_2O_{15}$	-76.53	2.51	Isothermal-jacket calorimeter: heat of solution in HCl, 26.61 H_2O (2.00 N at 25±0.8°C), 1g dissolved in 600g of solvent. Heat of dilution of aqueous $CaCl_2$, $AlCl_3$ and $FeCl_3$ in the same acid.	Newman and Hoffman (1956)

Table 15: Standard enthalpy of formation referred to the oxides component, experimental data. [a] This value corresponds to the enthalpy of formation at 800°C.

Chemistry	$\Delta H°_f$(KJ/mole)	Uncertainty (±)	Method of investigation	Sources
$Ca_2Fe_2O_5$	-2139.80	4.40	Same method as in Table 2.	Prasanna & Navrotsky, (1994)
	-2139.03	2.80	Same method as in Table 2.	Koehler et *al* (1961)
	-2131.14	-	Calculated values	FactSage database
	-2443.38	-		

$Ca_6Al_4Fe_2O_{15}$	-7375.02	-	Calculated values	Materials Project database
Ca_2FeAlO_5	-2575.57	-		

Table 16: Standard enthalpy of formation referred to the elements, calculated data from Materials Project database online and FactSage software.

The enthalpy of formation referred to the elements reported by Prasanna and Navrotsky (1994) were derived without heat content correction since $Ca_2Fe_2O_5$ heat capacities are not available. If we assume that formation reaction between 800°C and 25°C takes place with a $\Delta Cp(T,P)\sim 0$, $\Delta H°_f$ from elements can be calculated but in a less accurate way. Although this last result is in agreement with Koehler et *al* (1961), we can wonder about $\Delta H°_f$ referred to oxide used by the latter. According to Koehler et *al*, -44.18 KJ.mole^{-1} corresponds to the standard enthalpy of formation at 25°C. This value is more exothermic than Newman and Hoffman (1956): -31.13 KJ.mole^{-1}, but closer to that reported by Prasanna and Navrotsky (1994) at 800°C: $\Delta H°_f$ (800°C, oxides) =-45.00 KJ.mole^{-1}. Regarding the values stored in the thermodynamic databases, FactSage gave a $\Delta H°_f$ close to the published values while Materials Project calculated a more exothermic $\Delta H°_f$.

3.6 EXPERIMENTAL STUDIES

To investigate thermodynamic properties, we synthesized brownmillerite with varying alumina content by solid-state reaction. In this section, the experimental study of $Ca_2Fe_{2-x}Al_xO_5$ is discussed. Raw materials are $CaCO_3$, Fe_2O_3, and Al_2O_3, which were dried in a muffle furnace at 500°C under air for 24h. Four distinct compositions were defined (x=0, 0.5, 1 and 1.4) and the raw mix powders in appropriate amounts were mixed for 20 minutes. A first heat treatment of 1000°C was applied to calcine the $CaCO_3$. The synthesis was carried out under argon (30L/h, 200K/h) at 1200°C. Starting composition and sintering times are listed in Table 17. X-ray sdiffraction confirmed each phase with defined compositions by comparison of the measured lattice parameters with the published data (Table 17).

Chemistry	x=0	x=0.5	x=1.4	x=1	Supplier
$CaCO_3$	5.8937	6.2244	6.9231	4.9453	Alfa Aesar
Al_2O_3	0.0000	0.7924	2.4672	1.2589	Alfa Aesar
Fe_2O_3	4.6995	3.7223	1.6562	1.9714	WVR
Synthesis time (hours)	24	12	48	56	

Table 17: Composition table for $Ca_2Fe_{2-x}Al_xO_5$ synthesis.

Synthesis monitoring was done by X-ray diffraction after 12 hours of processing. Multiphase compounds are ground again and annealed until the pure intended phase is achieved. Fig. 44 illustrates each synthesis step including mechanical mixing (1), pellet de-carbonization (2) and heat treatment.

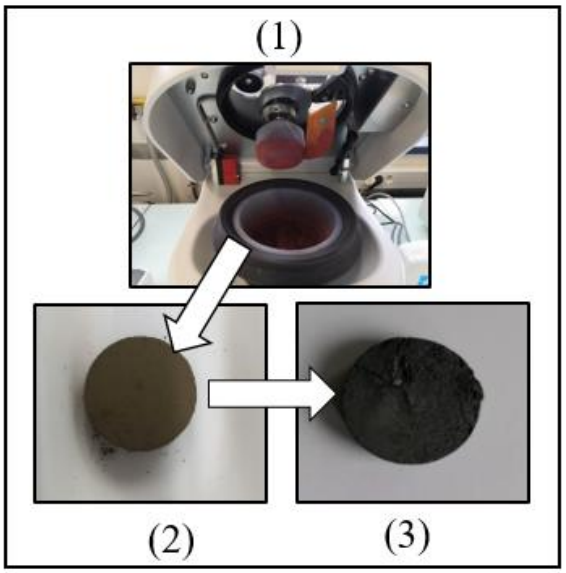

Fig. 44 : Synthesis step followed for each composition.

3.7 RELATIVE ENTHALPIES MEASUREMENT

Relative enthalpy values of the solid solution were measured for two distinct compositions by drop calorimeter MHTC96 (Type S thermophile, 1300°C max). Ca_2FeAlO_5 and the more alumina-rich compound $Ca_2Fe_{0.6}Al_{1.4}O_5$ were studied. Powders of identical composition to the samples studied were put at the bottom of the

crucible at a height of 15 mm in order to improve the sensitivity of the measurement and to soften dropped samples.

3.8 Ca_2FeAlO_5 MEASUREMENT RESULTS

For Ca_2FeAlO_5 the relative enthalpy was measured from 590 to 1096°C starting from room temperature as the starting point. Ca_2FeAlO_5 reaction of formation used to calculate relative enthalpies in FactSage software is given by equation [11]. The data from FTOxid are based on estimation using the Neumann- Kopp rule and the pure components. Table 18 reports raw experimental results obtained on the investigated compound. The measurements are carried out on six pellets for each temperature and the uncertainty on the results is less than 4%. In the case of Ca_2FeAlO_5 the initial uncorrected temperatures ranged from 22.5 to 25.9°C.

$$\frac{1}{2}Ca_2Fe_2O_5 + \frac{1}{2}Ca_2Al_2O_5 \rightarrow Ca_2FeAlO_5 \quad [11]$$

Heat Contents					
T(°C)		T (K)		H_T-H_{298K}	u(ΔH)
Initial	Final		J.mol^{-1}	J.mol^{-1}	%
Ca_2FeAlO_5 (mol. wt. 243)					
22.52	590.15	863.30	118119.42	4560.51	3.85
24.57	689.39	962.54	141167.68	4723.04	3.35
25.11	793.90	1067.05	163214.35	4723.32	2.88
25.63	894.45	1167.60	186393.16	4349.50	2.31
25.56	984.95	1258.10	200484.90	7525.71	3.75
25.90	1096.07	1369.22	227991.51	8603.93	3.72

Table 18: Relative enthalpies measured in function of temperature from 584.87°C to 1092.59°C.

Using the FTOxid database, we calculated the relative enthalpies on FactSage by setting the same temperature range as the ones measured. In Fig. 45, we plotted our results alongside those obtained using the Gibbs energy data included in the FTOxid database. The main discrepancy between both data sets is at high temperature, where the data points at 1096°C and 985°C are respectively

13.6KJ.mole^{-1} and 14.5KJ.mole^{-1} higher than the experimental results. Below these temperatures, FTOxid data are in agreement with the measured values.

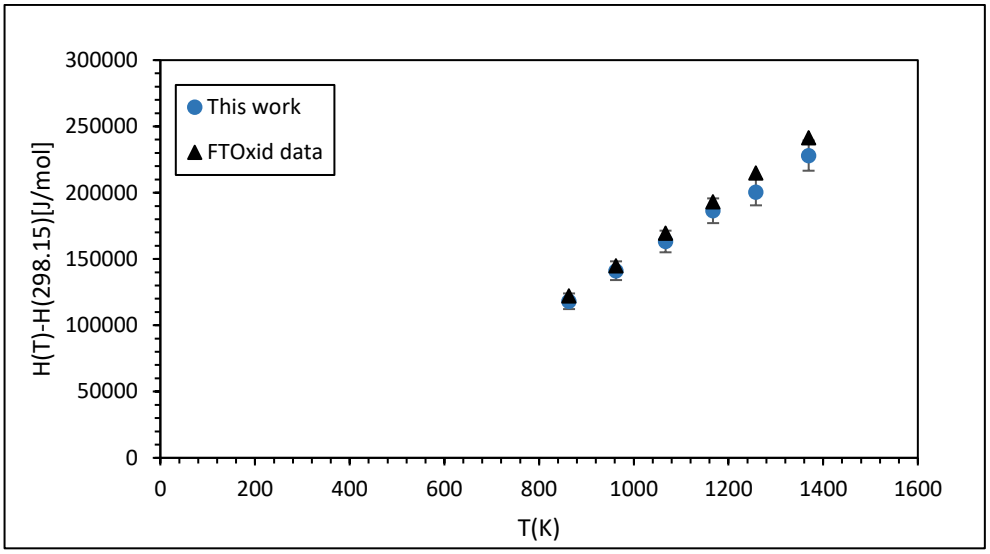

Fig. 45 : Ca_2FeAlO_5.relative enthalpy plotted with FTOxid data from FactSage Software.

3.9 $CA_2FE_{0.6}AL_{1.4}O_5$ MEASUREMENT RESULTS

A similar methodology was adopted as for the previous sample (Ca_2FeAlO_5). $Ca_2Fe_{0.6}Al_{1.4}O_5$, solid solution composition was measured from 584.87 to 1092.59°C, sample distributor temperature ranged from 24.4 to 27.78°C and peak error on the data was 5.04%. Results are reported in Table 19. Equation [12] was applied on FactSage to calculate the relative enthalpies for each implemented temperature and plotted with measured data in the Fig. 46.

$$\frac{3}{10}Ca_2Fe_2O_5 + \frac{7}{10}Ca_2Al_2O_5 \rightarrow Ca_2Fe_{0.6}Al_{1.4}O_5 \text{ [12]}$$

Relative enthalpy					
T (°C)		T (K)		H_T-H_{298K}	u(ΔH)
Initial	Final		J.mol^{-1}	J.mol^{-1}	%
$Ca_2Fe_{0.6}Al_{1.4}O_5$ (mol. wt. 231.4)					
24.40	584.87	858.02	110671.65	4342.96	3.92
25.00	692.79	965.94	129570.64	5027.50	3.88
25.05	793.90	1067.05	148575.79	6497.78	4.37
26.08	889.20	1162.35	174302.28	7557.37	4.34
27.00	984.95	1258.10	196654.49	8855.11	4.50
27.78	1092.59	1365.74	225405.01	11354.71	5.04

Table 19 : $Ca_2Fe_{0.6}Al_{1.4}O_5$ relative enthalpy plotted with FTOxid data from FactSage Software.

Lack of experimental data in the literature is a constraint to the establishment of relevant and predictive models of the thermodynamic properties of $Ca_2Fe_{2-x}Al_xO_5$ solid solution as a function of aluminium composition and temperature. In fact, comparison of both datasets, experiment and theoretical, reveals that FTOxid overestimated the relative enthalpies of $Ca_2Fe_{0.6}Al_{1.4}O_5$; the closest point to the experimental one is 584.9°C. Analysis of laboratories data of both compositions $Ca_2Fe_{0.6}Al_{1.4}O_5$ and Ca_2FeAlO_5 highlights that increasing Al ions in the solid solution leads to a lowering in relative enthalpy with respect to the modelled data in the FTOxid database in Factsage. A better description in the database would therefore need a remodelling.

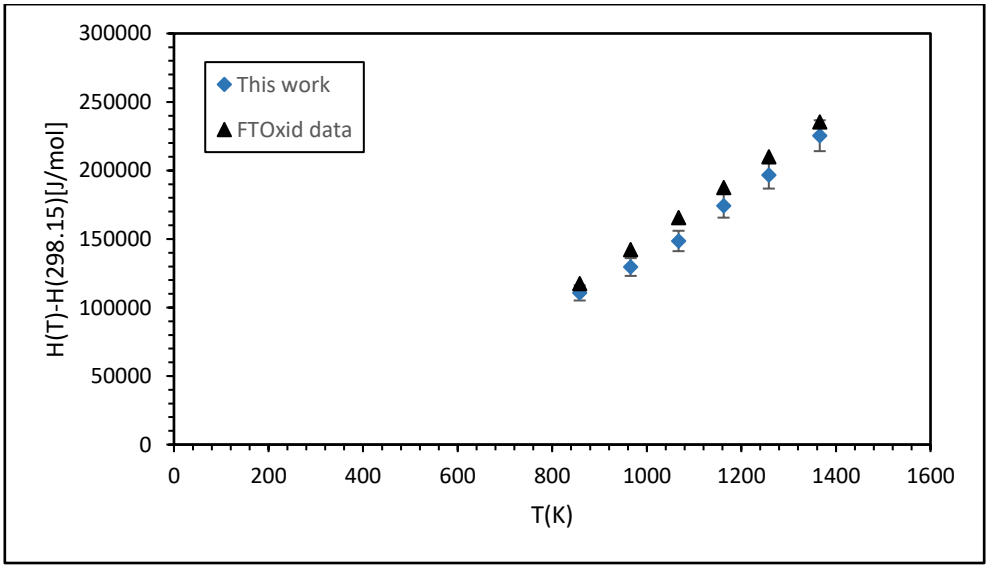

Fig. 46 : Relative enthalpy of $Ca_2Fe_{0.6}Al_{1.4}O_5$. plotted with FTOxid data from FactSage Software.

A particular issue concerning the calorimetric method applied for measuring relative enthalpy is related to the surrounding temperature control. For instance, the temperature inside the distributor above the calorimeter containing the dropped samples cannot be set. Initial temperature variation depends not only on meteorological changes, but also on furnace temperature in the calorimeter. Thus, it can be seen that in general initial temperature increases with measuring temperature (Table 18 and 19). However, an increase of 3°C cannot explain the difference with the modelled value in the FTOxid database. The relative enthalpy from 24 to 27°C is estimated to be of the order of a few 100 $J.mole^{-1}$ and is therefore in the reported uncertainty of the measurement. As there is no low temperature heat capacity data for the $Ca2Fe_{2-x}Al_xO_5$ solid solution available, it is not possible to correct all experimental values to the standard reference temperature of 25°C. Furthermore, in this type of equipment the absolute uncertainty increases with temperature, this is mainly due to radiation losses at high temperatures, which are difficult to monitor.

3.10 MELTING POINT

The melting point determinations were performed by differential scanning calorimetry Labsys^{TM} Evo (DSC). The scanning rates were 5K/min and 10K/min and the maximum temperature was set at 1508°C. In this study, we measured melting point of $Ca_2Fe_{2-x}Al_xO_5$ for the compositions x=0.5, x= 1 and x=1.4, the results are listed in Table 20.

Chemistry	Mass (mg)	Molar mass $g.mol^{-1}$	Al_x contents	$T_{fusion\ liquidus}$ (°C)	Scan rate (K/min)
$Ca_2Fe_{2-x}Al_xO_5$	103.1	254.4	0.5	1454±5	5
	55.7	242.9	1	1428±5	5 and 10
	66.94	231.4	1.4	1400±5	5 and 10

Table 20 : Melting proprieties of solid solution $Ca_2Fe_{2-x}Al_xO_5$ in function of Al ions contents.

The melting point of the solid solution depends on the Al content in the solid solution. It is observed that the insertion of Al ions leads to a reduction of the melting temperature, for the Ca_2FeAlO_5 composition the melting point we measured is 13°C higher than reported in the literature (1415°C±5). Pure $Ca_2Fe_2O_5$ melts at 1450°C (Lea, 1935), this value is close to that of the composition at x=0.5 but is still 4K higher. For this composition, a lower value than pure $Ca_2Fe_2O_5$ should be expected, as the insertion of Al influences the melting point in the solid solution.

3.11 Standard heat of formation of Ca_2AlFeO_5

The standard heat of formation was measured using dissolution calorimetry. Two series of Ca_2AlFeO_5 samples were dissolved in the basic slag solvent described in Chapter 1. The obtained results are presented in Fig. 47.

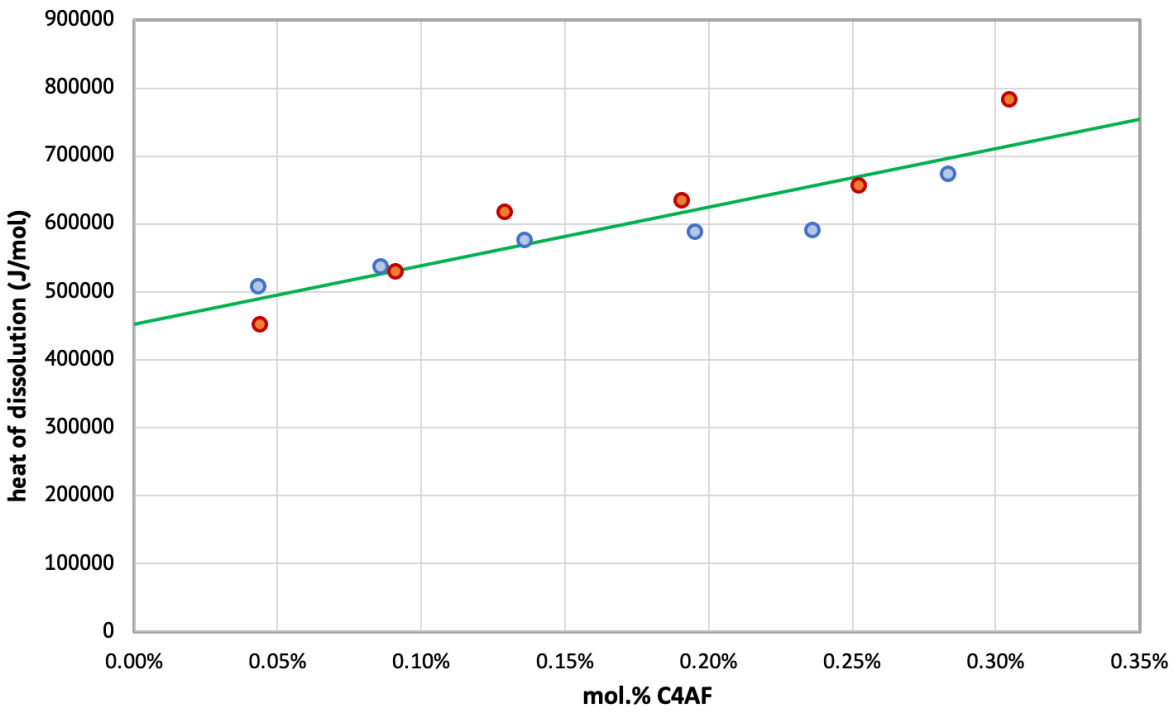

Fig. 47 : Experimental heat of dissolution of Ca_2AlFeO_5 in a basic slag solvent.

The heat of dissolution varies linearly with composition. Again, to calculate the standard heat of formation, we extrapolated the value to infinite dilution in the solvent using a linear regression. The obtained value is given by:

Q_{diss} (25°C) = 452618.7 ± 44015.3 J.mole^{-1}.

Similarly, using the dissolution data for pure CaO, Al_2O_3 and Fe_2O_3 from chapter 1, the standard heat of formation can be calculated and the value is:

$$\Delta_f H(25°C) = -46844.5 \pm 44512.5 \text{ J.mole}^{-1}.$$

Our new value agrees with the one reported by Ayed et *al* (1993) considering the uncertainty of our measurement.

3.12 CONCLUSION

The $Ca_2Fe_{2-x}Al_xO_5$ solid solution was studied experimentally and the results reported in this chapter; solid-solid synthesis under inert atmosphere is a necessary parameter to avoid any side reaction such as the formation of $Ca_{12}Al_{14}O_{33}$ stabilized by water vapour. The heat contents as a function of temperature were measured for two compositions relevant to cement systems x=1 and x=1.4. The calculated data from FTOxid agrees with the experimental data for the first composition while the second was overestimated. As far as the transition temperature measurements are concerned, the addition of aluminium reduces the melting point of the solid solution. The measured enthalpy of formation still has a considerable uncertainty but experimental value is in reasonable agreement with the only experimental data point available in the literature.

4 CHAPTER 4: THERMODYNAMIC STUDY OF THE C-A SYSTEM

4.1 INTRODUCTION

The knowledge of thermodynamic properties of $CaO\text{-}Al_2O_3$ is a major issue in different fields such as the cement industry, metallurgy, geology, ceramic materials and cosmology. Due to these numerous applications, the experimentally observed compounds present in cement have been the subject of various structural and thermodynamic investigations over the past century. Various authors studied the phase diagram containing aluminates component. The high melting point of the intermediate compounds in this system is one of the reasons. As early as 1909, Rankin and Wright (1915) reported a first version of the quasi-binary $CaO\text{-}Al_2O_3$ phase diagram. Later, investigations of portions of the diagram as well as thermodynamic and crystallographic properties of the intermediary compounds of this system completed this upstream work. The pioneering research work is probably the study of the moisture-free $CaO\text{-}Al_2O_3$ system (Nurse et *al* (1965)) by high temperature microscopy. From this study, many different versions of thermodynamic modelling and calculated phase diagrams were derived. Thanks to the development of time-temperature analysis methods otherwise differential thermal analysis, Jerebtsov and Mikhailov (2000) re-investigated this binary diagram and confirmed the general trend of the preliminary diagram. However, there are still important thermodynamic data missing. A review of available literature information on the $CaO\text{-}Al_2O_3$ system was carried out in this chapter in order to determine the various missing additional data. Starting from the literature, a new method of thermodynamic description based on the third generation Einstein model was used to describe the thermodynamic properties of the heat capacities of all calcium aluminates from 0K to the melting point. In addition, thermodynamic properties such as relative enthalpies and heat of formations were measured in particular for the compound $CaAl_{12}O_{19}$ as well as $Ca_5Al_6O_{14}$ for which no relevant thermodynamic data is reported in the literature up to now. Finally, a new version of the $CaO\text{-}Al_2O_3$ system was modelled and calculated. This chapter is divided into three parts: first, we will review the available literature, then we will present the additional experimental results obtained in the laboratory and finally we will finish with the modelling of the thermodynamic properties of calcium aluminates.

4.2 CRYSTALLOGRAPHIC DATA OF SOLID COMPOUNDS IN THE CaO-Al_2O_3 SYSTEM

There are five compounds and one solid solution in the CaO-Al_2O_3 pseudo-binary system. These phases are commonly noted according to the cement nomenclature as: CA ($CaAl_2O_4$), CA2 ($CaAl_4O_7$), C3A ($Ca_3Al_2O_6$), CA6 ($CaAl_{12}O_{19}$), C5A3 ($Ca_5Al_6O_{14}$), the high pressure phase C2A ($Ca_2Al_2O_5$) and the solid solution C12A7 ($Ca_{12}Al_{14}O_{32+x}$) with x ranging from 0 to roughly 1.5. The stability range of C5A3 phase is not clear. The compound is said to be metastable because it can be destabilized in the presence of excess oxygen. Rankin and Wright (1915) first identified this phase but its crystallographic structure was studied years later. The structure of C5A3 consists of alternating twisted sheets of deformed AlO_4 tetrahedra connected at the corners to form a network of five-membered rings and layers of Ca atoms. Two main, separate and concordant studies have shown that C5A3 crystallizes in an orthorhombic lattice of the Cmc21 space group (Aruja (1957) and Vincent (1978)). CA exists as two polymorphs. The first polymorph consists of an AlO_6-octahedral double layer structure; the Ca atoms are located in the interstitial sites and form a bridge between two layers of AlO_6-octahedral. While the second polymorph has a tunnel structure (Horkner & Muller-Buschbaum, 1976) . The structure of C3A consists of rings of six AlO_4 tetrahedra surrounding holes and Ca^{2+} ions holding the rings together (Jeffery and Mondal, 1975). C3A crystallizes in a cubic lattice of space groups Pm3m or Pa3 according to the most recent study (Jeffery and Mondal, 1975). The assessment of the crystal structure of CA2 has been the subject of various contradictory discussions; however, the most recent works agree that CA2 phase crystallizes in a monoclinic lattice (Table 21). C12A7 is a solid solution variable in oxygen $Ca_{12}Al_{14}O_{32+x}$, stable in air ($P(O_2)$ =0.21 atm, x>0), in the presence of H_2O ($Ca_{12}Al_{14}O_{33}(OH)_2$, it can therefore stabilized by traces of moisture. C12A7 has a capacity to absorb up to 1.3% H_2O from the furnace atmosphere at 950°-1350°C (Aggarwal et *al* (1972)). The formation of C12A7 occurs by the reaction of non-stoichiometric calcium aluminate (e.g. $5Ca_3Al_2O_6 + 9CaAl_2O_4 \leftrightarrow 2[Ca_{12}Al_{14}O_{32}]^{2+}: O^{2-}$) (Boysen et *al* 2007). The cubic crystal structure reported to belong to space group I4-3d according to different sources. Obtaining C12A7 crystals from the melt can also be done by the incorporation of various "modifiers" that can initiate the development of the nuclei of the structure. The C12A7 crystal is stabilized by the surrounding atmosphere (O_2, H_2O, CO_2, CO, SO_3)

or by the addition to the melt of CaF_2, $CaCl_2$, CaS, $CaSO_4$ or $CaCO_3$. Previous work by Jeevaratman et *al* (1964) on the structural stability of C12A7 by anion substitution in the cell led to three conclusions; firstly, C12A7 contains two reactive O^{-2} , which can be replaced totally or partially by four univalent ions, which will induce a probable modification.

4.3 PHASE DIAGRAM REVIEW

4.3.1 INVARIANTS REACTIONS

Upon cooling along the liquidus curve, compositions between C3A and CA form a eutectic liquid. Samples in this composition range were investigated by high-temperature microscopy by Nurse et *al* (1965) and the nature of the invariant reaction was confirmed by DTA under argon atmosphere by Jerebtsov (2000). The C3A solid compound dissociates incongruently into a mixture of liquid and CaO by a peritectic reaction. The incongruent melting point slightly differ according to the works published in the literature (Nurse (1965) and Jerebtsov (2000), but both values are in reasonable agreement when taking into account the uncertainties. Indeed, Rankin et *al's* (1915) preliminary work concluded on a temperature of 1808K while Nurse et *al* (1965) measured a temperature of 1539°C, which is in agreement with Jerebtsov (2000) recent work whose incongruent melting point value was 1540°C.

For CA, the melting type has been the object of contradictory discussion. In some works, it was reported that CA melts congruently. While, Nurse et *al* (1965) and later Jerebtsov (2000) measured an incongruent melting point. According to them, CA melts peritectically into CA2 and liquid with a composition close to CA. However, all authors agree on the melting temperature. Table 21 gathers the phase diagram data measured and modelled from the published papers. The equilibrium equations are for peritectic and eutectic mixtures but the melting type is specified.

C12A7 was first defined as being in reversible equilibrium with water molecules in the atmosphere in the form of $Ca_{12}Al_{14}O_{32}(OH)$. According to Nurse et al, it is not certain that the hydroxide group shown in the structure will be completely removed before the compound melts. The existence of C12A7 in the presence of moisture has been confirmed and its melting point measured. The stability of C12A7 in water free

environments has been debated, it is now established that this compound is able to incorporate an excess of oxygen in its framework.

There are different evaluations of the melting relations of CA2 in the literature. Rankin (1915) firstly identified this compound as C3A5. According to the author, C3A5 crystallizes in two forms, (I) stable and (II) unstable. The stable phase (I) melts congruently at 1720°C and forms a eutectic with CA and liquid. The melting point of the unstable phase (II) has not been determined and there is apparently no stability region for this phase according to Rankin and Wright (1915). Nevertheless, the congruent nature of the melting type was contradicted by the subsequent high-temperature microscope from Nurse et *al* (1965) and D.T.A from Jerebtsov and Mikhailov (2000) measurements, which concluded that CA2 melts incongruently. There are few studies on phase diagram data of CA6; the known peritectic melting point measured is 1830±5°C (Nurse et *al* 1965) and 1852±7°C (Jerebtsov and Mikhailov, 2000).

One issue concerning C12A7 is its stability in the C-A quasi-binary section. Preliminary work by Nurse indicated that this phase was stabilized by oxygen hydroxide (OH) molecules in air and in moisture nitrogen. In the same paper, Nurse measured the melting temperature of C12A7 and stated that the phase lost OH molecules before melting. Jerbestov's work also reported the presence of traces of water in the C12A7 phase. Recent work by Trofymluk indicates that C12A7 exists as a $[Ca_{12}Al_{12}O_{32-\delta}]^{+2\delta}(2\delta e^-)$, $0<\delta\leq 1$, solid solution from which $Ca_{12}Al_{12}O_{33}$ crystals can be obtained by the floating zone method. This oxygen variation thus suggests that it would be interesting to describe C12A7 in a ternary Ca-Al-O section rather than in the CaO-Al_2O_3 section. However, if one is interested in the CaO-Al_2O_3 quasi-binary system, the compound $Ca_{12}Al_{14}O_{33}$ must be considered. Regarding C5A3, it would appear that this phase is screened by C12A7 in an oxidizing environment and its synthesis therefore requires a neutral atmosphere. This phase exists in the C-A section but there are no relevant thermodynamic data in the literature that can be used in a phase diagram model.

Equilibrium	T(°C)	Melting type	Liquid composition		Method	Sources
			w%(CaO)	w%(Al_2O_3)		
CaO+Liquid→C3A	1539±5	Peritectic	57.2	42.8	High-temperature microscope (Thermocouples :95% Pt-5%Rh|80%Pt-20%Rh up to 1800°C and 80% Pt-20%Rh|60%Pt-40%Rh from 1800 to 1860°C)	Nurse et *al* (1965)
	1535±5	Peritectic	No data	No data	Melting point determined optically with optical pyrometer	Rankin and Wright (1915)
	1840±5	Peritectic	49±1	51±1	D.T.A in argon atmosphere (1.3 atm) equipped with tungsten-rhenium 5/20 thermocouple.	Jerebtsov and Mikhailov (2000)
C3A+CA→Liquid	1360±5	Eutectic	49.35	50.65	High-temperature microscope (Thermocouples :95% Pt-5%Rh|80%Pt-20%Rh up to 1800°C and 80% Pt-20%Rh|60%Pt-40%Rh from 1800 to 1860°C)	Nurse eT *al* (1965)
	1371±5	Eutectic	58±1	42±1	D.T.A in argon atmosphere (1.3 atm) equipped with tungsten-rhenium 5/20 thermocouple.	Jerebtsov and Mikhailov (2000)
CA→ CA2+Liquid	1602±5	Peritectic	36	64	High-temperature microscope (Thermocouples :95% Pt-5%Rh|80%Pt-20%Rh up to 1800°C and 80% Pt-20%Rh|60%Pt-40%Rh from 1800 to 1860°C)	Nurse eT *al* (1965)
	1604±5	Peritectic	37±1	63±1	D.T.A in argon atmosphere (1.3 atm) equipped with tungsten-rhenium 5/20 thermocouple.	Jerebtsov and Mikhailov (2000)
	1600	Congruently	-	-	Melting point determined optically	Rankin and Wright (1915)

Table 21 : Invariants reactions in the $Ca_3Al_2O_6$ -$CaAl_2O_4$ composition range without C12A7.

Equilibrium	T(°C)	Melting type	Method	Sources
Liquid+C3A+C12A7	1360	Eutectic	High-temperature microscope (Thermocouples :95% Pt-5%Rh|80%Pt-20%Rh up to 1800°C and 80% Pt-20%Rh|60%Pt-40%Rh from 1800 to 1860°C)	Nurse et al (1965)
	1395	Eutectic	Melting point determined optically with optical pyrometer	Rankin & Wright (1915)
	1403±5	Congruently	D.T.A in argon atmosphere (1.3 atm) equipped with tungsten-rhenium 5/20 thermocouple.	Jerebtsov and Mikhailov (2000)
	1392	Congruently	High-temperature microscope (Thermocouples :95% Pt-5%Rh|80%Pt-20%Rh up to 1800°C and 80% Pt-20%Rh|60%Pt-40%Rh from 1800 to 1860°C)	Nurse et al (1965)
C12A7 melting point	1455	Congruently	Melting point determined optically with optical pyrometer.	Rankin & Wright (1915)
	1360	Eutectic	High-temperature microscope (Thermocouples :95% Pt-5%Rh|80%Pt-20%Rh up to 1800°C and 80% Pt-20%Rh|60%Pt-40%Rh from 1800 to 1860°C)	Nurse et al (1965)
Liquid+CA+C12A7	1400	Eutectic	Melting point determined optically with optical pyrometer	Rankin & Wright (1915)

Table 22 : Data on C12A7 invariant and melting point. Nurse et *al* (1965) and Jerebtsov and Mikhailov (2000) reported that the C12A7 phase contained ~1 mass% water evaporated near to the melting point.

Equilibrium	T(°C)	Melting type	Liquid composition		Method	Sources
			w%(CaO)	w%(Al_2O_3)		
CA6+Liquid→CA2	1762±5	Peritectic	22	78	High-temperature microscope (Thermocouples :95% Pt-5%Rh|80%Pt-20%Rh up to 1800°C and 80% Pt-20%Rh|60%Pt-40%Rh from 1800 to 1860°C)	Nurse et *al* (1965)
	1762±5	Peritectic	26.5±1	73.5±1	D.T.A in argon atmosphere (1.3 atm) equipped with tungsten-rhenium 5/20 thermocouple.	Jerebtsov and Mikhailov (2000)
	1720	Congruent	No liquid composition study		Melting point determined optically with optical pyrometer	Rankin & Wright (1915)
Al_2O_3+Liquid→CA6	1830±5	Peritectic	16	84	High-temperature microscope (Thermocouples :95% Pt-5%Rh|80%Pt-20%Rh up to 1800°C and 80% Pt-20%Rh|60%Pt-40%Rh from 1800 to 1860°C)	Nurse et *al* (1965)
	1852±7	Peritectic	16.5±1	83.5±1	D.T.A in argon atmosphere (1.3 atm) equipped with tungsten-rhenium 5/20 thermocouple.	Jerebtsov and Mikhailov (2000)

Table 23 : Invariants reactions in the $CaAl_4O_7$-$CaAl_{12}O_{19}$ composition range

4.3.2 LIQUIDUS

One of the first studies providing the phase diagram of the CaO-Al_2O_3 system was carried out in 1915 (Rankin and Wright, 1915). In this system, four distinct intermediate compounds were identified in the binary section, namely $Ca_3Al_{10}O_{18}$, $CaAl_2O_4$, $Ca_5Al_6O_{14}$ and $Ca_3Al_2O_6$. Further research on this system has been conducted. Thus Filonenko and Lavrov (1950) identified by microscopic study the CA6 phase which was previously reported as $Ca_3Al_{32}O_{51}$ (Rankin and Wright, 1915). Later X-ray diffraction developments showed that $Ca_5Al_6O_{14}$ corresponds to C12A7, $Ca_3Al_{10}O_{18}$ to $CaAl_4O_7$. Various authors also published studies on the alumina-rich portions (references), but Nurse et *al* published the first complete experimental diagram in 1965 under controlled atmosphere. Subsequently, Jerebtsov and Mikhailov (2000) works carried out under argon confirmed the previous results of Nurse et *al* (1965).

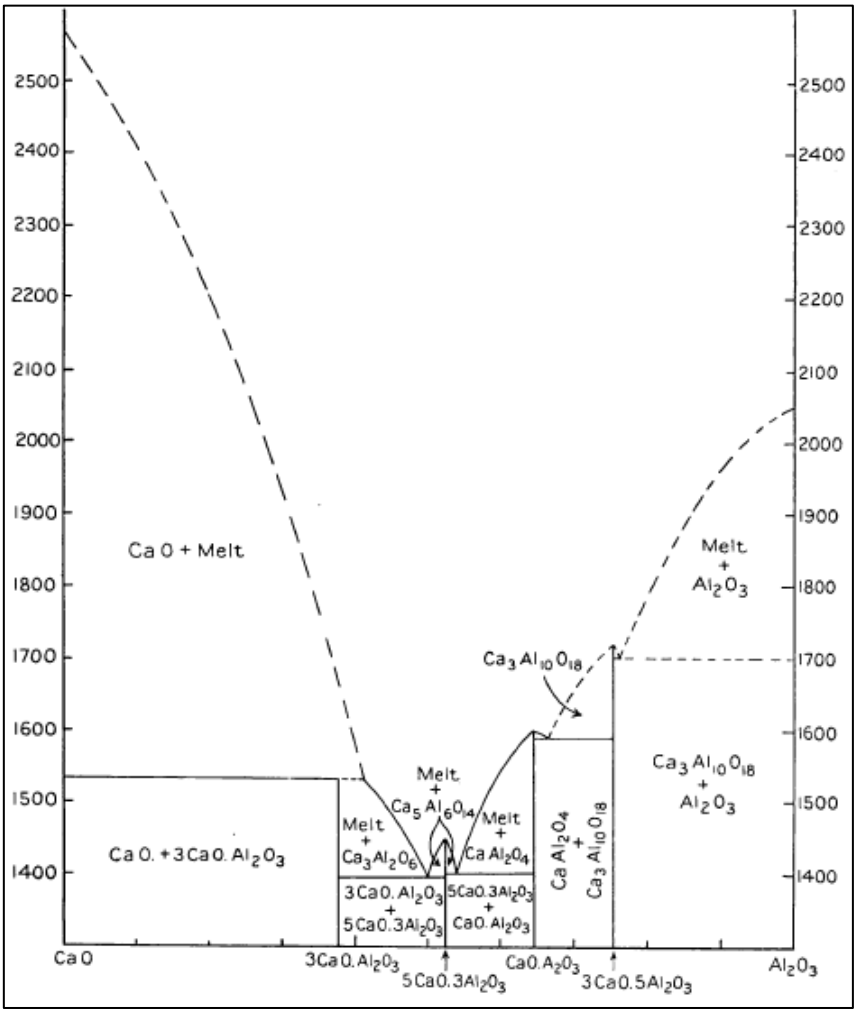

Fig. 48 : First CaO-Al_2O_3 phase diagram reported by Rankin and Wright (1915).

Only C3A melts incongruently in the Fig. 45 and forms a C3A-CaO-Liquid invariant. C3A is stable along the liquidus joining points E (eutectic) and P (peritectic) and then destabilizes above 1531°C into CaO and liquid. CA melts congruently and forms a first eutectic mixture with C5A3 and a second with C3A5. There is no CA6 phase reported by the authors in the $CaO\text{-}Al_2O_3$ section.

4.3.2.1$CaO\text{-}Al_2O_3$ in moisture-free atmospheres

Nurse et *al* (1965) was the first to provide relevant and accurate results and a more complete description of the aluminate quasi-binary phase diagram. Nurse synthesized aluminates from a mixture of $CaCO_3$ (99.9%) and Al_2O_3 (99.8%) as glass. The authors verified the purity and composition of the synthesized samples using different methods, including petrographic, X-rays diffraction and DTA. The binary compounds encountered under the liquidus curve are $Ca_3Al_2O_6$, $CaAl_2O_4$, $CaAl_4O_7$ and $CaAl_{12}O_{19}$.

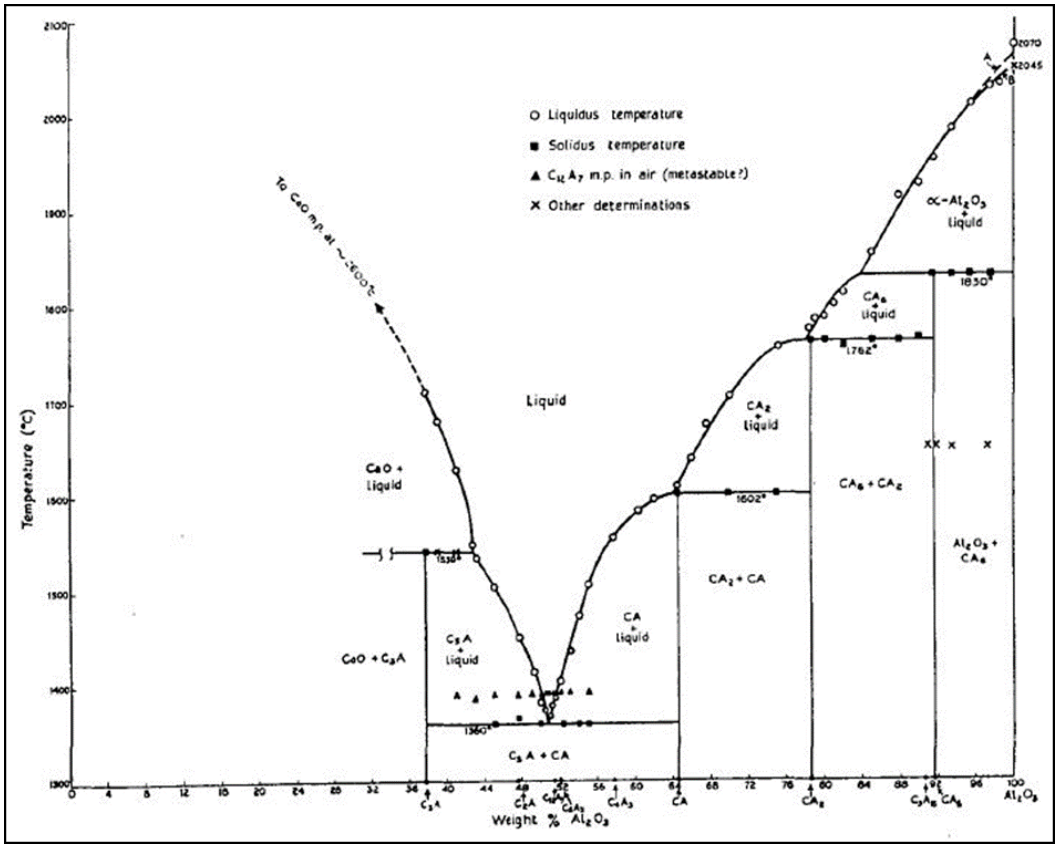

Fig. 49 : $CaO\text{-}Al_2O_3$ experiment phase diagram in moisture-free atmosphere without C12A7 (Nurse, Welch, & Majumdar, 1965).

All phases melt incongruently. C12A7 is assumed to be non-anhydrous, which means that it is not stable in the absence of air humidity.

4.3.2.2$CaO-Al_2O_3$ in argon atmosphere

Jerebtsov and Mikhailov (2000) conducted recently an additional study of the $CaO-Al_2O_3$ system by the differential thermal analysis DTA method. As reported by Nurse et *al* (1965), no C12A7 was detected by the authors in an dry atmosphere and all aluminates melt incongruently. Nevertheless, the existence of C12A7 in the presence of traces of moisture was confirmed through the eutectic at 1403°C.

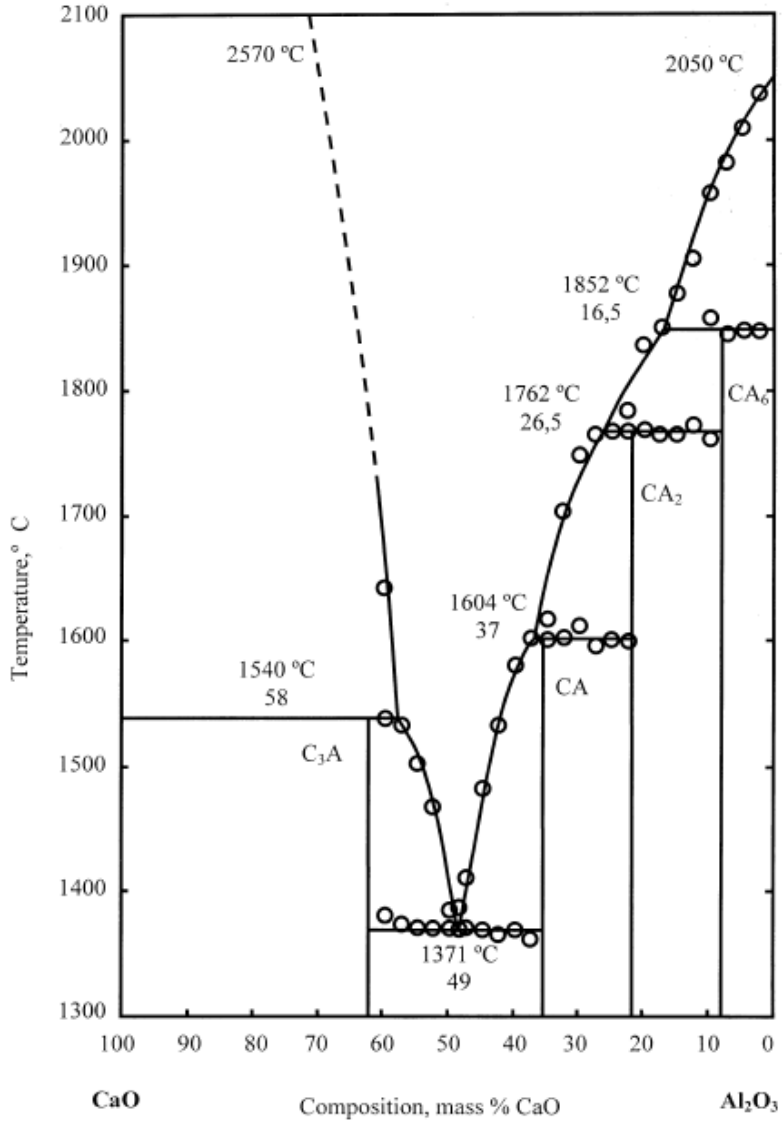

Fig. 50 : Experimental phase diagram by differential thermal analysis DTA method under argon atmosphere. Study conducted by Jerebtsov and Mikhailov (Jerebtsov and Mikhailov, 2000).

4.3.3 STABILITY OF C12A7 IN THE CaO-Al_2O_3 SECTION

Since the early works by Rankin and Wright (1915) on the CaO-Al_2O_3 system, it is now certain that C12A7 is not a polymorph of C5A3 but a distinct and isolated phase. Nevertheless, in the past, the focus of discussion around C12A7 has been on the stability of this phase in an dry environment of the CaO-Al_2O_3 condensed section. The results published on C12A7 by Nurse et *al* (1965) concluded that C12A7 is not completely anhydrous. Indeed, in that paper, C12A7 was synthesised by melting at 1500°C followed by annealing at 1000°C in nitrogen without moisture, D.T.A. and thermal equilibrium analyses indicated a mass gain of ~1.3% at 950°C and a loss of ~0.8% between 950°C and 1350°C. This result suggests that C12A7 crystals retain water molecules in their crystal structures until the melting point. From this observation, the authors (Nurse et *al* 1965) drew two conclusions on the CaO-Al_2O_3 system close to the composition of C12A7: firstly, the presence of hydroxyls in the lattice of C12A7 crystals indicates that this phase is present in the moisture-free atmosphere section as represented in Fig. 51. Secondly, a diagram containing C3A, C12A7 and CA as a phase assemblage can be reproduced when the experiments are carried out under nitrogen or argon gas as the model in Fig. 52.

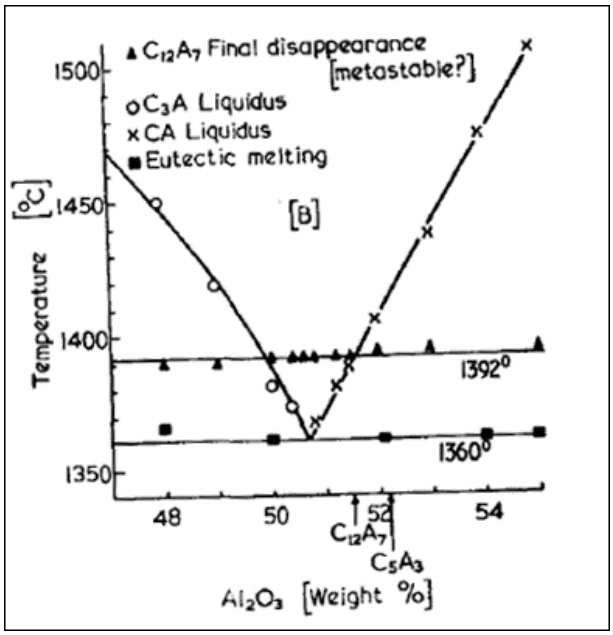

Fig. 51 : Portion of phase diagram: liquidus data near the C12A7 composition by very high-temperature microscopy, reported by Nurse et al (Nurse, Welch, & Majumdar, 1965).

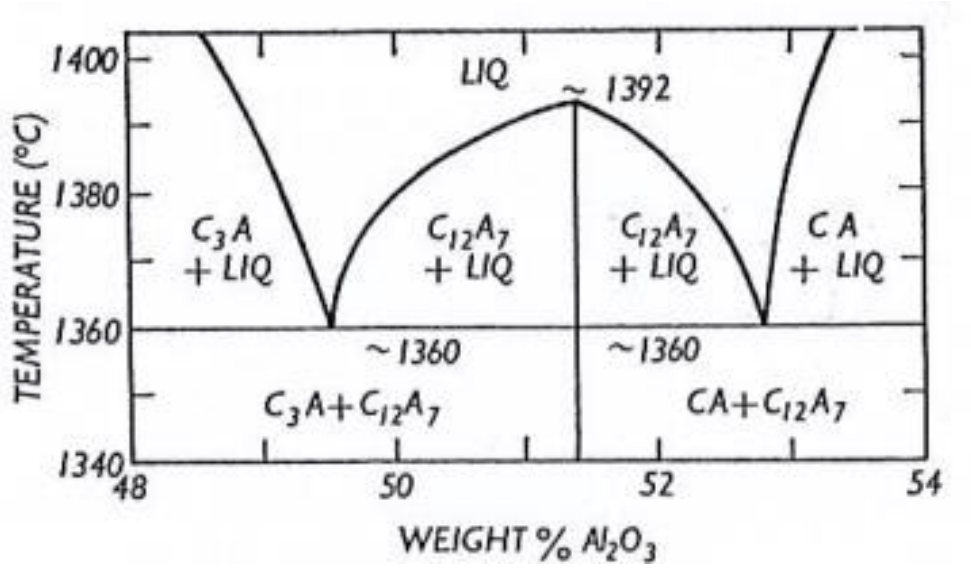

Fig. 52 : Currently accepted liquidus data near the C12A7 al (Nurse, Welch, & Majumdar, 1965).

4.3.4 PHASE DIAGRAM MODELLING IN THE LITERATURE

Thermodynamic modelling is a technique for calculating phase diagrams from optimized Gibbs energy datasets using the available experimental data. The general method consists of simultaneously evaluating all the experimental & theoretical information available for the system under study by simultaneous numerical modelling of the Gibbs energy of all the phases of the system. Using these Gibbs energy expressions as a function of temperature and composition, a phase diagram can be calculated. The particularity of this method is that it describes the thermodynamic properties from a mathematical model containing adjustable parameters and thus allows the prediction of properties in areas of the phase diagram where no experimental thermodynamic data are available. We reviewed the entire literature on optimized phase diagrams of the CaO-Al_2O_3 system. In this part, we will discuss the individual modelled results from the literature.

4.3.4.1 Calculated phase diagram based on the quasi-chemical model for the liquid phase

The phase diagram calculated and optimized by Eriksson and Pelton (1987) is shown in Fig. 53. The modified quasi-chemical model was used to describe the thermodynamic properties of the liquid phase. This model describes a binary system in which the particles of two compounds mix by substitution in a quasi-lattice [reference Pelton]. The evaluations are valid from room temperature to above liquid temperatures. As for the experimental phase diagram (Nurse et *al,* 1965), C12A7 has been excluded from the modelled CaO-Al_2O_3 section. This phase considered unstable in anhydrous surroundings. C3A and CA6 phases melt incongruently at temperatures close to the DTA measurements of Nurse et al, i.e. 1541°C (1539±5°C, Nurse et *al,* 1965 and 1833°C (1830±15°C Jerebtsov 2000). However, the CA and CA2 phases melt congruently, which is in contradiction with Nurse et *al* (1965) report. Although the melting point are in agreement with the experimental data. The nature of the melting of CA and CA2 was a subject of conflicting discussion. Authors have tended to prioritise the data concluding on congruent melting.

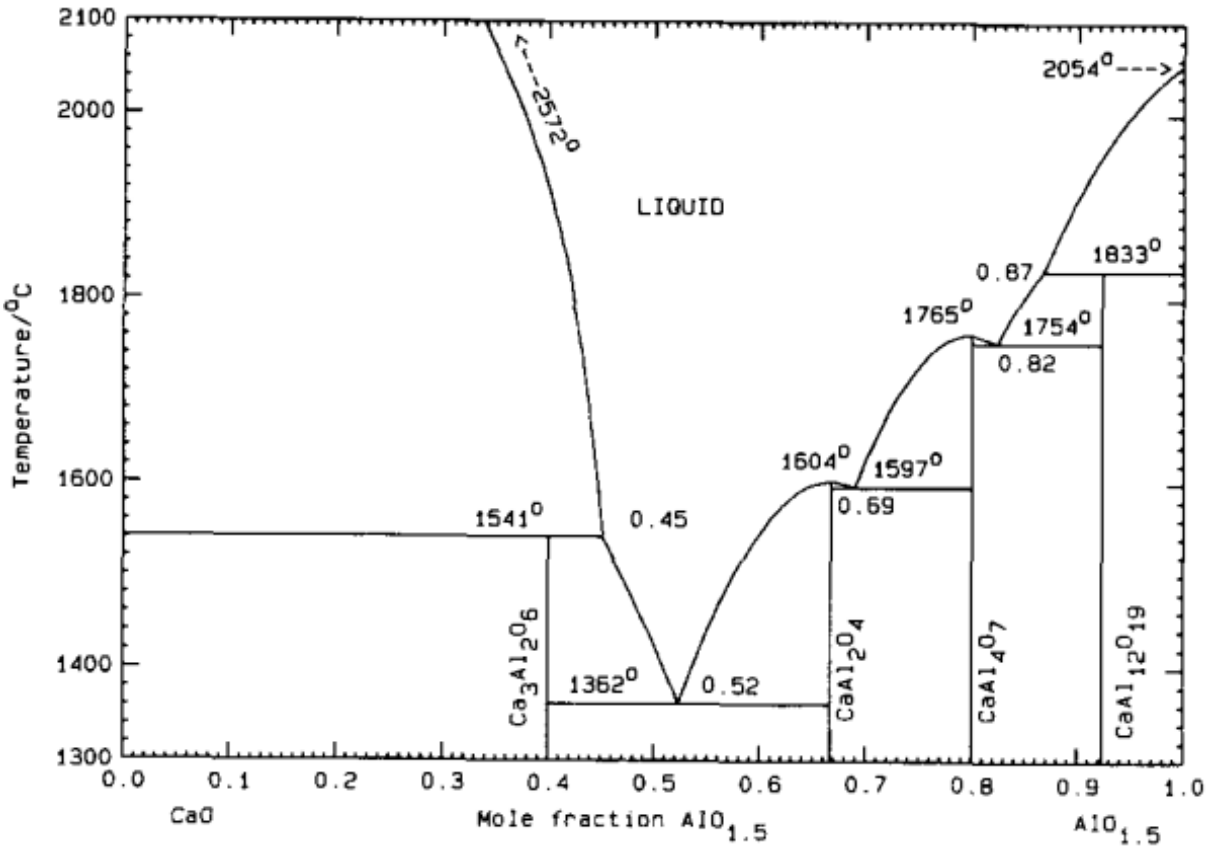

Fig. 53 : Liquidus CaO-Al_2O_3 optimized phase diagram. The authors defined the composition is in function of components CaO-$AlO_{1.5}$ (Eriksson and Pelton, 1987).

4.3.4.2 Calculated phase diagram based on two-sublattice model for the liquid phase

Hallstedt (1990) performed the modelling of CaO-Al_2O_3 phase diagram presented in Fig. 54. A two-sublattice subregular solution model was used to describe the liquid phase. In this model, the liquid consists of two sub-lattices, one for cations: $(Al^{3+}, Ca^{2+})_P$ and the other for anions and neutral species: $(Al^{3+}, Ca^{2+})_P$, where *P* and *Q* are the number of sites on each sublattice. The Gibbs energy of the liquid derived from Hillert et *al* (1985) model.

$$G_m = y_{Al^{3+}} + {}^\circ G_{Al_2^{3+}O_3^{2-}} + y_{Ca^{2+}} {}^\circ G_{Ca_2^{3+}O_2^{2-}} + 2RT(y_{Al^{3+}} \ln y_{Al^{3+}} + y_{Ca^{2+}} \ln y_{Ca^{2+}}) + G_m^E$$

[12]

There, P=*2* and $Q = y_{Ca^{2+}} + y_{Al^{3+}}$ where *y* is the mole fraction of each sublattice. G_m^E is the excess Gibbs energy depending on interaction between Al^{3+} and Ca^{2+} on the cation sublattice. These interactions are more precisely defined by a Redlich-Kister polynomial [13]:

$$G_m^E = y_{Ca^{2+}} y_{Al^{3+}} [{}^\circ L + L^1 (y_{Ca^{2+}} - y_{Al^{3+}})] \text{ [13]}$$

The *L* parameters are set to account for the temperature dependence. °*L* for the regular temperature dependent and L^1 for the temperature independent subregular. Pure solid phases stated by equation [14]

$${}^\circ G - H^{SER} = A + BT + CT\ln T + DT^2 + ET^3 + FT^{-1} \text{ [14]}$$

Equation [15] applied to the solid intermediate constituents of the CaO-Al_2O_3 section. All aluminates are dealt with as stoichiometric compounds and their Gibbs energy is calculated in relation with pure oxides.

$${}^\circ G^{C_X A_Y} = X {}^\circ G^{CaO} + Y {}^\circ G^{Al_2O_3} + A + BT + CT \ln T \text{ [15]}$$

The phase diagram computed in Fig. 54 is based on the two-subregular model for the liquid phase. The data on the invariant equilibria and the liquid are taken from the experimental work from (Nurse et *al* 1965). No constraints were set on the melting type of CA2 and CA, all compounds are stoichiometric and C12A7 is considered

unstable as reported by Nurse et *al* (1965) . Temperatures in brackets are from Nurse et *al* (1965) DTA measurement while Hallstedt (1990) calculated three-phase equilibria temperatures without brackets. The invariant temperatures are generally in agreement with the experimental data except for the CA6 + Al_2O_3 + Liquid equilibrium, which is 50 K above the measurements. As in the previous model Fig. 54, CA2 and CA melt congruently at temperatures in agreement with assessment. Hallstedt (1990) reported C3A and CA2 unstable at low temperatures. This conclusion is based on the extrapolation of the EMF experimental data (Allibert et *al* 1981) at low temperature.

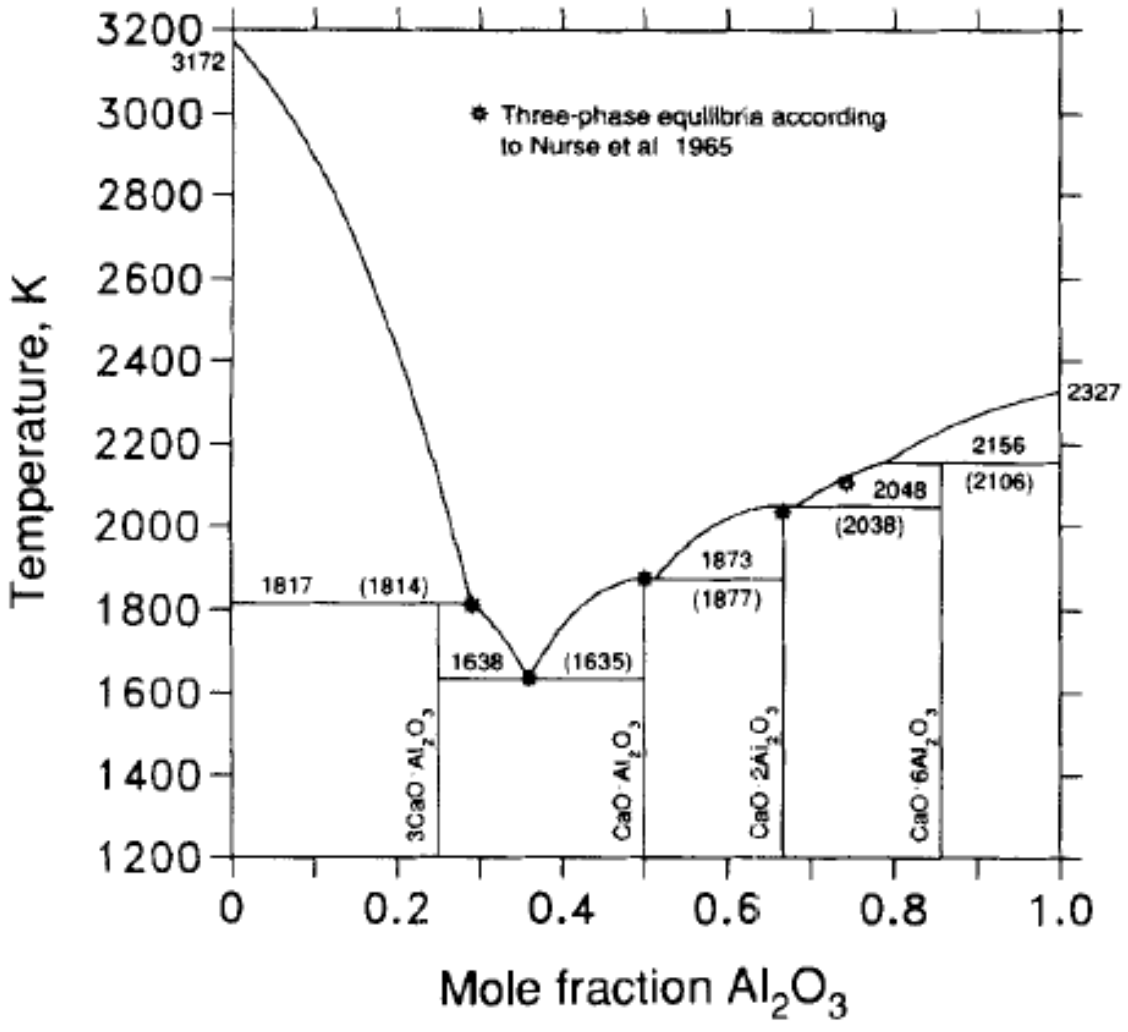

Fig. 54 : Phase diagram from Hallstedt (1990) optimization with three phase equilibrium data and invariant temperature from Nurse et *al* (1965) and calculated temperature.

The diagram including the experimental liquidus data is reproduced in Fig. 55. The agreement of the calculated Al_2O_3-rich liquidus with the experimental data is correct, but the CaO-rich part of the liquidus is not in agreement with the data of Nurse et *al* (1965). According to Hallstedt (1990), it was not possible to obtain a reliable CA6 Gibbs energy of formation by fitting CA6-Al_2O_3-liquid simultaneously. Nevertheless, the Gibbs energy curve seemed reasonable only when the temperature of the three equilibrium phases CA6-Al_2O_3-liquid was above the value of Nurse et *al* (1965). The lack of sufficient thermodynamic data on CA6 is clearly the reason of these discrepancies.

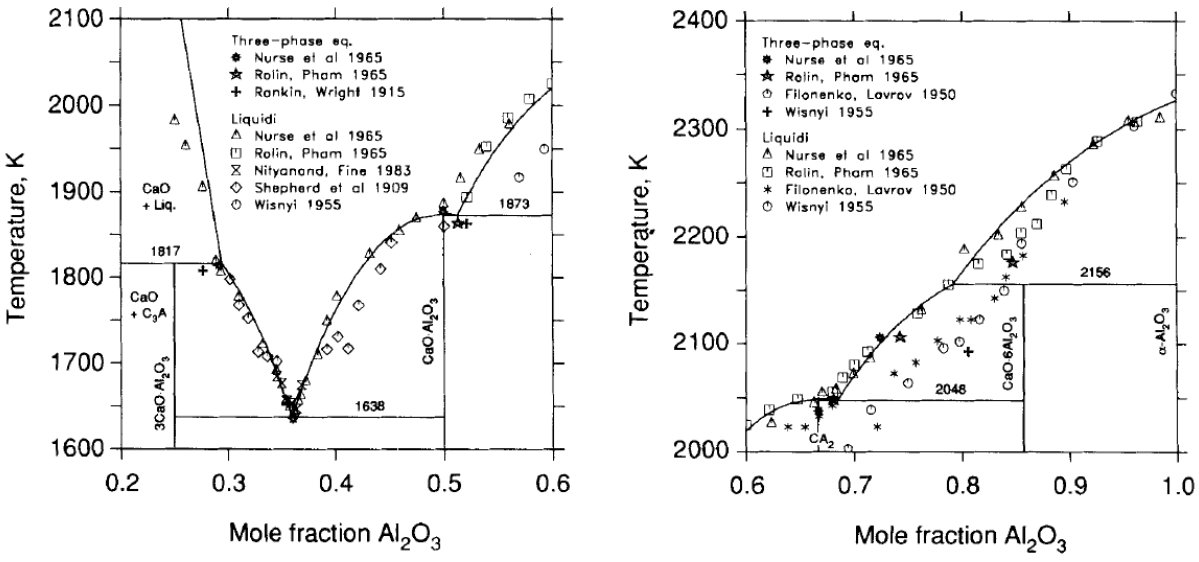

Fig. 55 : Hallstedt (1990) part of phase diagram from 20 to 100% alumina. Invariant three phase equilibria and liquidus are including. The experimental data come from various sources.

Mao et *al* (2004) also used the ionic two-sublattice model to describe the thermodynamic properties for the liquid phase of the CaO-Al_2O_3 system. A new AlO_2^{-1}species was introduced to describe the tetrahedral network. Hence, the model is described by the following formulas: $(Al^{+3}, Ca^{2+})_P\ (AlO_2^{-1}, O^{-2})_Q$ and Gibbs energy by equation [16].

$$G_m = y_{Al^{+3}} y_{AlO_2^{-1}} {}^{\circ}G_{Al^{+3}:AlO_2^{-1}} + y_{Al^{+3}} y_{O}^{-2} {}^{\circ}G_{Al^{+3}:O^{-2}} + y_{Ca^{2+}} y_{AlO_2^{-1}} {}^{\circ}G_{Ca^{+2}:AlO_2^{-1}} + y_{Ca^{+2}} y_{O}^{-2} {}^{\circ}G_{Ca^{+2}:O^{-2}} + P'RT(y_{Al^{3+}} \ln y_{Al^{3+}} + y_{Ca^{+2}} \ln y_{Ca^{+2}}) + Q'RT\left(y_{AlO_2^{-1}} \ln y_{AlO_2^{-1}} + y_{O}^{-2} \ln y_{O}^{-2}\right) + G_m^E \quad [16]$$

As in the two-sublattice subregular description, *y* is the site fraction; *P'* and *Q'* are adjustable parameters that ensure the electroneutrality condition. $^{\circ}G_{Al^{+3}:AlO_2^{-1}}$ and $^{\circ}G_{Ca^{+2}:O^{-2}}$ are respectively similar to the Gibbs energy of two moles of pure G(Al_2O_3) and G(CaO). The description of the solid phases is similar to those given in the two-sublattice subregular. The Gibbs energies of the pure liquid phases Al_2O_3 and CaO came from Hallstedt's (1990) assessment.

The calculated phase diagram as modelled by Mao et *al* (2004) is given in Fig. 56. The authors retained four solid and stoichiometric phases in the CaO-Al_2O_3 section, namely C3A, CA, CA2 and CA6. The experimental data of the liquid are the same as that of the literature review of Hallstedt (1990). The calculated phase diagram is compared with experimental data from various sources. The experimental data of the invariants are perfectly reproduced. The experimental liquid points of Nurse et *al* (1965), Rolin and Pham (1965) are also modelled correctly except for the lime rich liquidus. According to the authors, this discrepancy is due to the high melting point of the CaO used (2852°C). Regarding the CA6+Al_2O_3+Liquid invariant, there is a 40K difference between the calculated values and the experimental data as well as a difference of 1.65 mass% Al_2O_3 in the liquid composition. As Hallstedt indicated earlier, it was impossible to obtain a reasonable temperature dependence Gibbs energy of formation by fitting CA6 liquidus and these three phases in invariant equilibrium (CA6+Al_2O_3+Liquid) at the same time. In this description, only CA2 melts congruently at 1767.5°C while three other phases melt incongruently.

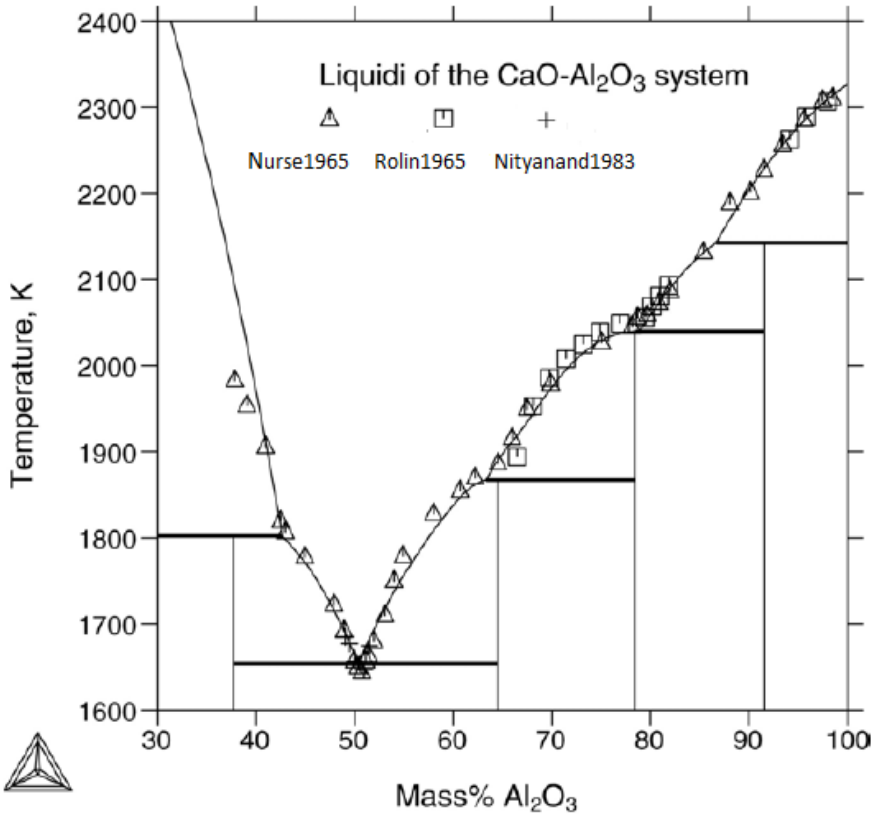

Fig. 56 : Phase diagram including calculated liquid of $CaO\text{-}Al_2O_3$ (Mao et *al,* 2004) system with experimental data from various authors.

4.3.5 C12A7 IN SECTION $CaO\text{-}Al_2O_3$

Oxygen concentration is an important parameter in C12A7 formation, stabilization at high temperature occurs by absorption of excess oxygen from any oxidizing atmosphere even when PO_2 pressure is as low as 10^{-8} atm (Zhmoidin and Chatterjee, 1985). Regarding the phase diagram, there are few modelling works in literature including this phase in an anhydrous section. In the Fig. 57, Li et *al* (2017) added C12A7 in $CaO\text{-}Al_2O_3$ section and calculated the interactions parameters in the liquid phase between CaO and Al_2O_3 by using a sub-regular Redlich-Kister equation. At the same time, the liquidus was also computed using the commercial software FactSage. Moreover, the authors synthesized C12A7 also. The synthesis consisted in mixing Al_2O_3 and CaO powders, pre-treated in a furnace at 1000°C for 2h and then transferred to a Mo crucible for heat treatment at 1500°C during 2h in open atmosphere (Air). Finally, XRD analysis confirmed the obtaining of C12A7 phase but the authors did not measure the oxygen content.

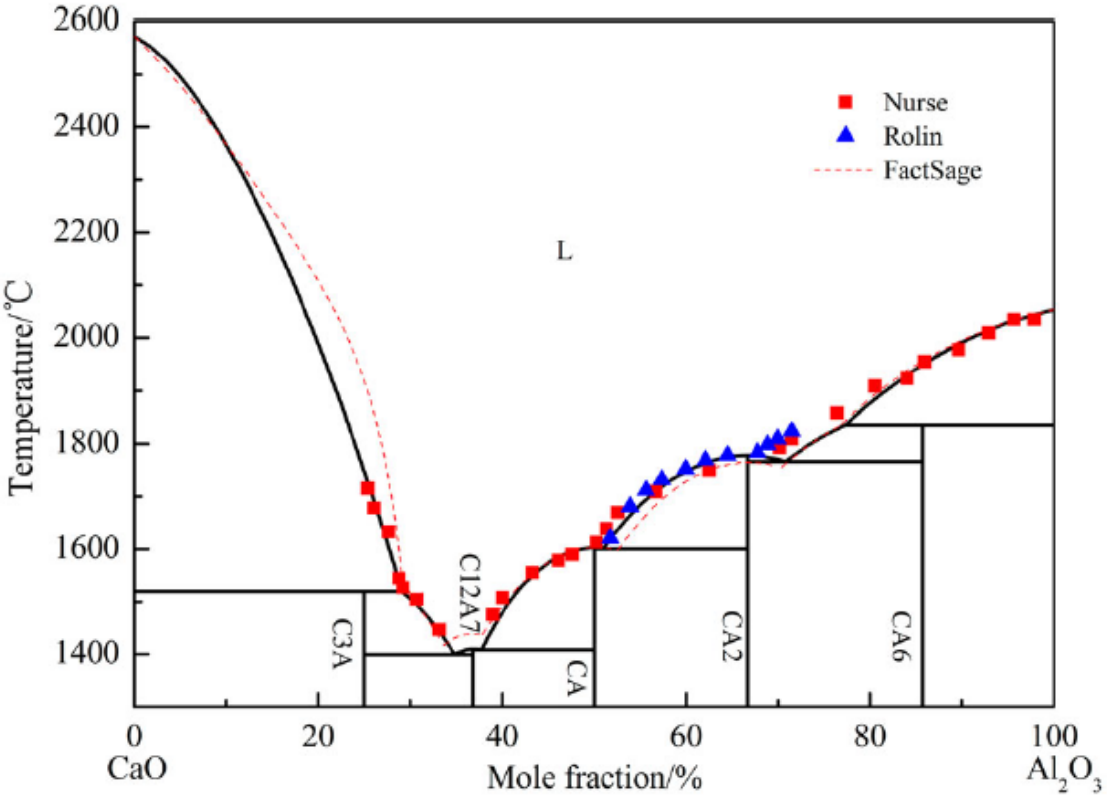

Fig. 57 : Li et *al* (2017) Computed phase diagram of $CaO\text{-}Al_2O_3$ including C12A7 in the section.

In this diagram the melting relation for CA2 and CA6 do not fit correctly. Results obtained by FactSage calculation indicates discrepancies between the experimental data and the liquidus near C12A7 and C3A. C12A7 melting point is higher in the FactSage results, while Li et *al* (2017) reported 1415°C, which is in better agreement with the experimental values. Temperature of existence of CA6-Al_2O_3-Liquid invariant is not given but by graphical observation we deduce a value of ~1835°C in agreement with Nurse et *al* (1965) experiment (1830°±15°C) but ~ 17°C lower than Jerebtsov and Mikhailov (2000) value (1852°C). The intermediate compounds melt congruently except for C3A and CA6.

Hallstedt (1990) did the modeling of C12A7 separately without including it in the main $CaO\text{-}Al_2O_3$ diagram. As shown in Fig. 58, C12A7 melts congruently in his version and forms two eutectics with CA and C3A, although the melting temperature is higher than that given by Nurse et *al* (1965). According to the author, the appearance of C12A7 should not significantly influence the equilibrium of C3A and CA. As can be seen in Nurse et *al* (1965) phase diagram in Fig. 49, the two eutectics formed on either

side of C12A7 are at the same temperature indicating a destabilization of CA and C3A in relation to liquid.

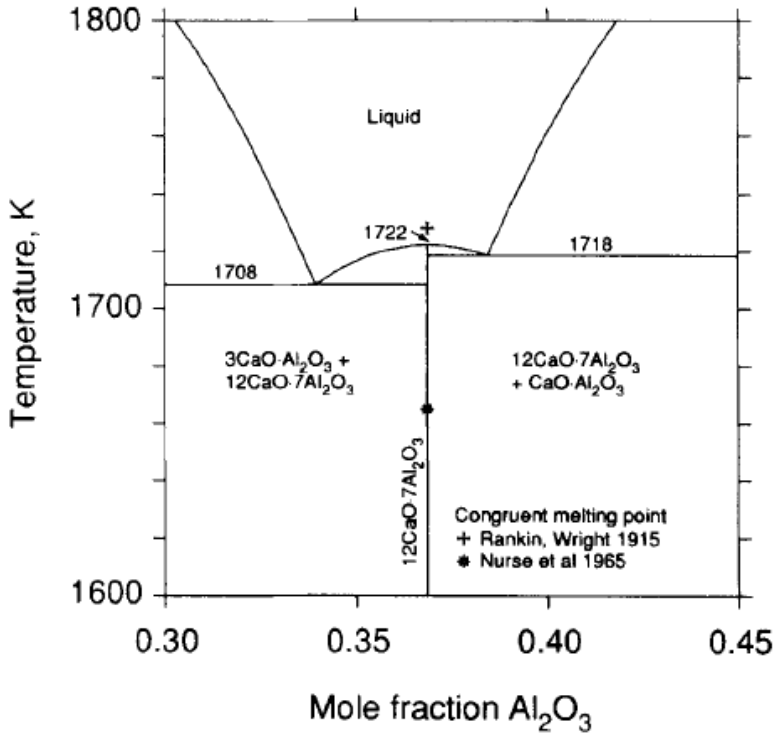

Fig. 58 : Part of the phase diagram including C12A7 calculated in isolation (Hallstedt, 1990). The experimental data are from the congruent melting reported by Rankin and Wright (1915) and Nurse et *al* (1965).

Ball et *al* (1993) used a non-ideal interacting associated species to describe thermodynamics properties of oxides melts in the $CaO\text{-}Al_2O_3$ system and recalculated another phase diagram. In this model, the thermodynamic data comes from Scientific Group Thermodata Europe (SGTE) substance database while for the stoichiometric solids come from $CaO\text{-}Al_2O_3$ assessed by Hallstedt (1990). The calculated phase diagram is computed by using experiment liquids data from Nurse et al (1965).

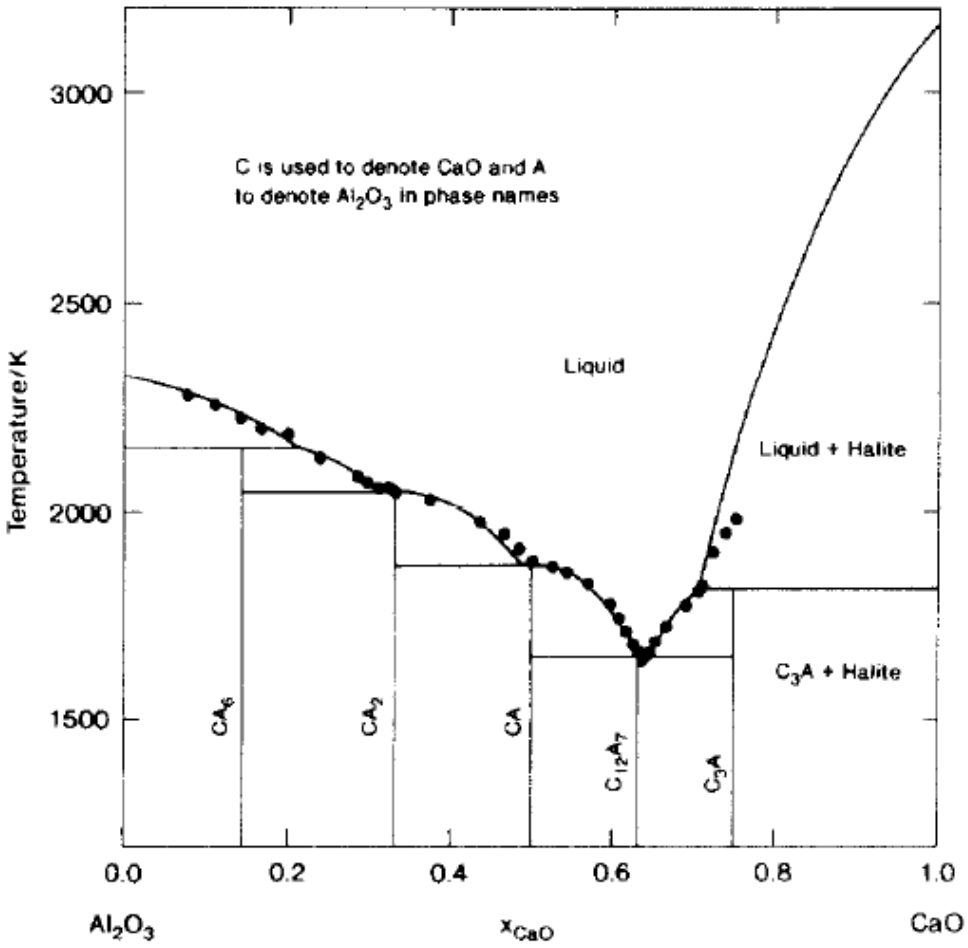

Fig. 59 : Calculated binary phase diagram from Ball et *al* (1993), based on Associate model. Experimental data come from Nurse et *al* (1965).

4.3.6 HIGH ALUMINA PORTION IN CaO-Al_2O_3

One of the most frequently encountered contradictions concerns the melting type of intermediate compounds in the CaO-Al_2O_3 section. Although the most consistent studies by Nurse et *al* (1965), Jerebtsov, and Mikhailov (2000) conclude that, with the exception of C12A7, all other aluminates in the binary section melt incongruently, CA and CA2 compounds are often represented as congruently melting in some calculated phase diagrams. On the one hand, the lack of experimental data of liquidus and solidus explains discrepancies between some phase diagrams reported in the past Fig. 60. On the other hand, the difficulty to reproduce the new thermodynamic values can also explain some differences between the experimental data and the calculated.

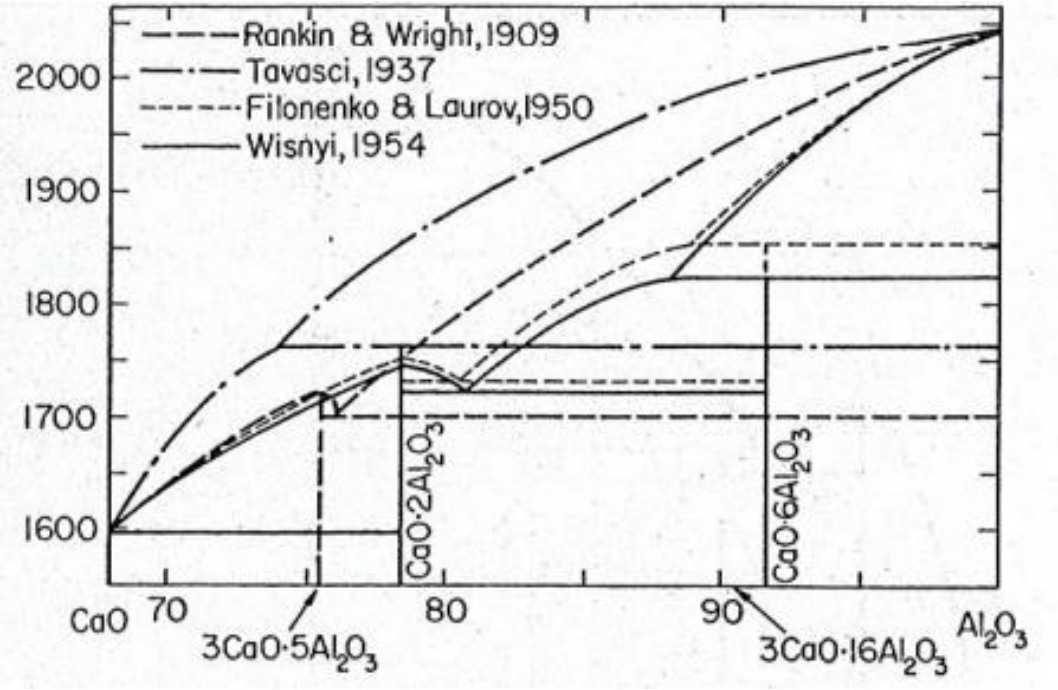

Fig. 60 : High Alumina portion in $CaO\text{-}Al_2O_3$. Comparison between various studies by L. G. Wisnyi, Doctor's thesis, Rutgers University, State University of New Jersey, New Brunswick, New Jersey, January 1955.

A private communication between Auriol, Hausser et *al* (1961) already predicted the CA and CA2 aluminates as incongruent melting compounds as shown in Fig. 61. Moreover, the temperatures of the invariants $CA6\text{-}Al_2O_3$-Liquid and CA2-CA6-Liquid are in agreement with the work of Jerebtsov and Mikhailov (2000), i.e. 8°C above the experimental measurements. Similarly, the peritectic melting temperature of CA is in agreement with those reported by Nurse et *al* (1965) and then Jerebtsov and Mikhailov (2000) some years later.

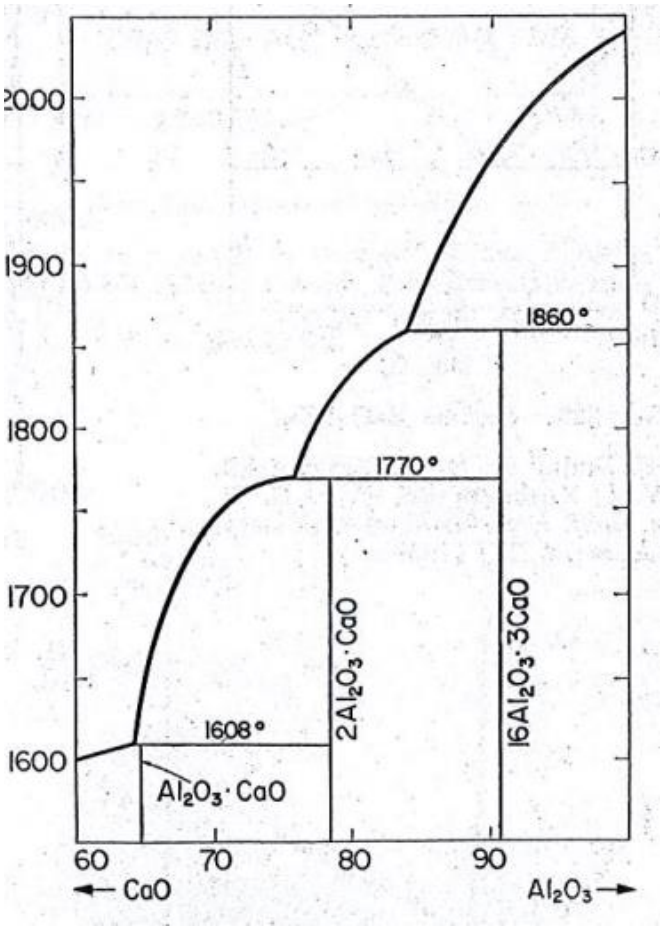

Fig. 61 : Part of the system $CaO\text{-}Al_2O_3$ from Phase diagrams for Ceramists: A. Auriol, G. Hauser, and J. G. Wurm, private communication, Nov. 19, 1961.

4.4 THERMODYNAMIC PROPERTIES

4.4.1 HEAT CAPACITY AND RELATIVE ENTHALPY

In our work, we measured the heat content values of CA6 and C5A3 by drop calorimetry. The lack of studies on heat contents and Cp measurements for these compounds does not allow us to compare the various data in the literature. However, the measurement techniques used by the authors, in particular calorimetry; make it possible to obtain precise and relevant values. The ΔH and Cp values reported in the literature for calcium aluminates are provided in Table 24.

Chemistry	Measurement	Temperature range (K)	Method of investigation	Sources
$Ca_3Al_2O_6$	Heat capacity	53.86→298.16	Calorimeter referred to Nernst Method.	King (1955)
$Ca_{12}Al_{14}O_{33}$	Heat capacity	53.89→298.16		
$CaAl_4O_7$	Heat capacity	53.50→298.16		
$CaAl_2O_4$	Heat capacity	53.52 →298.16		
$Ca_3Al_2O_6$	Relative enthalpy	373.6→1807.9	High temperature drop Calorimeter: platinum-rhodium capsules.	Bonnickson (1955)
$Ca_{12}Al_{14}O_{33}$	Relative enthalpy	394.4→1672.6		
$CaAl_2O_4$	Relative enthalpy	402.6→1800.2		
$CaAl_4O_7$	Relative enthalpy	403.7→1801.5		

Table 24 : Thermodynamic data for aluminates in the CaO-Al_2O_3 pseudo-binary.

4.4.2 HEAT OF FORMATION

Enthalpy of formation is a characteristic thermodynamic value determined experimentally for a wide range of chemical compounds. The calorimetric method is the most commonly used to determine these thermodynamic data. Two types of calorimeters are commonly used, namely isothermal, in which the temperature surrounding the calorimeter is kept constant. Various authors using the calorimetric method have measured the standard enthalpy of formation of aluminates experimentally. The study of the literature has enabled us to collect existing data (Table 25 & 26).

4.4.2.1$\Delta_f H°$ Referred to the elements

Coughlin (1956) measured the heat of formation of C3A, C12A7 and CA by calorimetric method in hydrochloric acid solution as solvent. For C3A and C12A7, Koehler et *al* (1961) found a more exothermic value than those of Coughlin (Coughlin, heats of formation of of crystalline CaO.Al2O3, 12CaO.7Al2O3 and 3CaO.Al2O3, 1956). This difference is mainly due to the standard heat of formation values of Al_2O_3 used by the authors. C3A calculated from experimental values by Eliezer et *al* (1981)

and corrected by heat capacity (Bonnickson, 1955) is in agreement with Koehler et *al* (1961) while the Materials Project database (using DFT calculations) reports more negative heat of formation (C3A and C12A7) than Coughlin et *al* (1956). For CA the literature data globally agree, but there is -18.3kJ.mole^{-1} difference between Coughlin (1956) and the Materials Project database. Discrepancies between CA2 heats of formations in Table 25 are mainly due to disagreement on the relevance of the reported experimental values. Indeed, Hemingway (1982) rejected the heat of formation reported by Eliezer et *al* (1981) and argued there was an error in Hess cycle applied by Koehler et *al* (1961), whereas Eliezer et *al* (1981) assumed that the error lies in original experiment. The other data in Table 25 were estimated (Eysel & Hahn, 1970) or calculated (MaterialsProject, s.d.). Regarding C5A3 the only value is reported by Materials project.

4.4.2.2$\Delta_f H°$ Referred to the oxides

Trofymluk et *al* (2005) measured the heat of formation of C12A7 as a function of oxygen content by solution drop calorimetry; the value obtained confirms Coughlin (1956) previous result. Similarly, the experimental heat of formation data for CA from literature agrees (Coughlin, 1956). Koehler et *al* (1961) determined the enthalpy of formation of CA2 from the heat of formation of gibbsite from α-Al_2O_3 and liquid water ($\Delta H°_f$ = 30.8±2.6KJ.mole^{-1} unpublished work of R. Barany one of the author) combined to overall calorimetric reaction. The result is 9.0 and 14.5kJ.mole^{-1} smaller than Coughlin (1956) and Geiger et *al* (1988), respectively. In addition, the error bar is quite large. As suggested by Eliezer (1970), this gap may be related to the original experiment. For CA6 the only experimental data is that measured at 1060K i.e. $\Delta H°_f$ = -33±9.7 KJ.mole^{-1} (Geiger et *al* 1988).

Phase	$\Delta H°_f$(kJ/mole)	Uncertainty (±)	Method of investigation	Sources
$Ca_2Al_2O_5$	-2970.7		Calculated from Materials Project	Materials Project
$Ca_3Al_2O_6$	-3617.0		Calculated from Materials Project	Materials Project
	-3587.6	2.8	Based on Coughlin (1956) heat measurement and mean heat of formation Al_2O_3 (α, corundum): -400,290±310 cale.mole^{-1} from Holley and Huber (1951) and -400,480±200 cale.mole^{-1}from Mah (1957)	Koehler et *al* (1961)
	-3587.8	3.0	Phase diagram CaO-$AlO_{1.5}$: obtained from phase equilibria correcting by using the heat capacity of Bonnickson (1955).	Eliezer et *al* (1981)
	-3557.4	5.2	Calorimeter : heat of solution measurement in hydrochloric acid as solvent (37.5% acid diluting in distilled water)	Coughlin (1956)
$Ca_{12}Al_{14}O_{33}$	-19611.1		Calculated from Materials Project	Materials Project
	-19430.2	12.9	Based on Coughlin (1956) heat measurement and mean heat of formation Al_2O_3 (α, corundum): -400,290±310 cale.mole^{-1} from Holley and Huber (1951) and -400,480±200 cale.mole^{-1}from Mah (1957)	Koehler et *al* (1961)
	-19374.01	23.4	Calorimeter : heat of solution measurement in hydrochloric acid as solvent (37.5% acid diluting distilled water)	Coughlin (1956)
$CaAl_2O_4$	-2321.3	2.1	Calorimeter : heat of solution measurement in hydrochloric acid as solvent (37.5% acid diluting distilled water)	Coughlin (1956)
	-2326.3	2.0	Phase diagram CaO-$AlO_{1.5}$: obtained from phase equilibria correcting by using the heat capacity of Bonnickson (1955)	Eliezer et *al* (1981)

	2326.2	1.5	Based on Coughlin (1956) heat measurement and mean heat of formation Al_2O_3 (α, corundum): -400,290±310 cale.mole^{-1} from Holley and Huber (1951)and -400,480±200 cale.mole^{-1}from Mah (1957)	Koehler et *al* (1961)
	-2339.6		Calculated from Materials Project	Materials Project
$CaAl_4O_7$	-4021.1		Calculated from Materials Project	Materials Project
	-3995.2	3.0	Phase diagram CaO-$AlO_{1.5}$: obtained from phase equilibria correcting by using the heat capacity of Bonnickson.	Eliezer et *al* (1981)
	-4023.8	4.8	Recalculated value from Koehler et *al* experiment data. The value is revised because the authors advanced that there are errors on the Hess cycle used by Koehler et *al.*	Hemingway (1982)
	3979.1	4.8	Solution calorimeter with 20.10w% hydrofluoric acid as the reaction medium.	Koehler et *al* (1961)
	-4007	5.2	High-temperature oxide melt solution calorimetry. Measurement performed in a Ni-block, Calvet type with eutectic mixture $(Li,Na)_2B_2O_4$ as solvent.	Geiger et *al* (1988)
$Ca_5Al_6O_{14}$	-8324.2		Calculated from Materials Project	Materials Project
$CaAl_{12}O_{19}$	-10614.9		Calculated from Materials Project	Materials Project
	-10605.2	10	Phase diagram CaO-$AlO_{1.5}$: obtained from phase equilibria correcting by using the heat capacity of Bonnickson (1955)	Eysel and Hahn (1970)
	-10813	20	Estimated value from relationship between heat of reaction and gram formula weight.	Hemingway (1982)
	-10722	12	High-temperature oxide melt solution calorimetry. Measurement performed in a Ni-block, Calvet type with eutectic mixture $(Li,Na)_2B_2O_4$ as solvent.	Geiger et al (1988)

Table 25 : Enthalpy of formation of calcium aluminates referred to the elements (298.15K).

Chemistry	dH°f(KJ/mole)	Uncertainty (±)	Method of investigation	Sources
$Ca_2Al_2O_5$	-28.10	3.8	Drop solution calorimetry with $2PbO.B_2O_3$ solvent at 978K.	Kojitani et *al* (2009)
$Ca_3Al_2O_6$	-6.7	1.38	Calorimeter : heat of solution measurement in hydrochloric acid as solvent (37.5% acid diluting in distilled waterc	Coughlin (1956)
	-7.2	1.7	Based on Coughlin [ref] heat measurement and mean heat of formation Al_2O_3 (α, corundum): -400,290±310 cale.mole^{-1} from Holley and Huber and -400,480±200 cale.mole^{-1}from Mah.	Koehler et *al* (1961)
$Ca_{12}Al_{14}O_{33}$	-79.4	11.1	Calorimeter : heat of solution measurement in hydrochloric acid as solvent (37.5% acid diluting in distilled water)	Coughlin (1956)
	-82.9	12.6	Based on Coughlin (1956) heat measurement and mean heat of formation Al_2O_3 (α, corundum): -400,290±310 cale.mole^{-1} from Holley and Huber (1951)and -400,480±200 cale.mole^{-1}from Mah (1957)	Koehler et *al* (1961)
	-79.4	4.4	High-Temperature drop-solution calorimetry at 1080K performed using a Tian-Calvet micro-calorimeter with molten $2PbO.B_2O_3$ as solvent.	Trofymluk et *al* (2005)
$CaAl_2O_4$	-15.40	1.46	Calorimeter : heat of solution measurement in hydrochloric acid as solvent (37.5% acid diluting in distilled water)	Coughlin (1956)

	-15.9	1.7	Based on Coughlin (1956) heat measurement and mean heat of formation Al_2O_3 (α, corundum): -400,290±310 cale.mole^{-1} from Holley and Huber (1951)and -400,480±200 cale.mole^{-1}from Mah (1957)	Koehler et *al* (1961)
	-16.90	1.04	Solution calorimetry with $2PbO.B_2O_3$ as solvent: calculated based on heat of solution measurement and CaO & Al_2O_3 unpublished data from Navrotsky and Coons, 1976.	Trofymluk et *al* (2005)
$CaAl_4O_7$	-20.9	4.7	High-temperature oxide melt solution calorimetry. Measurement performed in a Ni-block, Calvet type with eutectic mixture $(Li,Na)_2B_2O_4$ as solvent at 1060±10K.	Geiger et *al* (1988)
	-6.4	5.4	Solution calorimeter with 20.10w% hydrofluoric acid as the reaction medium	Koehler et *al* (1961)
$CaAl_{12}O_{19}$	-22.2	-	Calculated from two-sublattice model	Hallstedt (1990)

Table 26 : Enthalpy of formation of calcium aluminates referred to oxides (298.15K).

4.5 COMPONENT ACTIVITIES IN THE LIQUID PHASE

Sharman and Richardson (1961) measured the capacities of sulphides in a solution containing a mixture of CaO and Al_2O_3. From the data collected, the activities of CaO and Al_2O_3 were established at 1500°C. Work by Allibert et al also yielded composition-dependent activities of CaO and Al_2O_3 by mass spectroscopy at 1787°C (Allibert et *al* 1981). The experiment was first carried out in an induction furnace containing a block of Mo in which CaO and Al_2O_3 were placed. The mixture under He (gas) was heated above the melting point of Al_2O_3. The block was then heated in a vacuum spectrometer. Results from both works are given in the Table 27. We have gathered all the data from the available literature: calculated and measured.

Sources	Temperature (°C)	Method of investigation	xCaO (mole)	a(CaO)	a(Al_2O_3)
Alibert et *al* (1981)	1787	Mass spectrometer equipped with multi effusion cell containing homogenous melt of different composition. CaO satured melt and pure Al_2O_3 used as reference.	0.645	0.42	0.02
			0.578	0.2	0.05
			0.548	0.14	0.06
			0.495	0.082	0.2
			0.438	0.048	0.41
			0.414	0.04	0.25
			0.352	0.025	0.5
Sharma and Richardson, (1961)	1500.16	Gas & slag equilibrium technique: activities obtained from Sulphide capacities measurement containing CaO and Al_2O_3.	0.58	0.21	0.15
			0.6	0.25	0.115
			0.62	0.3	0.085
			0.64	0.38	0.06
			0.66	0.5	0.04
			0.68	0.67	0.025
			0.71	1	0.007

Table 27 : Component activities at 1787°C (Allibert, Chatillon, Jacob, & Lourtau, 1981) and 1500.16K (Sharma & Richardson, 1961).

4.6 STANDARD MOLAR GIBBS FREE ENERGIES OF FORMATION

Standard free energies of formation of the $CaO-Al_2O_3$ system were studied in the literature for the compositions CA3, C12A7, CA, CA2 and CA6; Gibbs free energy data are not available for C5A3. We have gathered various data for each composition in Tables (28-31). In order to compare the different data collected we have plotted the evolution of Gibbs energy as a function of temperature for each composition (Fig. 62-65). For C12A7 the Gibbs free energies were only measured by Allibert et *al* (1981), thus it is not possible to compare the data for this compound from other sources.

4.6.1 TRICALCIUM ALUMINATE: C3A

Table 28 gathers the Gibbs free energy of formation data of C3A. As the results plotted in Fig. 62 indicate, the data from Kumar et *al* (1985) are in agreement with Rog et al (1993). The data from Nagata et al (1989) are more negative than those from Popov et *al* (1979) and Rog et *al* (1993). When extrapolated to the temperature range of the other two authors we find a mean deviation of 2.51KJ. $mole^{-1}$. Although Allibert et *al* (1981) could not quantify the C3A data by EMF, the authors suggested the following equation: $\Delta G°=-1700-32.0T$ (±1500) $J.mole^{-1}$. This equation is based on Gibbs energies calculated from the properties of the liquid phase with an entropy compatible with the heat capacity data. The plot of the data from this equation reveals significant discrepancies with others experimental data.

4.6.2 MAYENITE: C12A7

For C12A7, Allibert et *al* (1981) measured the Gibbs free energy of formation by the EMF method. According to them, the results are probably not relevant due to the dissolution of the solvent CaF_2 in C12A7. Equation [17] was established based on thermochemical data (Allibert, Chatillon, Jacob, & Lourtau, 1981).

$$12/7CaO(s) + Al_2O_3(s) \rightarrow 12/7\ CaO.Al_2O_3\ (s) \quad [17]$$

$$\Delta G°= -12300-29.3T\ (\pm 2500)\ J.\ mole^{-1}$$

Dissolution of CaF_2 in C12A7 leads to the formation of a highly stabilised solid solution. As stated by Jeevaratman et *al* (1964), the O^{-2} ions are partially or totally replaced by univalent ions. The attractive inductive effect of fluorine enhances the

stability of C12A7, probably forming the compound $Ca_{12}Al_{14}O_{32}F_2$ (Allibert et *al* 1981). This stabilization effect results in very negative Gibbs energies.

4.6.3 MONOCALCIUM ALUMINATE: CA

Table 29 provides the Gibbs free energies of formation as a function of temperature. In Fig. 63, the data of Kumar et al are also in agreement with those of Rog et al. The data of both Allibert et al and Nagata et *al* (1989) are more negative than Kumar and Kay (1985) in the same temperature range. The mean differences between Allibert and Kumar then Nagata and Kumar are respectively 3.4KJ and 1.62KJ.mole^{-1}. In contrast to CA6 and CA2, the extrapolated data of Nagata et *al* (1989) are less negative than Allibert et *al* (1981). The CaF_2 solvent used by the authors can explain this discrepancy in values. Indeed, Allibert et *al* (1981) indicate the possibility of the formation of a ternary compound $3CaO.3Al_2O_3.CaF_2$, which can affect the EMF measurement results.

4.6.4 GROSSITE CA

CA2 Gibbs free energies of formation are given in Table 30 and plotted in Fig. 64. As in the case of CA6, the experiments of Kumar and Kay (1985) and Rog et al (1993) agree. The data from Allibert et *al* (1981) are more negative than Kumar and Rog et *al* (1993)by ~2 and ~2.3KJ.mole^{-1} respectively. Similarly, evolution of the Gibbs free energies of formation as a function of temperature reported by Nagata et *al* (1989) have an average deviation of 1.4kJ.mole^{-1} from those of Kumar and Kay (1985). However, extrapolating these data to low temperature shows a similarity with reported Gibbs free energy by Allibert et *al* (1981).

4.6.5 HIBONITE: CA6

The comparison of experimental Gibbs free energy data of CA6 formation shows some disagreement between the different authors. Allibert et *al* (1981)and Popov et *al* (1979) both used an EMF technique with CAF_2 as electrolyte; the difference between their experiments is mainly the nature of the reference electrodes used in the measurements. Indeed, Popov et *al* (1979) used a mixture of $Ca_{0.17}Zr_{0.83}O_{1.83}$ and $CaZrO_3$ under oxidising atmosphere as reference electrode while Allibert et al had CaO under air as reference electrode. Despite the experimental similarities, the temperature dependence of the Gibbs energy of the two studies are very different. The Gibbs

energies reported by Popov et *al* (1979) are more negative. The galvanic cell method in the presence of Ca Caβ"-alumina solid electrolytes was used by Kumar and Kay (1985) and Rog et al (1993), in both studies the reference electrodes were CaO/air and O_2 respectively. The Gibbs energy curves of the two studies overlap over the common temperature range of 827°C to 927°C. Kumar and Kay (1985) are ~0.37KJ.mole^{-1} more negative than Rog et *al* (1993), and extrapolating data to higher temperatures, both studies remain in agreement. Nagata et *al* (1989) used $4CaO.P_2O_5$ as a solvent in the galvanic cells, the Gibbs energy found to be less negative ~4KJ.mole^{-1}than Kumar and Kay (1985). Additionally, extrapolating Nagata et *al* (1989) curve, we find the result is in agreement with Allibert et *al* (1981).

Reactions	Temperature (K)	dG(J)=A-BT(K) [J.mol^{-1}]		Estimated error	Method	Sources
		A(J)	B(J/K)			
$3CaO+Al_2O_3 \rightarrow C3A$	1050-1320	-7818.6408	-29.4972	±836.8	Galvanic Cells using Caβ"-alumina solid electrolytes	Kumar and Kay (1985)
	1000-1200	-6530	-30.6	-	Galvanic Cells using Caβ"-alumina-CaF_2 solid electrolytes	Rog et *al* (1993)
	1373-1635	-11790	-28.27	±1190	Galvanic Cells using $4CaO.P_2O_5$	Nagata et *al* (1989)

Table 28 : Standard Gibbs free energy of C3A.

Reactions	Temperature (K)	dG(J)=A-BT(K) [J.mol^{-1}]		Estimated error (J)	Method	Sources
		A(J)	B(J/K)			
$CaO+Al_2O_3 \rightarrow CA$	1050-1500	-15113.026	-18.2004	±836.8	Galvanic Cells using Caβ"-alumina solid electrolytes	Kumar and Kay (1985)

	1373-1843	-17910	-17.38	±790	Galvanic Cells using $4CaO.P_2O_5$	Nagata et *al* (1989)
	1000-1200	-13980	-19	-	Galvanic Cells using Caβ"-alumina-CaF2 solid electrolytes	Rog et *al* (1993)
	923-1223	-18120	-18.61	±1800	EMF with CaF2 electrolyte	Allibert et *al* (1981)

Table 29 : Standard Gibbs free energy of CA.

Reaction	Temperature (K)	dG(J)=A-BT(K) [J.mol^{-1}]		Estimated error (J)	Method	Sources
		A(J)	B(J/K)			
$CaO+2Al_2O_3 \rightarrow CA2$	1100-1500	-12916.426	-26.74	±1255.2	Galvanic Cells using Caβ"-alumina solid electrolytes	Kumar & Kay (1985)
	1373-1873	-15650	-25.82	±900	Galvanic Cells using $4CaO.P_2O_5$	Nagata et *al* (1989)
	1000-1200	-11870	-27.5	-	Galvanic Cells using Caβ"-alumina-CaF_2 solid electrolytes	Rog et *al* (1993)
	923-1223	-16070	-25.7	±800	EMF with CaF_2 electrolyte	Allibert et *al* (1981)
	1260-1400	-18409.6	-18.78		EMF method with CaF_2 as electrolyte	Popov et al (1979)

Table 30 : Standard Gibbs free energy of CA2.

Reaction	Temperature (K)	dG(J)=A-BT(K) [J.mol^{-1}]		Estimated error (J)	Method	Sources
		A(J)	B(J/K)			
CaO(s)+6Al_2O_3(s) →CA6(s)	1100-1500	-17869.45	-39.3296	±836.8	Galvanic Cells using Caβ"-alumina solid electrolytes	(Kumar & Kay, 1985)
	1373-1873	-16380	-37.58	±1730	Galvanic Cells using 4CaO.P2O5	Nagata et *al* (1989)
	1000-1200	-15460	-41.1		Galvanic Cells using Caβ"-alumina-CaF_2 solid electrolytes	Rog et *al* (1993)
	923-1223	-17430	-37.2	±1500	EMF with CaF_2 electrolyte	Allibert et *al* (1981)
	1260-1400	-31380	-28.36752		EMF method with CaF_2 as electrolyte	Popov et al (1979)

Table 31 : Standard Gibbs free energy of CA6.

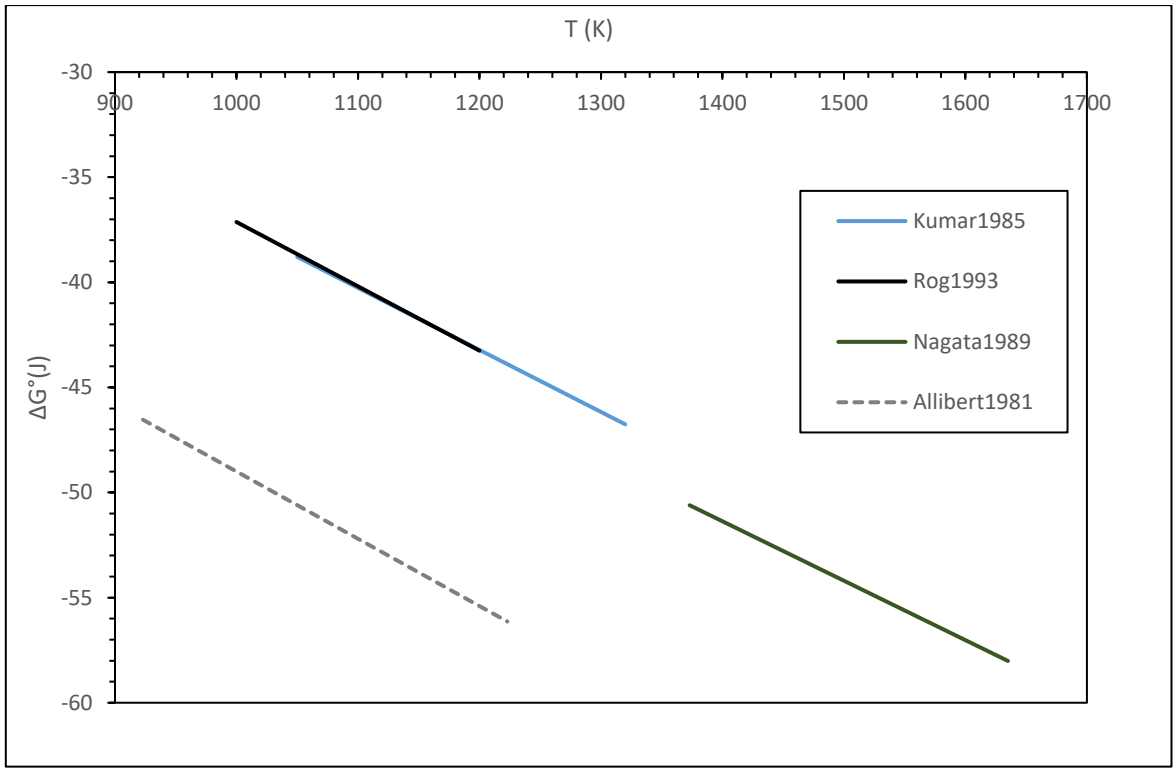

Fig. 62 : C3A Gibbs energy plotted in function of temperature.

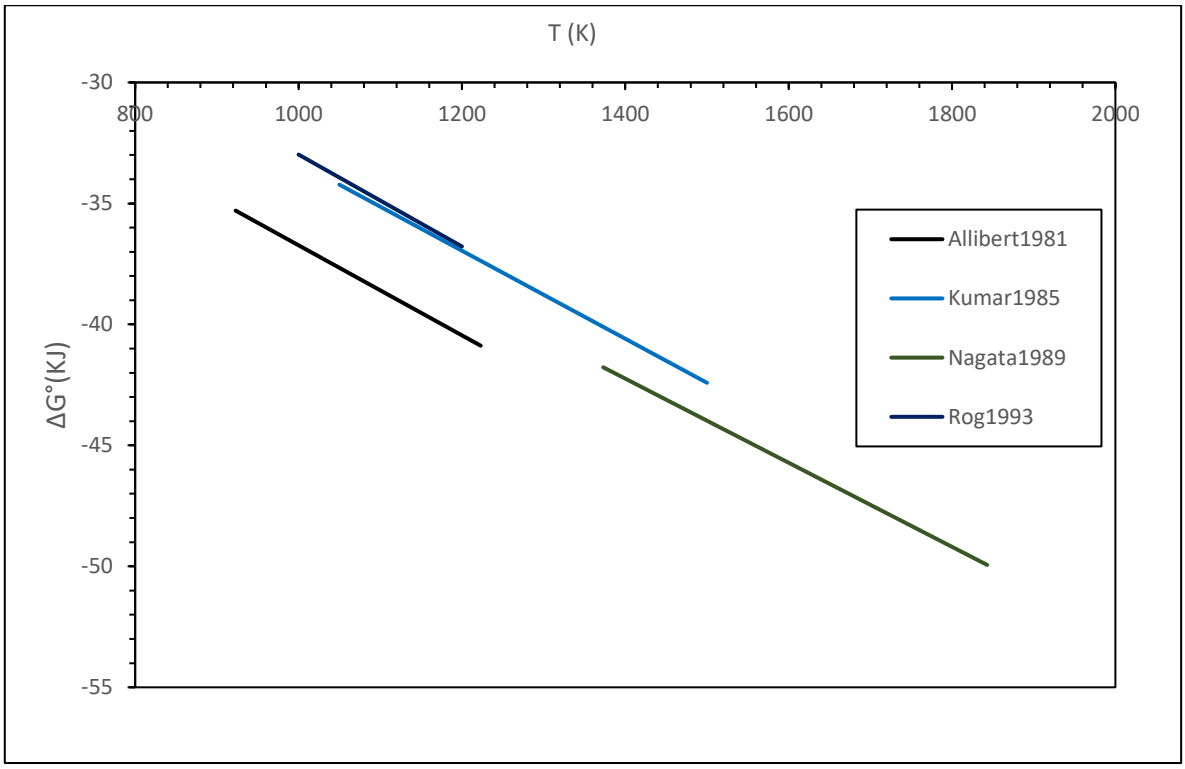

Fig. 63 : CA Gibbs energy plotted in function of temperature.

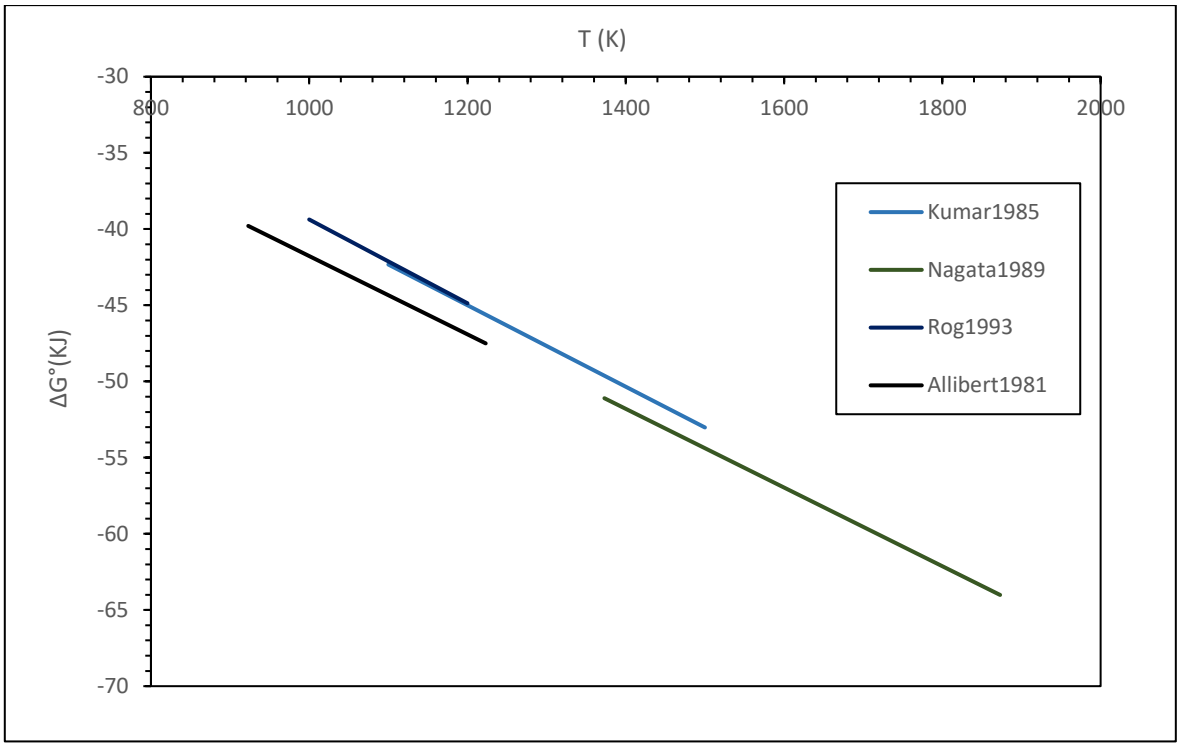

Fig. 64 : CA2 Gibbs energy plotted in function of temperature.

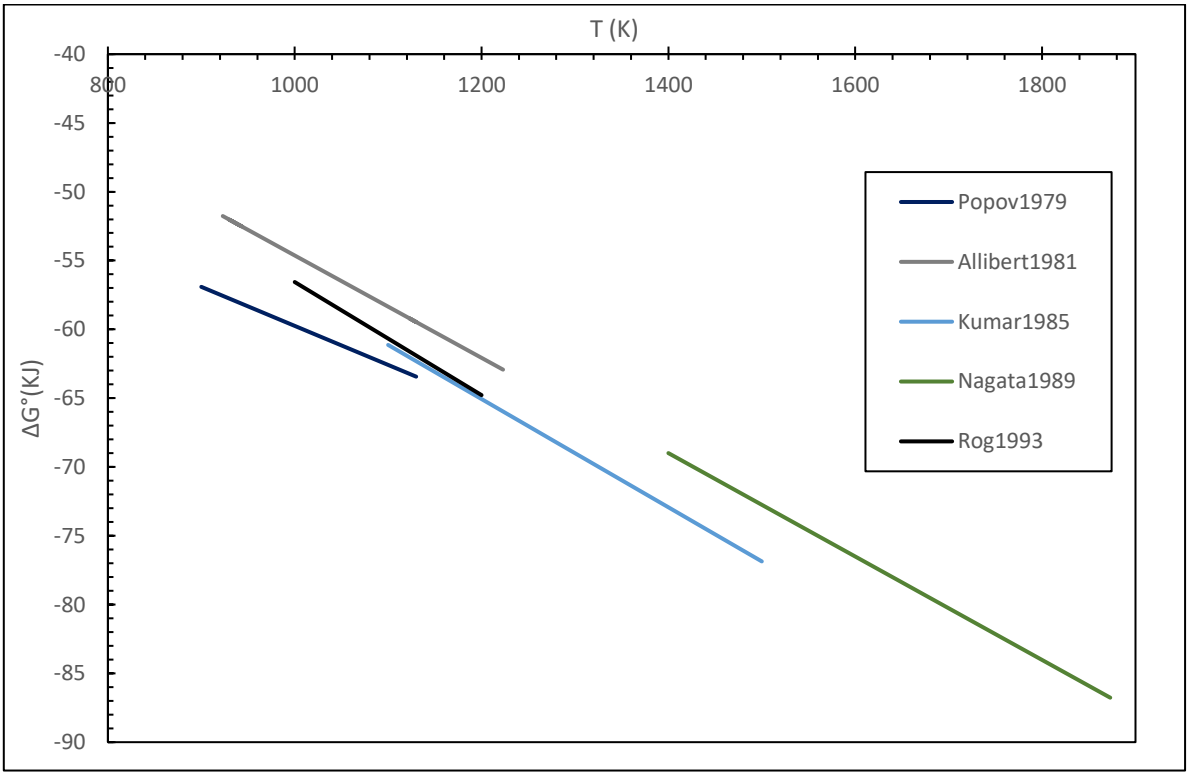

Fig. 65 : CA6 Gibbs energy plotted in function of temperature.

4.7 EXPERIMENTAL STUDIES OF ALUMINATES

4.7.1 SYNTHESIS AND CHARACTERISATION OF C5A3 AND CA6

The synthesis of C5A3 was done under argon in order to avoid the formation of C12A7, which is more stable in an oxidizing environment. A first synthesis with a heat treatment duration of 6h showed the formation of the first diffraction peaks attributed to a minority phase C5A3, two other phases corresponding to CA and C3A were also identified. During the synthesis of C5A3, the intermediate phases CA and C3A are formed first for kinetic reasons and then react according to the following equation: $2CaAlO_4 + Ca_3Al_2O_6 \rightarrow Ca_5Al_6O_{14}$. This synthesis is slow most likely due to a small difference in the enthalpy of reaction and a low driving force. After 48 H of reaction, a second X-ray analysis showed an increase in the diffraction peaks of the C5A3 phase. This confirms the slow nature of the reaction but also the thermodynamic stability of this compound. Finally, after 18 days of reaction combined with intermediate grinding every 24 to 48h of reaction, X-ray analysis allowed us to identify C5A3 as the major phase. However, two minor phases remain CA and C3A. The amounts of these two phases are too small to react to completion, and the distribution of these two phases seems to be inhomogeneous, which prevents the synthesis of a 100% pure sample.

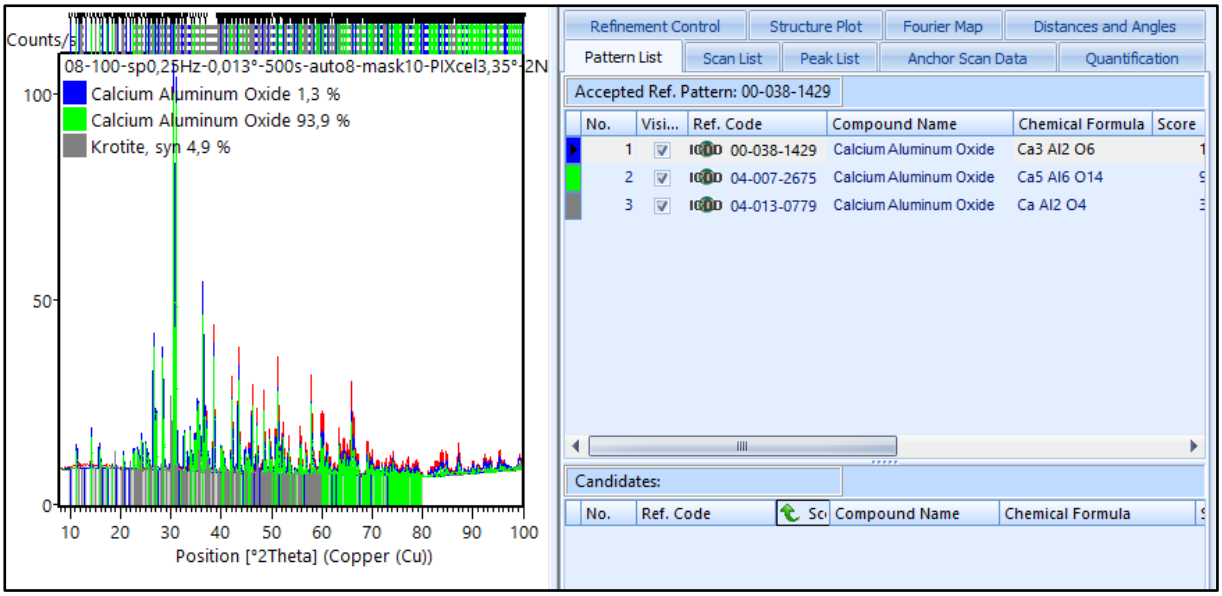

Fig. 66 : Quantitative estimation of phases obtained after $Ca_5Al_6O_{14}$ synthesis.

Fig. 67 shows the evolution of the major phase C5A3 as a function of reaction time. The quantification of the phase amounts was done using a Rietveld analysis and the HighScore software as shown in Fig. 66. The quantitative analysis of the constitutive phases of the synthesized material showed that we had reached 93.9% of C5A3, 1.3% C3A and 4.9% CA.

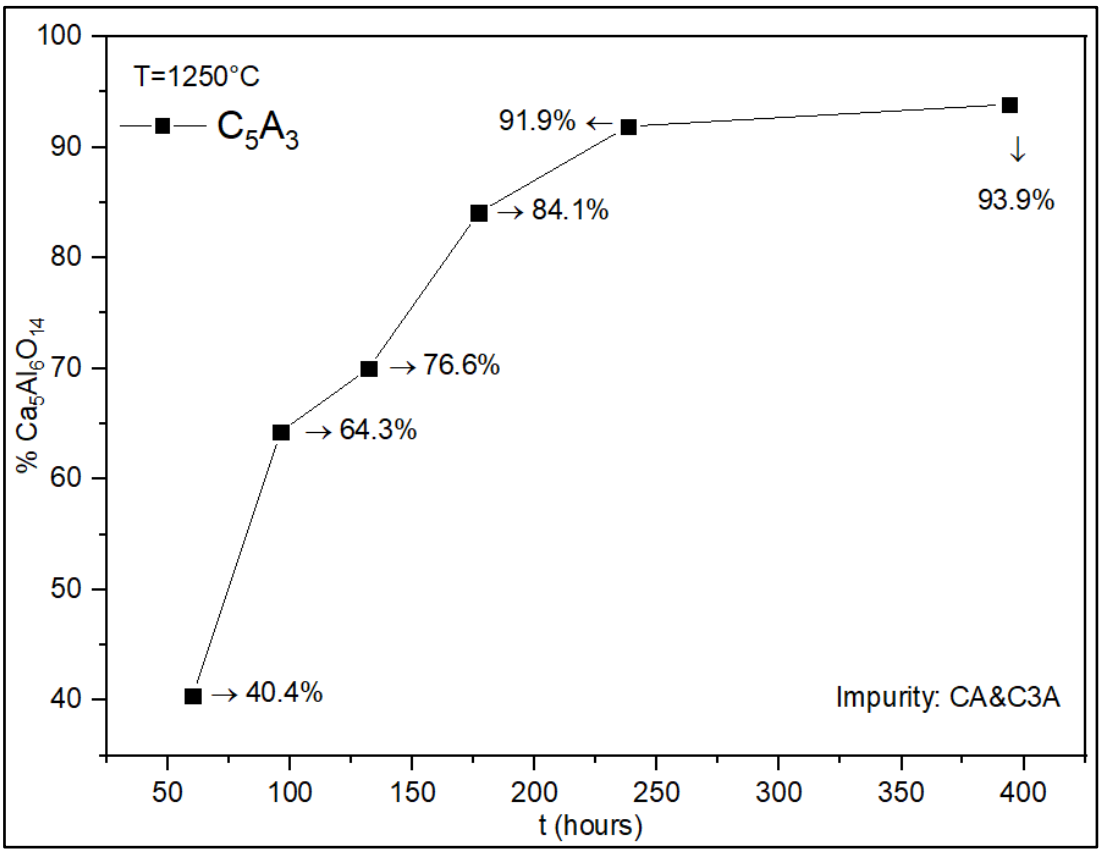

Fig. 67 : Evolution of $Ca_5Al_6O_{14}$ as main phase in function of time of sintering.

We did not obtain a pure CA6 phase either. There was additional CA2 phase and Al_2O_3 coexisting with the major phase. After a second thermal annealing, the CA2 phase totally reacted but there was still some Al_2O_3 which remained stable, knowing that the formation of CA6 is done according to the equation $CaAl_4O_7 + 4Al_2O_3 \rightarrow CaAl_{12}O_{19}$, it is thus admitted that the quantity of $CaAl_4O_7$ formed was not sufficient to react with the remaining Al_2O_3. We were able to quantify the percentage of Al_2O_3 by quantitative analysis on HighScore Fig. 68 and we obtained 12.2% Al_2O_3 as impurity.

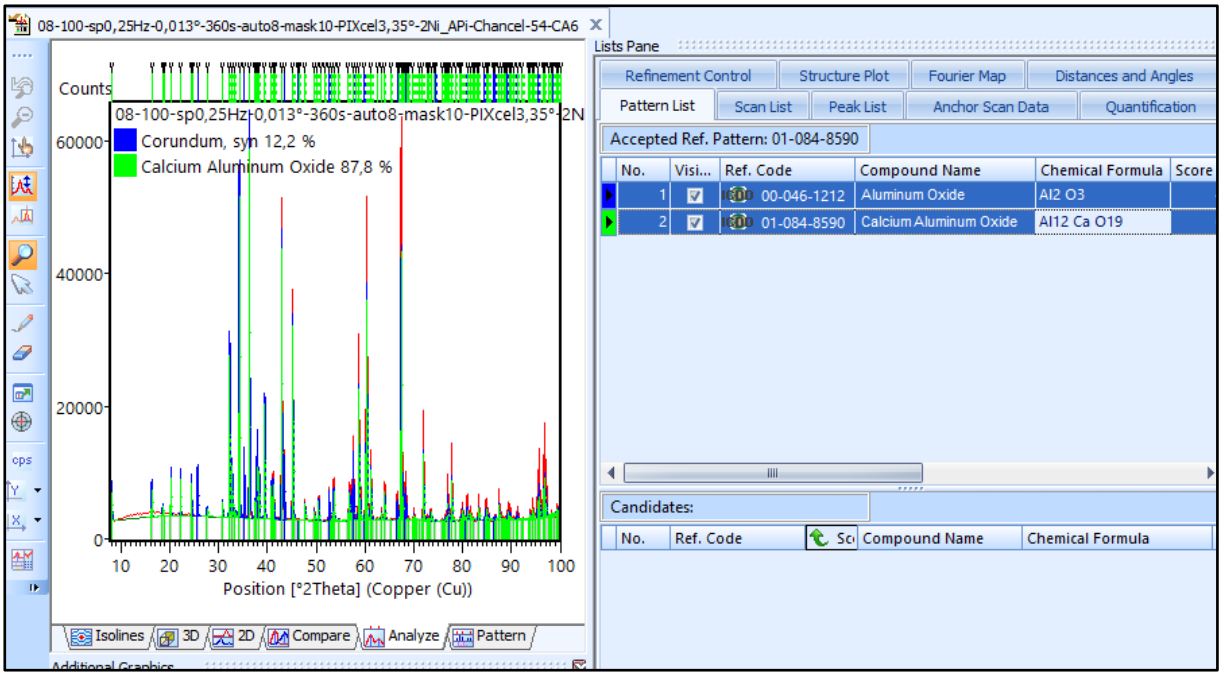

Fig. 68 : Quantitative estimation of phases obtained after $CaAl_{12}O_{19}$.

4.7.2 CRYSTALLOGRAPHIC DATA OF THE SYNTHESISED PHASE

The lattice parameters from the crystallographic analysis are given in Table 32. C5A3 crystallises in an orthorhombic lattice of space group $Cmc2_1$. The values of the crystallographic parameters of the major phase are in agreement with the literature (Aruja, 1957) (Vincent & Jeffery, 1978). The CA phase present in the material has similar structural characteristics to that of Horkner and Muller-Buschbaum (1976). Despite the presence of the minor phase Al_2O_3, the lattice parameters of the synthesised CA6 are in agreement with the literature (Utsunomiya et *al* (1988)).

	$Ca_5Al_6O_{14}$	$CaAl_{12}O_{19}$
Space group	$Cmc2_1$	$P6_3/mmc$
Lattice parameter a (Å)	11.281	5.559
Lattice parameter b (Å)	10.994	5.559
Lattice parameter c (Å)	10.306	21.902

Table 32 : Lattice parameters of $Ca_5Al_6O_{14}$ and $CaAl_{12}O_{19}$ synthesis compounds.

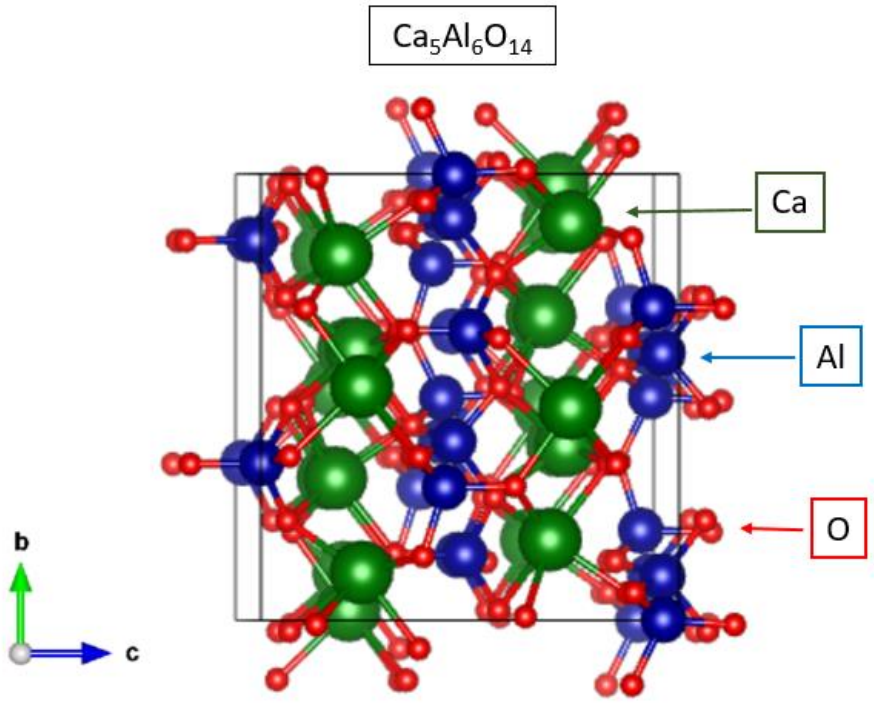

Fig. 69 : Crystallographic representation of $Ca_5Al_6O_{14}$.

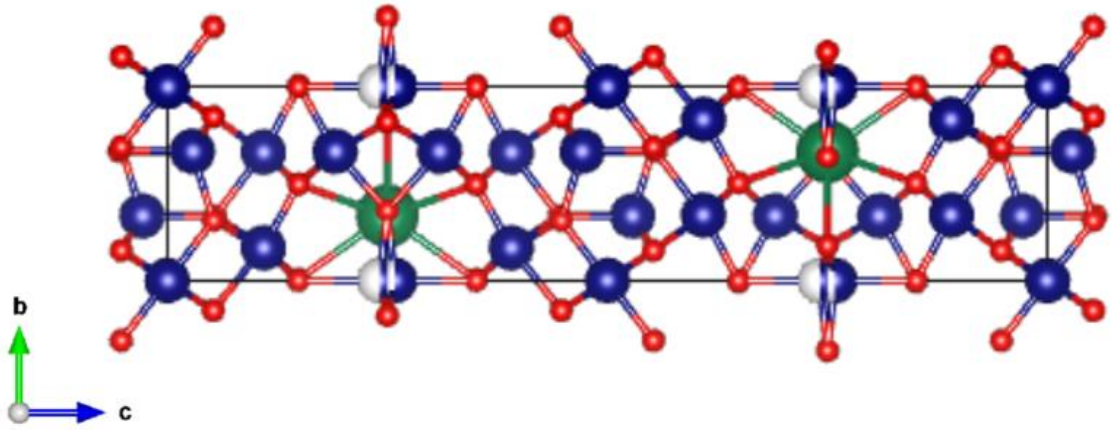

Fig. 70 : Crystallographic representation of $CaAl_{12}O_{19}$..

4.7.3 RELATIVE ENTHALPY MEASUREMENTS RESULTS

Table 33 summarises the results of measuring heat contents of C5A3. The values obtained are corrected using the enthalpies of CA and C3A as the compound has a purity of 93.9%. The measurements were carried out at five different temperatures from room temperature to the high temperature of measurement; the error on the values did not exceed 3%, Measurements on C5A3 are made with a 95%

confidence interval. Lack of thermodynamic description in the literature does not allow for comparisons between experimental and modelled values.

Relative enthalpy				
T	T	H_T-H_{298K}		u(ΔH)
°C	K	J.mol^{-1}	J.mol^{-1}	%
$Ca_5Al_6O_{14}$ (mol. wt. 586.28)				
799.66	1072.81	434459.97	13076.42	3.01
898.51	1171.66	489697.91	10738.37	2.19
998.72	1271.87	559500.72	8864.55	1.58
1099.26	1372.41	602791.62	11466.47	1.90
1198.03	1471.18	628306.37	13984.21	2.23

Table 33 : Relative enthalpy data from Drop calorimetry for $Ca_5Al_6O_{14}$.

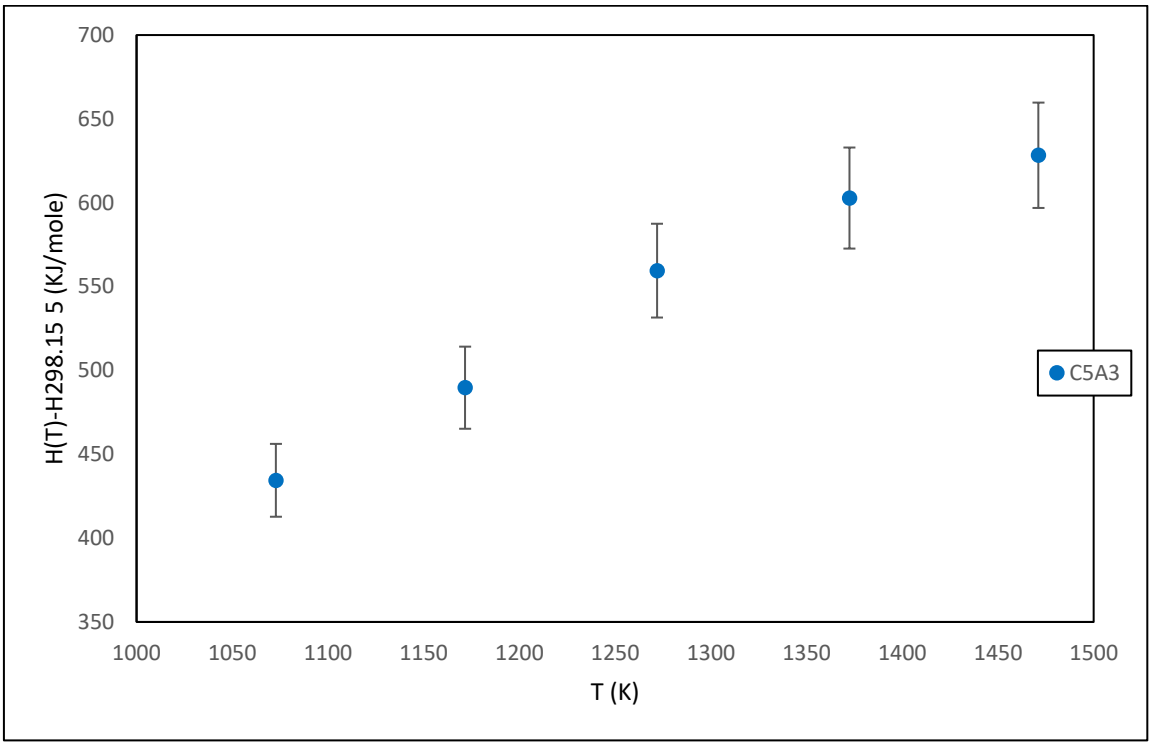

Fig. 71 : $Ca_5Al_6O_{14}$ Heat contents evolution in function of temperature.

As in the case of C5A3, the literature review highlighted a lack of thermodynamic data for CA6, including heat contents and Cp. The results of the CA6 heat content measurements are summarised in Table 34. Fig. 72 is a comparison of the

experimental values and the model described in the FTPs database. The measurements are done under the same experimental conditions as for C5A3. The experimental results confirm the estimated data as recorded in the FTPs database. The largest differences observed are 12.98 and 12.26KJ.mole^{-1} at temperatures of 798.25 and 1099.3°C, which represent 2.4 and 1.55% difference respectively.

Relative enthalpy				
T	T	H_T-H_{298K}		u(ΔH)
°C	K	J.mol^{-1}	J.mol^{-1}	%
$CaAl_{12}O_{19}$ (mol. wt. 668)				
798.25	1071.4	540485.80	37002.39	6.85
898.52	1171.67	630690.80	14907.19	2.36
999.25	1272.40	724678.83	20164.40	2.78
1099.30	1372.45	780197.91	15950.61	2.04
1198.03	1471.18	880310.10	36400.92	4.14

Table 34: Relative enthalpy data from Drop calorimetry for $CaAl_{12}O_{19}$.

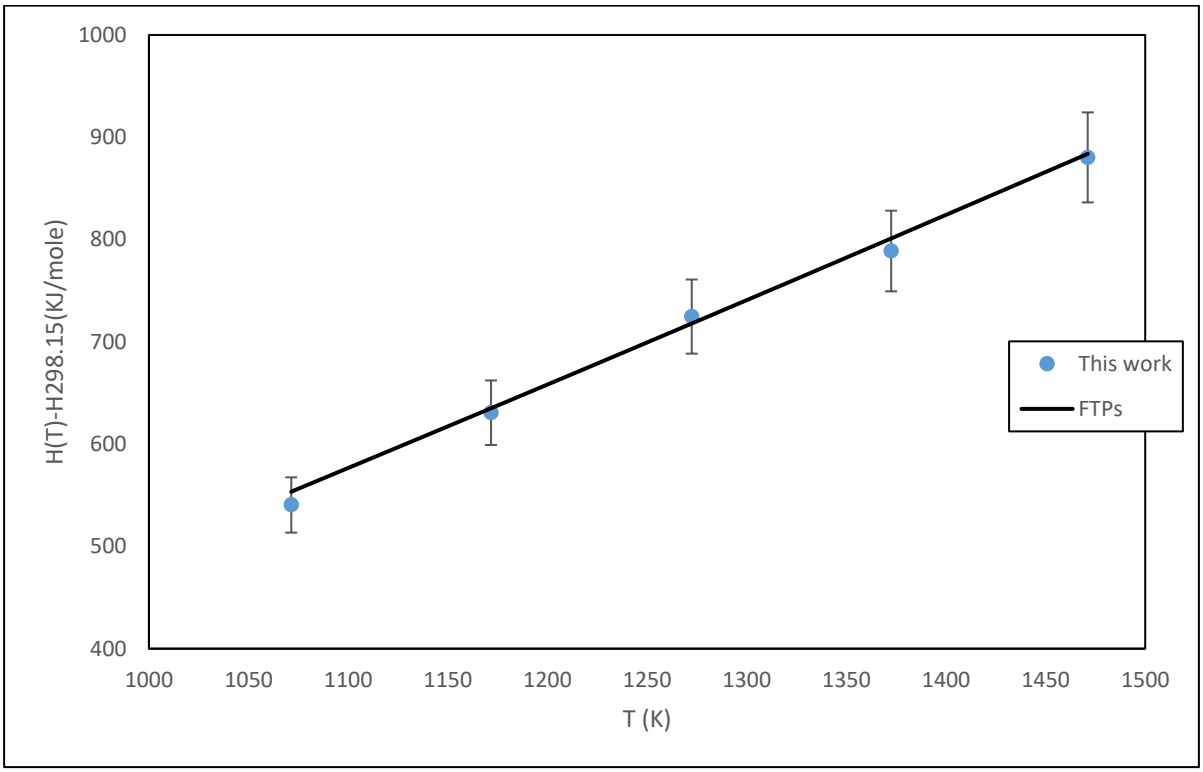

Fig. 72 : Comparison between measurement and FTPs database.

4.7.4 HEAT OF FORMATIONS MEASUREMENT

The standard heat of formation was measured using dissolution calorimetry by dissolving $Ca_5Al_6O_{14}$ and $CaAl_{12}O_{19}$ samples in the basic slag solvent used for $Ca_3Si_2O_7$ and Ca_2AlFeO_5. The obtained results are respectively presented in Fig. 73 and Fig.74.

Q_{diss} (25°C) = 957461.7 ± 71451.2 J.mole^{-1} heat of dissolution for $Ca_5Al_6O_{14}$.

Q_{diss} (25°C) = 984697.7 ± 34196.2 J.mole^{-1} heat of dissolution for $CaAl_{12}O_{19}$.

To calculate the enthalpy of formation we proceeded as follows: using the dissolution data for pure CaO and Al_2O_3 measured in chapter 1, the standard heat of formation can be calculated and the value is given by:

Δ_fH(25°C) = -123559.2 ± 73126.1 J.mole^{-1} for $Ca_5Al_6O_{14}$.

Δ_fH(25°C) = -15513.3 ± 37847.3 J.mole^{-1} for $CaAl_{12}O_{19}$.

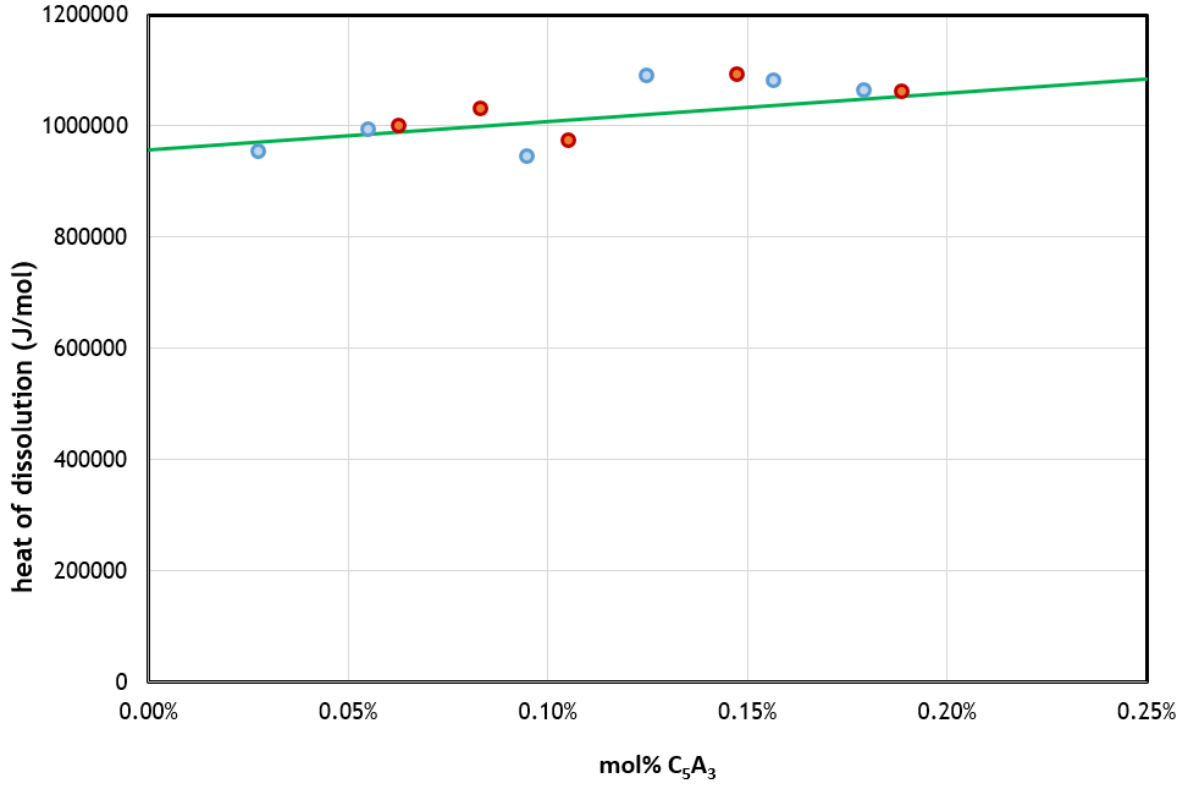

Fig. 73 : Heat of dissolution of C5A3.

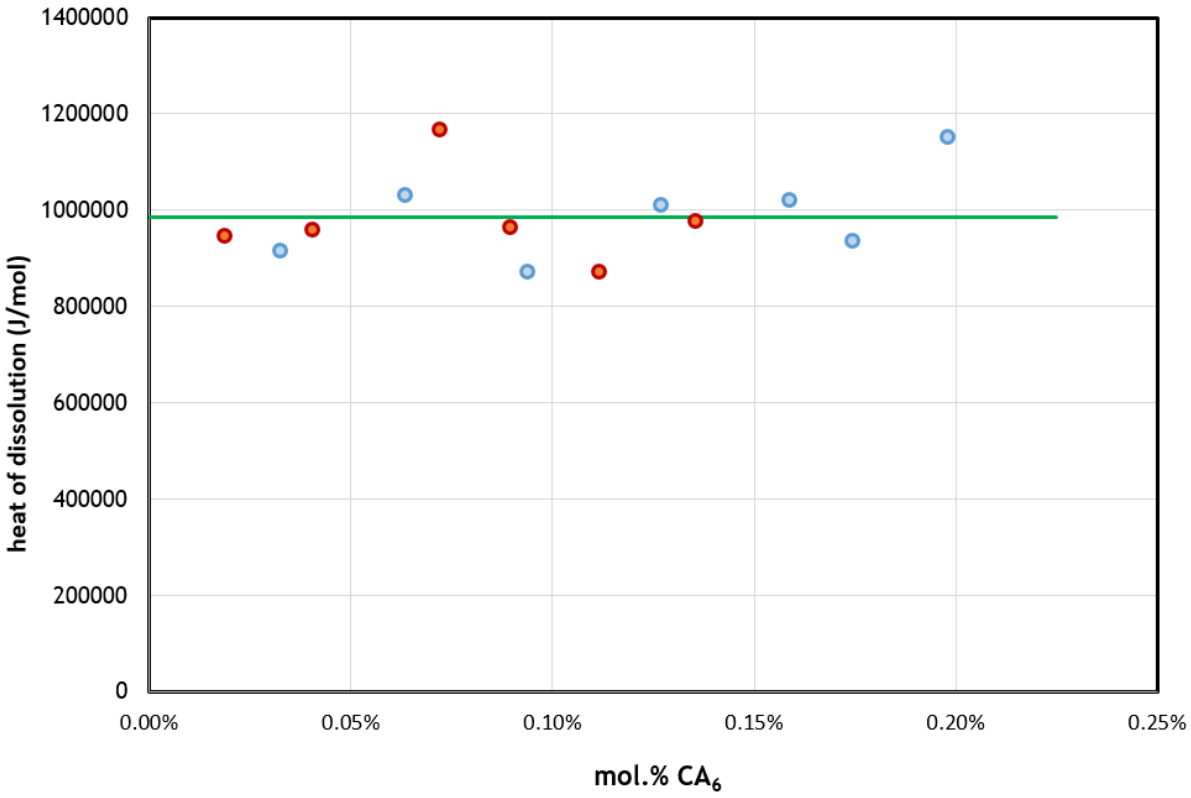

Fig. 74 : Heat of dissolution of CA6.

4.8 THERMODYNAMIC MODELLING

4.8.1 HEAT CAPACITY MODELLED

The heat contents of the aluminates (C12A7, C3A, CA2 and CA) were measured over a temperature range of 53.50 to 298.16K (1955); no other values above these temperatures are reported in the literature. However, Bonnickson (1955) measured heat contents above 298.16K on the above-mentioned aluminates, over a temperature range of 373.6 to 1807.9K. The modelling of heat capacities and the parameter optimization of the multiple Einstein model was carried out using the PARROT module of ThermoCalc. The experimental data used combined the low temperature heat capacity (1955) and the high temperature heat contents (Bonnickson, 1955). For this work 3 Einstein temperatures were used for the description of the heat capacities and we added a polynomial function to take into account the anharmonic contributions at high temperature. The thermodynamic description of aluminates is valid from 0K by extrapolation to the melting temperature of each modelled solid.

Chemistry	Θ_1	Θ_2	Θ_3	α_1	α_2	α_3	a_1	a_2
C12A7	1156.49	502.74	206.20	15.80	27.05	16.15	1.15E-01	-
C3A	1020.131	480.050	195.44	2.74	5.31	2.96	1.16E-02	-
CA2	1109.65	508.76	209.97	4.69	4.65	2.66	1.03E-02	-
CA	1047.39	458.84	178.70	2.75	2.73	1.52	1.32E-03	4.24E-06

Table 35: Einstein and polynomial parameters from room temperature to melting point.

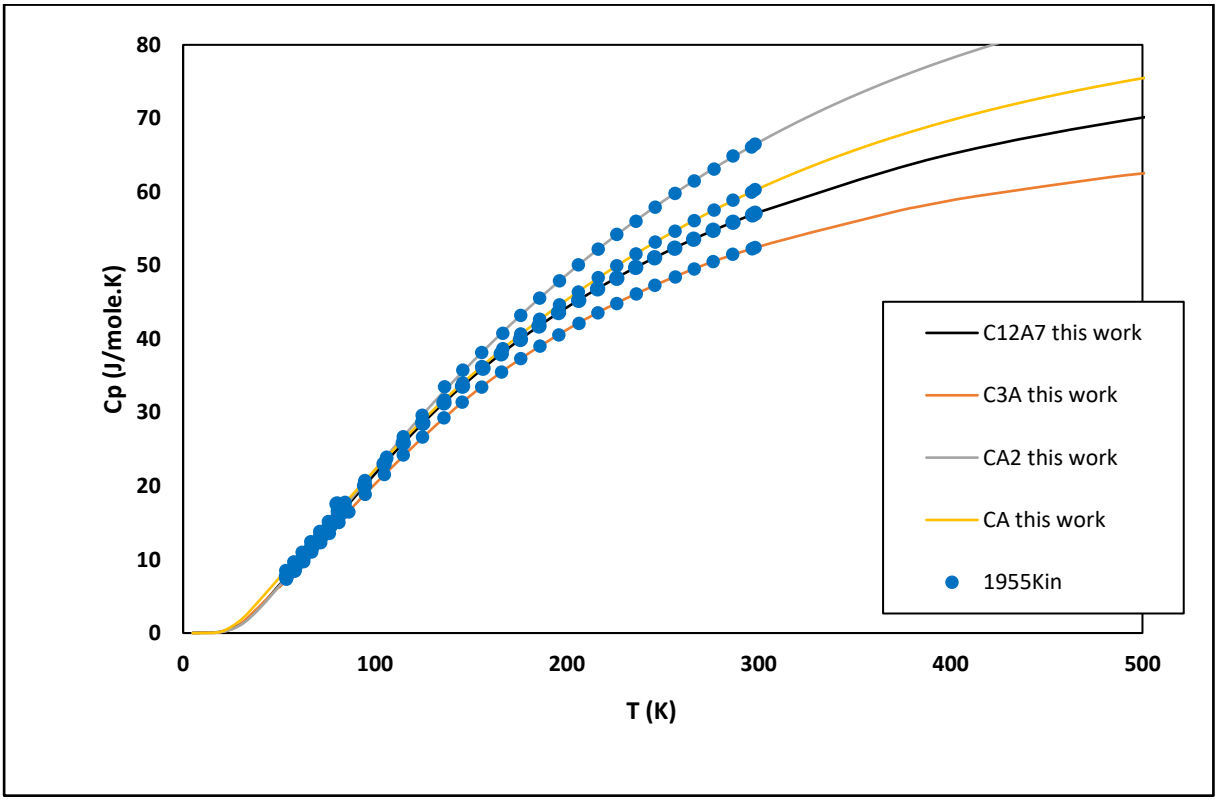

Fig. 75 : Calcium Aluminates modelled heat capacity compared with literature (1955) normalized to 1 mole of oxide.

4.8.2 HEAT CONTENTS CALCULATED

The thermodynamic description of the heat capacities of aluminates is in agreement with the experimental values of King (1955) at low temperature. In order to verify the validation of the high temperature model, we calculated the heat contents using the heat capacities from the high temperature model. The calculated heat content values are plotted in Fig. 76. The data are in agreement with the experimental values of Bonnickson (1955). The proposed model is therefore valid from low temperature to the melting temperature of the studied aluminates. The evolution of the energy values (Cp and ΔH) are closely linked to the stoichiometry of the compound. Its Alumina-rich compositions increase the amount of heat: ΔH (CA2)> ΔH (CA)> ΔH (C12A7)> ΔH (C3A). As mentioned before, the fitting parameters a_1 and a_2 ensure the continuity of the optimized data at high temperatures. The choice of a reduced number of parameters also ensures the reduction of the standard error of the parameters estimated by optimization. The modelling of C3A, CA2 and C12A7 required only one a_1 parameter, but we added an a_2 parameter for a more accurate optimization of CA. The results obtained in Fig .74 are in full agreement with the experimental values from literature.

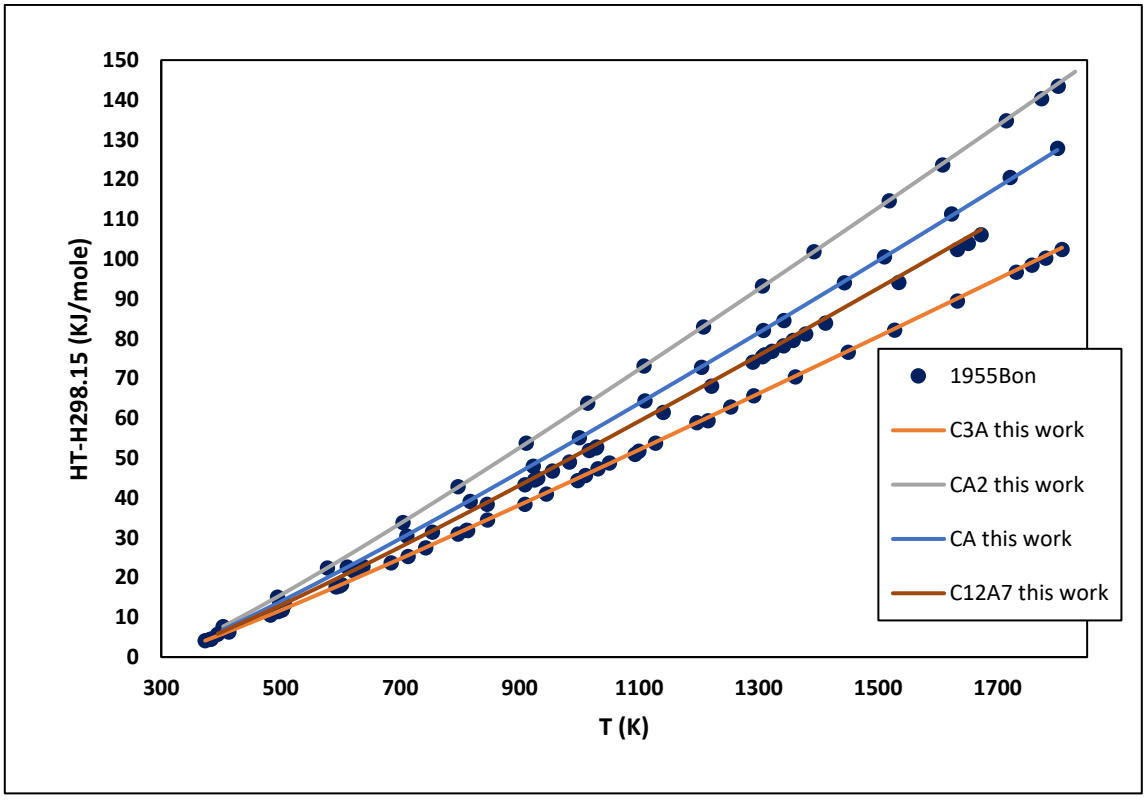

Fig. 76 : Modelled heat content of calcium aluminates compared with the literature data (Bonnickson, 1955) normalized to 1 mole of oxide.

4.9 PHASE DIAGRAM COMPUTED

A new phase diagram based on the 3rd generation CALPHAD functions combined with the associate model to describe the liquid phase was computed. The pure CaO description is based on the evaluation of Deffrennes et *al* (2020). The alumina-rich liquid data are in agreement with the model; the shape of the CaO-rich liquid is related to the effects of the associate and shows a discrepancy with the experimental data. Nevertheless, this simple description is sufficient. For CA6, the heat capacities used for the modelling are the ones derived from Haas et al (1981) as they agree well with our measurements. We have measured the relative enthalpies but low temperature Cp experimental data is missing. For C5A3 the experimental data are not enough for a complete thermodynamic description of this phase.

G_{Liquid} (C, C3A, A):

G_{Liquid} (C, C3A, A):

$G_C = 2 * G_{CaO}^{Liquid}$ based on (Deffrennes et *al* (2020).

$G_A = 2.5 * G_{Al_2O_3}^{Liquid}$

$G_{C3A} = 6 * G_{CaO}^{Liquid} + 5 * G_{Al_2O_3}^{Liquid} - 150000$

$L_{Liquid,A,C;0} = -111284 + 3.87532 * T$

$L_{Liquid,A,C3A;1} = -360702 + 54.0135 * T$

$L_{Liquid,C,C3A;0} = -89679.7 + 69.9359 * T$

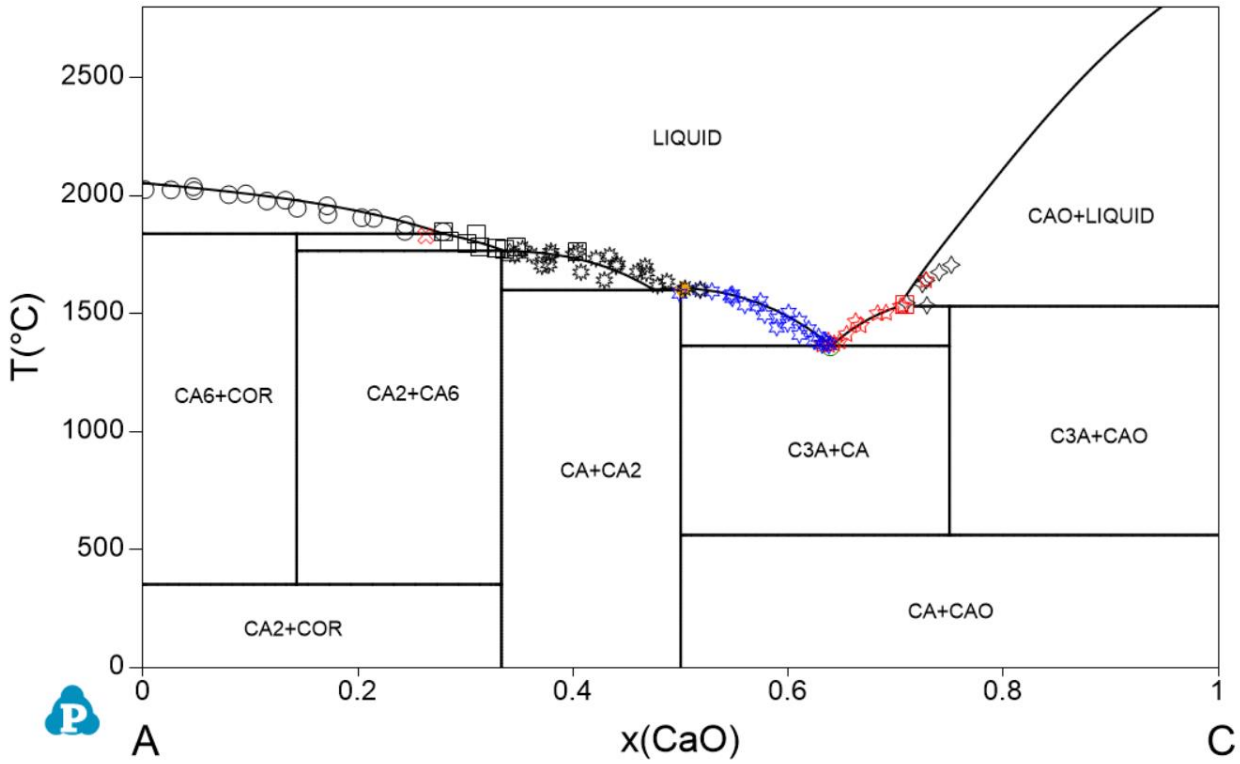

Fig. 77 : Calculated CaO-Al_2O_3 phase diagram computed with experiments data from Nurse et al (1965), Jerebtsov and Mikhailov (2000), Wisnyi (1955) and Rolin and Pham (1965).

		T(°C)	
Invariant	This study	Nurse et *al* (1965)	Jerebtsov and Mikhailov (2000)
CaO+Liquid→C3A	1531.7	1539	1540
C3A+CA→Liquid	1364.0	1360	1361
CA2+Liquid→CA	1600.4	1602	1604
CA6+Liquid→CA2	1766.6	1762	1762
Al_2O_3+Liquid→CA6	1839.3	1830	1852

Table 36: Invariant melting point from this study and assessment.

Chemistry	$S_{298.15}$ (J/(mol.K)	
	This work	King (1955)
$Ca_3Al_2O_6$	202.5	205.4
$CaAl_2O_4$	112.9	114.2
$CaAl_4O_7$	174.9	177.8
$CaAl_{12}O_{19}$	388.9	-

Table 37: Standard entropy for the calcium aluminates as compared to values from King (1955).

We have plotted activities of as a function of Al_2O_3 and CaO composition. The areas in which the activities are constant indicate two-phase field. In the single-phase areas, i.e. for stoichiometric solids, the activities decrease along a horizontal curve. Activity of Al_2O_3 is one for x (CaO) = 0 since is pure compound at this temperature and is used as reference state. Additionally, the value of Al_2O_3 activity decrease until zero at x (CaO) = 1.

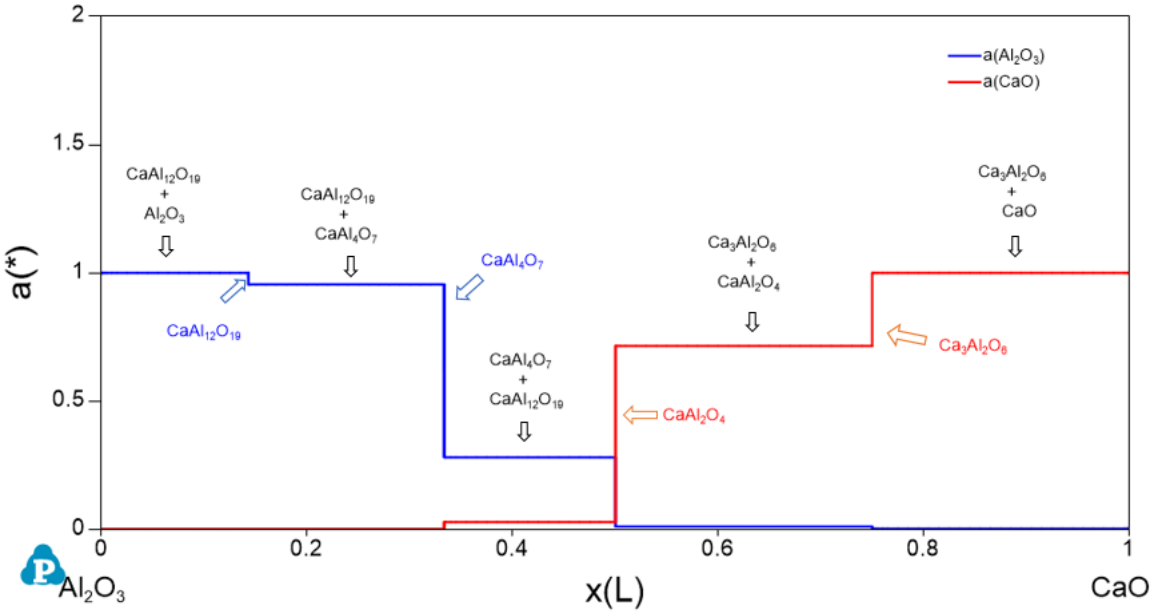

Fig. 78 : Activity at 1000°C in relation to the composition.

4.10 CONCLUSION

In this section, we have critically evaluated the literature and highlighted a certain lack of thermodynamic data, especially on CA6, but also an absence of experimental data on C5A3. The formation of C5A3 requires a neutral gas atmosphere to avoid the formation of C12A7. The reaction is slow due to the small enthalpy of reaction difference with respect to CA and C3A and the compound obtained contains these two secondary phases. Both aluminates were synthesized and the relative enthalpies measured. The literature review allowed us to propose a phase diagram based on the associated model and 3rd generation CALPHAD function. Subsequently, it is expected to measure the heat capacities of the aluminates in order to re-examine the phase diagram.

5 GENERAL CONCLUSION

Increasing greenhouse gas pollution is a global concern. The Kyoto Protocol of 1997, which entered into effect in 2005, aims to reduce emissions of the six greenhouse gases CH_4, N_2O, HFCs, PFCs, SF_6 and CO_2. The latter is particularly produced by the cement industries, whose overall pollution of the sector accounts for 8% of emissions into the air. Since the implementation of the near zero emission policy by the year 2050, the cement industries are investing in research and development to reduce the carbon footprint effects of cement production. As limestone ($CaCO_3$) is the major CO_2-producing element in the cement industry, one of the solutions is to find an alternative to produce cements with low limestone content. A thorough knowledge of the thermodynamic properties of the key oxides contained in Portland clinkers allows a better understanding of the physico-chemical processes and stability of the major constituents of Portland cement. Reliable experimental data and modelling using the CALPHAD approach allows the complex clinker formation process to be modelled and the process to be optimised. For this purpose, it is necessary to build up a high quality database based on experimental measurements of the various oxides constituting clinker (raw material used for cement manufacture). In this thesis, we focused on the thermodynamic properties study of Belite (C2S), Rankinite (C3S2), Alumino-ferrite (C4AF) and selected calcium aluminates (CA6, C5A3). Measurements of the enthalpy

of formation, relative enthalpy and melting point of these oxides provide new data that can be used to predict the formation and properties of clinkers.

For Belite, the relative enthalpy data of the γ, α' α,- Ca_2SiO_4 polymorphs complement those of β- Ca_2SiO_4 measured by Coughlin (reference). Similarly, the transition temperatures are consistent with data reported in the literature. By studying Rankinite, we were able to measure relative enthalpies not reported in the literature and to confirm the melting point of this compound. For C4AF, the enthalpies of formation and relative enthalpies of the solid solution were measured for the first time and will be the subject of a future article. The synthesis of C5A3 resulted in a 93.9% pure compound, it is difficult to go beyond this percentage given the slow kinetics linked to the low enthalpy of reaction, moreover the conditions of synthesis require an inert gas environment to avoid any formation of C12A7. Nevertheless, we were able to measure the first relative enthalpies on this compound. The study of CA6 allowed us to measure the relative enthalpies mainly, which also contributes to enrich the database of the oxides of the C-A system. We were also able to model the heat capacities of the aluminates CA, CA2, C3A and C12A7 from the low-temperature Cp and then to compute the Gibbs energy dependence as a function of temperature.

One of the major challenges encountered during this thesis was the time constraint. Indeed, the Covid-19 confinement has affected the progress of the work, from an experiment point of view, some experiments have been rescheduled. Practical training on the use of the SEM, for example, was cancelled. We also started the study of the solubility limits of minor elements such as MgO in C3A but due to time constraints, these results could not be fully exploited. Similarly, it was planned to measure the heat capacities of C5A3 and CA6, but unfortunately, this could not be done due to delays in the delivery of the equipment planned for this experiment. As a continuation of this work, it would be interesting to complete the missing thermodynamic data and to produce a complementary phase diagram of the C-A system including these missing data. The introduction of C5A3 in the quasi-binary C-A section would be a first, as in all the phase diagram models reported in the literature this phase has always been excluded. It would also be interesting to study the premelting effects of C3S2 on the heat capacities and to measure the enthalpy. Concerning the $Ca_{12}Al_{14}O_{32+x}$ solid solution, the stability of this phase could have been studied as a function of the quantity of oxygen and the quantity of OH^- measured in

case of synthesis in a free-moisture environment and the melting point of this phase could have been re-evaluated. The work presented in this manuscript nevertheless brings new data of primary importance in the study of the major constituents of Portland clinker. However, it is planned to write articles on the results obtained on C4AF solid solution and the C-A system. In spite of these undesirable points outside of our control, through these three years of work, we were able to contribute in a non-negligible way to the conception of a solid database and open new perspectives on future work that will be carried out in the laboratories in order to complete this preliminary work.

REFERENCES

Abdul, W., Mawalala, C., Pisch, A., & Bannerman, M. N. (2022). CaO-SiO_2 Assessment: 3rd generation modelling of thermodynamic properties. *Submitted article*.

Aggarwal, P. S., Gard, J. A., Glasser, F. P., & Biggar, G. M. (1972). Synthesis and Properties of Dicalciumm Aluminate, 2CaO.Al_2O_3. *Cement and Concrete Research, 2*, 291-297.

Agrell, S. O., & Gay, P. (1961, March 4). Kilchoanite, a Polymorph of Rankinite. *Nature*, 743.

Allibert, M., Chatillon, C., Jacob, K. T., & Lourtau, R. (1981). Mass-Spectrometric and Electrochemical Studies of Thermodynamic Properties of Liquid and Solid Phases in the System CaO-Al_2O_3. *J. Am. Ceram. Soc., 64*(5), 307-314.

Aruja, E. (1957, December 24). The Unit Cell of Orthorhombic Pentacalcium Trialuminate 5CaO.3Al2O3. *Acta Cryst., 10*, 337.

Auriol, A., Hausser, G., & Wurm, J. G. (1961, November 19). Part of the system CaO-Al_2O_3 phase diagrams for Ceramists. *Private communication*.

Ayed, F., Sorrentino, F., & Castanet, R. (1993). Determination par calorimetrie de dissolution des enthalpies de formation de quelques silicates, aluminates et alumino-silicates de calcium. *Journal of Thermal Analysis, 41*, 755-766.

Bajenova, I., Khvan, A., Dinsdale, A., & Kondratiev, A. (2020). Implementation of the extended Einstein and two-state liquid models for thermodynamic description of pure SiO_2 at 1 atm. *Calphad, 68*, 1-21. doi:https://doi.org/10.1016/j.calphad.2019.101716

Ball, R. G., Mignanelli, M. A., Barry, T. I., & Gisby, J. A. (1993). The calculation of phase equilibria of oxide core-concrete systems. *Journal of Nuclear Materials, 201*, 238-249.

Barbier , J., & Hyde, B. G. (1985, July). The structures of the Polymorphs of Dicalcium Silicate, Ca2SiO4. *Acta Cryst., B41*, 383-390.

Benz, R., & Wagner, C. (1961, August). Thermodynamics of the solid system CaO-SiO_2 from electromtive force data. *J. Phys. Chem., 65*, 1308-1311.

Bertaut, E. F., Blum, P., & Sagnières, A. (1959). Structure du Ferrite Bicalcique et de la Brownmillerite. *Acta Cryst., 12*, 149-159.

Bonnickson, K. R. (1955). High temperature heat contents of aluminates of calcium and magnesium. *J. Phys. Chem, 59*, 220-221.

Bouhifd, M. A., Gruener, G., Mysen, B. O., & Richet, P. (2002, August). Premelting and calcium mobility in gehlenite ($Ca_2Al_2SiO_7$) and pseudowollastonite ($CaSiO_3$). *Phys Chem Minerals, 29*, 655-662. doi:DOI 10.1007/s00269-002-0276-0

Boyko, E. R., & Wisnyi, L. G. (1958, March 21). The optical properties and structures of $CaO.2Al_2O_3$ and $SrO.2Al_2O_3$. *Acta cryst., 11*, 444.

Boysen, H., Lerch, M., Stys, A., & Senyshyn, A. (2007, June). Structure and oxygen mobility in mayenite ($Ca_{12}Al_{14}O_{33}$): a high-temperature neutron powder diffraction study. *Acta Cryst.*, 675–682.

Bredig, M. A. (1950, June). Polymorphism of Calcium Orthosilicate. *Journal of The American Ceramic Society, 33*, 188-192.

Brunauer, S., Kantro, D. L., & Weise, C. H. (1956, August). The heat of decomposition of tricalcium silicate into β-dicalcium silicate and calcium oxide. *The Journal of Physical Chemistry, 60*(6), 771-774.

Büssem, V. W., & Eitel, A. (1936). Die Struktur des Pentacalciumtrialuminats. *Zeitschrift für Kristallographie, 95*(1-6), 175-188.

Carlson, E. T. (1931). The decomposition of tricalcium silicate in the temperature range, 100°-1300°C. *US. Bureau of Standard Journal of Research, 7*, 893-902.

Chan, C., Kriven, W. M., & Young, J. F. (1988). Analytical Electron Microspic Studies of Doped Dicalcium Silicates. *J Am Ceram Soc., 71*, 713-719.

Chase, M. W., Ansara, I., Dinsdale, A., Eriksson, G., Gremwall, G., Hglund, L., & Yokokawa, H. (1995). Thermodynamic models and data for pure elements and

other enmembers of solutions. (E. S. Ltd, Ed.) *Calphad, 19*(4), 437-447. doi:https://doi.org/10.1016/0364-5916(96)00002-8

Chromy, S. (1967). High-Temperature Microscopic Investigation of Tricalcium Silicate and Dicalcium Silicate Phases in Portland Cement Clinker. *J. Amer. Ceram. Soc.*, 677-680.

Cockayne, B., & Robertson, D. S. (1964). Calcium aluminate single crystals: growth, lattice parameters and transmittance. *Solid State Communications, 2*, 359-360.

Colville, A. A., & Geller, S. (1971). The Crystal Structure of Brownmillerite, Ca_2FeAlO_5. *Acta Cryst.*, 2311-2315.

Colville, A. A., & Geller, S. (1972). Crystal Structures of $Ca_2Fe_{1.43}Al_{0.57}O_5$ and Ca2Fe1.28Al0.72O5. *Acta. Cryst., B28*, 3196-3200.

Coughlin, J. P. (1956, June 7). heats of formation of of crystalline $CaO.Al_2O_3$, $12CaO.7Al_2O_3$ and $3CaO.Al_2O_3$. *J; Am. Chem. Soc., 78*(21), 5479-5481.

Coughlin, J. P., & O'Brien, C. (1957). High temperature heat contents of calcium orthosilicate. *Journal of Physical Chemestry, 61*, 767-769.

Cuesta, A., Aranda, M. A., Sanz, J., de la Torre, A. G., & Losilla, E. R. (2014). Mechanism of stabilization of dicalcium silicate solid solution with aluminium. *Dalton Trans.*, 2176-2182.

Deffrennes, G., Pisch, A., Alvares, C. M., Nuta, I., Pasturel, A., Khvan, A., & Pisch, A. (2020). Thermodynamic modelling of the Ca–O system including 3rd generation description of CaO and CaO_2. *Calphad*, 1-15.

Eitel, V. W., & Richter, H. (1942). Thermochemische Untersuchungen der Bildung des Portlandzementklinkers. *Zementtechnischer Teil*, 506-512.

Eliezer, I., Elizier, N., Howald, R. A., & Viswanadham, P. (1981, May 12). Thermodynamic properties of calcium aluminates. *J. Phys. Chem., 85*, 2835-2838.

Elsner, V. H., Gronow, V., & Schwiete, H. E. (1935). Die Berchnung des exothermen Effekts bei der Bildung von Portlandzement aus der Zusammensetzung des

gebrannten Klinkers. *Mitteilung aus dem Kalser-Wilhelm fur Silikatforschung, Berlin-Dahlem*, 542-544.

Eriksson, G., & Pelton, A. D. (1987). Critical Evaluation and Optimization of the Thermodynamic Properties and Phase Diagrams of the CaO-Al_2O_3, Al_2O_3-SiO_2, and CaO-Al_2O_3-SiO_2 Systems. *Metallurgical Transactions B, 24*, 807-816.

Eriksson, G., & Pelton, D. (1993, October). Critical Evaluation and Optimization of the Thermodynamic Properties and Phase Diagrams of the CaO-Al_2Oa3 Al_2O_3-SiO_2, and CaO-Al_2O_3-SiO_2 Systems. *Meta. Trans. B., 24B*, 807-815.

Eysel , W., & Hahn, T. (1970). Polymorphism and solid solution of Ca_2GeO_4 and Ca_2SiO_4. *Z. Kristallogr.*, 322-341.

Filonenko, N. E., & Lavrov, I. V. (1950). Equilibrium Conditions in the Al2O3 angle of the Ternary System CaO-Al2O3-SiO2. *Zh. Prikl. Khim., 23*, 1040-1046.

Forest, J. (1971). Connaissance de l'orthosilicate de calcium. *Bulletin de la Société française de Minéralogie et de Cristallographie, 94*, 118-137.

Fukuda, k., & Ando, H. (2002, October). Determination of the Pcmn/Ibm2 Phase Boundary at High Temperatures in the System $Ca_2Fe_2O_5$–$Ca_2Al_2O_5$. *J. Am. Ceram., 85*(5), 1300-1302.

Fukuda, K., Maki, I., & Adachi, K. (1992). Structure Change of Ca2SiO4 Solid Solutions with Ba Concentration. *J. Am. Soc.*, 884-888.

Galuskin, E. V., Gfeller, F., Savelyeva, V. B., Armbruster, T., Lazic, B., Galuskina, I. O., . . . Gazeev, V. M. (2012). Pavlovskyite $Ca_8(SiO_4)_2(Si_3O_{10})$: A new mineral of altered silicate-carbonate xenoliths from the two Russian type localities, Birkhin massif, Baikal Lake area and Upper Chegem caldera, North Caucasus. *American Mineralogist, 97*, 503–512.

Geiger, C. A., Kleppa, O. J., Mysen, B. O., Lattimer, J. M., & Grossman, L. (1988, June). Enthalpies of formation of $CaAl_4O_7$ and $CaAl_{12}O_{19}$ (hibonite) by high temperature, alkali borate solution calorimetry. *Geo. Cosmo. Acta., 52*(6), 1729-1736.

Geller, S., & Colville, A. A. (1971). Magnetic space group of brownmillerite, Ca_2FeAlO_5. *Solid State Communications, 9*, 1307-1308.

Ghosh, S. N., Rao, P. B., Paul, A. K., & Raina, K. (1979). Review The chemestry of dicalcium silicate mineral. *Journal of Materials Science, 14*, 1554-1566.

Gies, A., & Knofel, D. (1986). Influence of Alkalies on the composition of Belite-rich cement clinkers and the technological properties of the resulting cements. *Cement and Concrete, 16*, 411-422.

Goodwin, D. W., & Lindop, A. J. (1970). The Crystal Structure of $CaO.2Al_2O_3$. *Acta Cyrst.*, 1230-1235.

Grant, R. W., & Geller, S. (1968). Spin Orientation and Magnetic Properties of Ca_2FeAlO_5. *Journal of Applied Physics, 39*(2), 1122-1123.

Greig, J. W. (1927). Immiscibility in Silicate Melts. *Am. J. Sci., 5*(73), 1-44.

Grevel, K. D., Bellman, F., Majzlan, J., Dachs, E., Benisek, A., & Ludwig, H. M. (2022, February). Thermodynamic data of belite polymorphs. *Cement and Concrete Research, 152*, 1-9. doi:https://doi.org/10.1016/j.cemconres.2021.106621

Guirado, F., Gali, S., & Chinchon, S. (1996). X-ray profile analysis of $Ca_2Fe_{2-x}Al_xO_5$ solid solutions. *Word Cement and Development*, 73-76.

H.F.W Taylor, B. I. (1972). *Trans J. Br. Ceram. Soc*, 71.

Haas , J. L., & Fisher, J. R. (1976, April). Simultaneous evaluation and correlation of thermodynamic data. *American Journal of Science, 276*(4), 525-545. doi:https://doi.org/10.2475/ajs.276.4.525

Haas, J., Gilpin, R., & Hemingway, B. (1981). Thermodynamic Tabulations for Selected Phases in the $CaO\text{-}Al_2O_3\text{-}SiO_2\text{-}H_2O$ at 101.325kPa (1atm) between 273.15 and 1800K. *J. Phys.Chem.Ref. Data*, 575-668.

Hallstedt, B. (1990). Assessment of the $CaO\text{-}Al_2O_3$ System. *J. Am. Ceram. Soc, 73*, 15-23.

Hanic, F., Kamarad, J., Stracelsky, J., & Kapralik, I. (1987). The P-T Diagram of Ca_2SiO_4. *Br. Ceram. Trans. J., 86*, 194–198.

Hanic, F., Kamarad, J., Stracelsky, J., & Kapralik, I. (1987). The P-T Diagram of Ca_2SiO_4.. *Br. Ceram. Trans., 86*, 194-198.

Hansen, W. C., Brownmiller, L. T., & Bogue, R. H. (1928). Studies on the system calcium oxide-alumina-ferric. *Journal of American Chemical Society, 50*, 396-433.

Hemingway, B. S. (1982). Comment on "Thermodynamlc Properties of Calcium". *J. Phys. Chem.*, 2802-2803.

Hillert, M., Janson, B., Sundman, B., & Agren, J. (1985). A two-Sublattice Model for Molten Solutions with Different Tendency for Ionization. *Metall. Trans; A, 16A*, 261-266.

Hillert, M., Sundman, B., & Wang, X. (1990, April). An Assessment of CaO-SiO_2 system. *Metallurgical Transactions B, 21*, 303-312. doi:https://doi.org/10.1007/BF02664198

Hodgson, D., Vass, T., & Hugues, P. (2022). Retrieved from ea.org: https://www.iea.org/reports/cement

Hofmeister, A. M., Wopenka, B., & Locock, A. J. (2004, March 3). Spectroscopy and structure of hibonite, grossite, and CaAl2O4: Implications for astronomical environments. (Elsevier, Ed.) *Geochim. Cosmochim. Acta, 68*(21), 4485-4503.

Holley, C. E., & Huber, E. J. (1951). The Heats of Combustion of Magnesium and Aluminum. *Jour. Am. Chem. Soc., 73*, 5577.

Horkner, W., & Muller-Buschbaum, H. (1976). Zur Kristallstruktur von $CaAl_2O_4$. *J. inorg. nucl. Chem., 38*, 983-984.

Jeevaratman, J., Glasser, F. P., & Dent Glasser, L. S. (1964, February). Anion Substitution and Structure of 12CaO7$A1_2O_3$. *J. am. ceram. soc.*, 105.

Jeffery, J. W., & Mondal, P. (1975). The Crystal Structure of Tricalium Aluminate, Ca3AI206. *Acta. cryst.*, 689-697.

Jerebtsov, D. A., & Mikhailov, G. G. (2000, March). Phase diagram of CaO-Al_2O_3 system. *Ceramics International*, 25-28.

Johannson, O. K., & Thorvaldson, T. (1934). Studies on the Thermochemistry of the Compounds Occurring in the System CaO—Al_2O_3—SiO_2. V. The Heats of Formation of Tricalcium Silicate and Dicalcium Silicate. *J. Am. Chem. Soc., 56*(11), 2327-2330. doi:https://doi.org/10.1021/ja01326a032

Jost, K. H., Ziemer, B., & Seydel, R. (1977). Redetermination of the Structure of β-Dicalcium Silicate. *Acta Cryst.*, 1696-1700.

Kahlenberg, V., Fischer, R. X., & Shaw, C. S. (2000). Rietveld analysis of dicalcium aluminate ($Ca_2Al_2O_5$)-A new high pressure phase with the Brownmillerite-type structure. *Am. min., 85*, 1061–1065.

Kim , Y., & Hong, S. (2004). Influence of Minor Ions on the Stability and Hydration Rates of β-Dicalcium Silicate. *J. Am. Ceram. Soc., 87*, 900-905.

Kim, G. Y., Roh, K. S., & Yo, C. h. (1995). Structural and Magentic Properties of Brownmillerite Ca2AlxFe2-xO5 System. *Bull. Korean. Chem. Soc., 16*(10), 933-938.

Kim, Y. J., Nettleship, I., & Kriven, W. M. (1992). Phase Transformations in Dicalcium Silicate: II, TEM Studies of Crystallography, Microstructure, and Mechanisms. *J. Am. Ceram Soc., 75*, 2407-2419.

King, E. G. (1951). Heats of Formation of Crystalline Calcium Orthosilicate, Tricalcium Silicate and Zinc Orthosilicate. *J. Am. Chem. Soc., 73*, 656–658. doi:https://doi.org/10.1021/ja01146a046

King, E. G. (1955, March 1). Heat capacities at low temperatures and entropies at 298.16°K of crystalline calcium and magnesium aluminates. *Am. Chem. Soc., 59*, 218-219.

King, E. G. (1957, October 20). Low Temperature Heat Capacities and Entropies at 298.15 °K of Some Crystalline Silicates Containing Calcium. *J. Am. Chem. Soc, 79*, 5437–5438.

Koehler, M. F., Banary, R., & Kelley, K. K. (1961). Heats and free energies of foramtion of ferrites and aluminates of calcium, magnesium, and lithium. *US. Bur. Mines, Rep. Invest.*(5711), 8-9.

Kother, V. W., & Muller, F. (1978). Thermochemische Untersuchung zur Stabilitat von Orthosilicaten und-germanaten. *Z. Anorg. allg. Chem., 444*, 77-90.

Kojitani, H., Wakabayashi, Y., Tejima, Y., Kato, C., Haraguchi, M., & Akaogi, M. (2009, April). High-pressure phase relations in $Ca_2AlSiO_{5.5}$ and energetics of perovskite-related compounds with oxygen defects in the $Ca_2Si_2O_6$–$Ca_2Al_2O_5$ join. *Physics of the Earth and Planetary Interiors, 173*(3-4), 349-353.

Koryttseva, A., & Navrotsky, A. (2017). High-temperature calorimetric study of oxide component dissolution in a CaO–MgO–Al_2O_3–SiO_2 slag at 1450° C. *Journal of the American Ceramic Society, 100*(3), 1172-1177.

Kumar, R. V., & Kay, D. A. (1985, March). The Utilization of Galvanic Cells Using Caβ"-Alumina Solid Electrolytes in Thermodynamic Investigation of CaO-Al_2O_3 System. *Metall Mater Trans, B16*, 107-112.

Kusachi, I. (1975, October). The structure of rankinite. *Mineralogical Journal, 8*, 38-47.

Lai, G., Nojiri, T., & Nakano, K. (1992, July). Studies of the stability of β-Ca_2SiO_4 doped by minor ions. *Cement and Concret, 22*, 743-754.

Landa-Cánovas, A. R., & Hansen, S. (1999). Transmission electron microscopic study of ferrite in sulfate-resisting Portland cement clinker. *Cement and Concrete Research, 29*, 679–686.

Lazić, B., Kahlenberg, V., Konzett, J., & Kaindl, R. (2006, March 20). On the polymorphism of CaAl2O4—structural investigations of two high pressure modifications. *8*, 589-597.

Lea, F. M. (1935). The chemestry of Cement and Concrete. *Third edition*.

Lehne, J., & Preston, F. (2018). Making concrete change: Innovation in low-carbon cement and concrete. *Chatham House Report* .

Levin, E. M., Robbins, C. R., & McMurdie, H. F. (1964). Phase diagrams for ceramists. *A. C. society.*, 104.

Li, Y., Liu, C., Zhang, T., Tian, M., & Peng, C. (2017, May 18). Phase diagram assessment of $CaO–Al_2O_3–La_2O_3$ system. *The Canadian Journal of Metallurgy and Materials Science, 56*(3), 245-251.

Mah, A. D. (1957). Heats of Formation of Alumina, Molybdenum Trioxide, and Molybdenum Dioxide. *Jour. Phy. Chem., 61*, 1572.

Mao, H., Selleby, M., & Sundman, B. (2004, September). A re-evaluation of the liquid phases in the $CaO–Al_2O_3$ and $MgO–Al_2O_3$ systems. *Calphas, 28*(3), 307-312.

MaterialsProject. (n.d.). Retrieved from https://legacy.materialsproject.org/

McMurdie, H. F. (1937, February). Studies on portion of the system: $CaO\text{-}Al_2O_3\text{-}Fe_2O_3$. *Journal of Research of the National Bureau of Standards, 18*, 475-484.

Midgley, C. (1952). The Crystal Structure of β Dicalcium Silicate. *Acta Cryst., 5*, 307-312.

Mistuda, T., & Fukuo, K. (1969, December). Synthesis of kilchoanite. *Mineralogical Journal, 6*, 17-35.

Moody, K. M. (1953, March). The space-group and cell-dimensions of rankinite. *Miner. Mag., 20*(220), 79. doi:https://doi.org/10.1180/minmag.1953.030.220.09

Mumme, W., Cranswick, L., & Chakoumakos, B. (1996). Rietvielld crystal structure refinements from high temperature neutron powder diffraction for the polymorphs of dicalcium silicate. *Neues Jahrbuch fuer Mineralogie - Abhandlungen, 170*(2), 171-188.

Nagata, K., Tanabe, J., & Goto, K. S. (1989). Standard Free Energies of Formation of $CaO\text{-}Al_2O_3$ Intermediate Compounds by Means of EMF Measurement of Galvanic Cells. *Tetsu-to-Hagané, 75*(11), 2023-2030.

Navrotsky, A. (1977). Progress and new directions in high temperature calorimetry. *Physics and Chemistry of Minerals, 2*(1), 89-104.

Neuville, D. R., Cormier, L., Roux, J., Henderson, G. S., Ligny, D., Flank, A. M., & Lagarde, P. (2007). Investigation of Aluminate and A1203 Crystals and Melts at High Temperature Using XANES Spectroscopy. *American Institute of Physics*, 419-421. doi:https://doi.org/10.1063/1.2644545

Neuville, D. R., Henderson, G., Cormier, L., & Massiot, D. (2010). The structure of crystals, glasses, and melts along the CaO-Al2O3 join: Results from Raman, Al L- and K-edge X-ray absorption, and 27Al NMR spectroscopy. *American Mineralogist, 95*, 1580-1589. doi:https://doi.org/10.2138/am.2010.3465

Newkirk, T. F., & Thwaite, R. D. (1958). Pseudoternary System Calcium Oxide-Monocalcium Aluminate ($CaO{\cdot}Al_2O_3$)-Dicalcium Ferrite ($2CaO{\cdot}\ Fe_2O_3$). *Journal of Research of the National Bureau of Standards, 61*(4), 233-245.

Newman, E. S., & Hoffman, R. (1956, June 6). Heats of Formation of Hexacalcium Dialumino Ferrite and Dicalcium Ferrite. *Journal of Research of the National Bureau of Standards, 56*(6), 314-318.

Nurse, R. W., Welch, J. H., & Majumdar, A. J. (1965). The 12CaO.7A Al_2O_3 phase in CaO- Al_2O_3 system. *Trans. Brit. Ceram. Soc., 64*, 323-332.

Nurse, R. W., Welch, J. H., & Majumdar, A. J. (1965). The CaO- Al_2O_3 System in a Moisture-free Atmosphere. *Brit. Ceram. Soc.*, 409-418.

O'Daniel, H., & Tscheischwili, L. (1942). Zur Struktur von γ-Ca_2SiO_4 und Na_2BeF_4. *Zeitschrift für Kristallographie*, 124-141.

Palacios, L., De La Torre, G. A., Bruque, S., Garcıa-Muoz, J. L., Garcıa-Granda, S., Sheptyakov, D., & Aranda, M. A. (2007, April 14). Crystal Structures and in-Situ Formation Study of Mayenite Electrides. *Inorg. chem., 46*, 4167–4176.

Pelton, A. D., & Blander, M. (1986). *Metall. Trans. B., 17B*, 805-815.

Phan, T., Tran, N., Kim, D. H., Tho, P. T., Huy, B. T., Dang, T. N., . Lee, B. (2018). Electronic structure and magnetic properties of Al-doped $Ca_2Fe_2O_5$ brownmillerite compounds. *J. Am. Ceram. Soc., 101*, 2181-2189. doi:10.1111/jace.15357

Phillips, B., & Muan, A. (1959). Phase Equilibria in the System CaO-Iron Oxide-SiO2 in Air. *J. Am. Ceram. Soc., 42*(9), 413-423. doi:https://doi-org.gaelnomade-1.grenet.fr/10.1111/j.1151-2916.1959.tb12966.x

Popov, S. G., Levitskii, V. A., Skolis, Y. Y., & Karlin, V. V. (1979). Thermodynamic stabibility of calcium hexaaluminate $CaO.6Al_2O_3$ and its reaction with oxides. *Inorganic Materials., 15*(7), 968-971.

Prasanna, T. S., & Navrotsky, A. (1994). Energetics sin the brownmillerite-perovskite pseudobinary $Ca_2Fe_2O_5$-$CaTiO_3$. *Journal of Materials Research*, 3121–3124. doi:https://doi.org/10.1557/JMR.1994.3121

Rankin, G. A., & Wright, F. E. (1915, Junuary). The Ternary System CaO-Al_2O_3-SiO_2. *Am. Jour. Sci., 229*, 1-79.

Rankin, G. A., & Wright, F. E. (1915, January). The ternary system CaO-Al_2O_3-SiO_2 with optical study. *Am. Jour. Sci., XXXIX*(229), 1-78.

Redhammer, G. J., Tippelt, G., Roth, G., & Amthauer, G. (2004). Structural variations in brownmillerite series $Ca_2(Fe_{2-x}Al_x)O_5$: Single-crystal X-ray diffraction at 25°C and high-temperature X-ray powder difraction (25°<T<1000°C). *American Mineralogist, 89*, 405-420.

Regourd, M., Bigaré, M., Forest, J., & Guinier, A. (1968). Synthesis and crystallographic investigation of some belites. *Proc. 5th Int. Symp. Chem. Cement, 1*, 44-48.

Remy, C., Guyot, F., & Madon, M. (1995, May). High Pressure Polymorphism of Dicalcium Silicate Ca2SiO4. A Transmission Electron Microscopy Study. *Phys Chem Minerals, 22*, 419-427.

Richet, P., Ingrin, J., Mysen, B. O., Courtial, P., & Gillet, P. (1994, February). Premelting effects in minerals: an experimental study. *Earth and Planetary Science Letters, 121*(3-4), 589-600. doi:https://doi.org/10.1016/0012-821X(94)90093-0

Rog, G., Kozlowska-Rog, A., & Zakula-Sokol, K. (1993). Determination of standard Gibbs free energies of formation of calcium aluminates from the oxydes by e.m.f measurements. *J. Chem. Thermodynamics, 25*, 807-810.

Rolin, M., & Pham, H. T. (1965). ’M. Rolin and H.T. Pham, “Phase Diagrams of Mixtures not Reacting with Molybdenum". (2, Ed.) *Rev. hautes Temp. Réfract.*, 175-185.

Roy, D. M. (1958). The system CaO- Al_2O_3 -SiO_2-H_2O. IV. Phase equilibriums in the high lime portion of the system CaO-SiO_2-H_2O. *American Mineralogist, 43*, 1009-1028.

S. Udagawa, K. U. (1980). in Review of 34th General Meeting. *Cement Association of Japon*, 37.

Saalfeld, H. (1975). X-Ray Investigation of Single Crystals of β-Ca_2SiO_4 (Larnite) at High Temperatures. *American Mineralogist, 60*, 824-827.

Saburi, S., Kusachi, I., Henmi, C., Kawahara, A., Henmi, K., & Kawada, I. (1976, October). Refinement of the structure of rankinite. *Mineralogical Journal, 8*, 240-246.

Sakakura, T., Tanaka, K., Takenada, Y., Hosono, H., & Kishimoto, S. (2011, February 11). Determination of the local structure of a cage with an oxygen ion in $C_{12}Al_{14}O_{33}$. *Acta Cryst.*, 193–204.

Scrivener, K. L. (2014). Options for the future of cement. *Indian Concr. J, 88*(7), 11-21.

Sharma, R. A., & Richardson, F. D. (1961). Activities in lime-alumina melts. *J. Iron. Stee. Inst.l , 198*(4), 386-390.

Smith, D. K. (1962). Crystallographic Changes with the Substitution of Aluminum for Iron in Dicalcium Ferrite. *Acta Crsyt., 15*, 1146-1151.

Smith, D. K. (1962). Crystallographic Changes with the Substitution of Aluminum for Iron in Dicalcium Ferrite. *Acta Cryst., 15*.

Smith, D. K., Majumdar, A. J., & Ordway, F. (1961, August). Re-Examination of the Polymorphism of Dicalcium Silicate. *J. Am. Ceram. Soc., 44*(8), 405-411. doi: https://doi.org/10.1111/j.1151-2916.1961.tb15472.x

Smith, D. K., Majumdar, A., & Ordway, F. (1965). The Crsytal Structure of γ-Dicalcium Silicate. *Acta Cryst., 18*, 787-795.

Solacolu, S. (1932). *Zement, 21*, 301.

Spencer, P. J. (2008, March). A brief history of CALPHAD. *32*(1), 1-8. doi:https://doi.org/10.1016/j.calphad.2007.10.001

Steel, J. (1960, December 31). New Data for the Calcium Silicate, 'Phase Z'. *Nature*, 1187-1188.

Steele, F. A., & Davey, P. W. (1929, August 7). The cristal structure of tricalcium aluminate. *J. am. chem. soc., 51*(8).

Suzuki, K., Ito, S., Nishikawa, T., & Shinno, I. (1986). Effect of Na, K and Fe on the formation of α- and β-Ca2SiO4. *Cement and Concret, 16*, 885-892.

Suzuki, K., & Yamaguchi, G. (1968). A structural study on α'Ca_2SiO_4. (I. Press, Ed.) *Proc. Fifth Int. Symp. on the Chemistry of Cement*.

Suzuki, M., Umesaki, N., & Ishii, Y. (2021, August). Highly disordered ionic distribution in α- dicalcium silicate for structure relaxation. *J Am Ceram Soc.*, 700-711.

Taylor, H. (1990). *Cement Chemestry.* London: Academic press.

TAYLOR, H. (1990). *Cement Chemestry.* London: Academic press.

Taylor, H. W. (1971, March). The crystal structure of kilchoanite, $Ca_6(SiO_4)(Si_3O_{10})$ with some comments on related phases. *Mineralogical Magazine, 38*, 26-31.

Taylor, J., & Dinsdale, A. (1987). National Physical Laboratory. *unpublished research*.

Todd, S. S. (1951, July). Low-temperature Heat Capacities and Entropies at 298.16°K of Crystalline Calcium Orthosilicate, Zinc Orthosilicate and Tricalcium Silicate. *J. Am. Chem. Soc., 73*(7), 3277-3278. doi:https://doi.org/10.1021/ja01151a084

Trofymluk, O., Toda, Y., Hosono, H., & Navrotsky, A. (2005). Energetics of Formation and Oxidation of Microporous Calcium Aluminates: A New Class of Electrides and Ionic Conductors. *Chem. Mater., 17*(22), 5574-5579.

Udagawa, S., Urabe, K., Natsume, M., & Yano, T. (1980). Refinement of the crystal structure of γ-Ca2SiO4. *Cement and Concrete, 10*, 139-144.

Ullrich , A., Garbev, K., & Bergfeldt, B. (2021). In Situ X-ray Diffraction at High Temperatures: Formation of Ca_2SiO_4 and Ternesite in Recycled Autoclaved Aerated Concrete. *Minerals* , 1-22.

Utsunomiya, A., Tanaka, K., Morikawa, H., & Marumo, F. (1988, January 4). Structure Refinement of $CaO.6Al_2O_3$. *J. Solide State Chem.*, 197-200.

Vicat, L. (1818). *Vicat, L. J. (1818). Recherches expérimentales sur les chaux de construction, les bétons et les mortiers ordinaires.* Goujon.

Vincent, M. G., & Jeffery, J. W. (1978). The Crystal Structure of Pentacalcium Trialuminate, $5CaO.3Al_2O_3$. *Acta. Cryst., B34*, 1422-1428.

Weeks, W. F. (1956, Septemeber). Heats of Formation of Metamorphic Minerals in the System CaO-MgO-SiO_2-H_2O and their Petrological Significance. *64*, 456-472.

Xiuji, F., & Shizong, L. (1986). Investigation of the effect of minor ions on the stability of C2S and the mechanism of stabilisation. *Cement and concrete, 16*, 587-601.

Yannaquis , N., & Guinier, A. (1959). La transition polymorphique β-γ de l'orthosilicate de calcium. *Bull. Soc. Franç. Crist., 82*, 126-136.

Zhmoidin, G. I., & Chatterjee, A. K. (1985, May). Sorption of gases by rystalline and molten $12CaO.7 Al_2O_3$. *Cement and Concret Research, 15*(3), 442-452.

Zhou, H. D., & Goodenough, J. B. (2005, April 18). Rotation of magnetocrystalline easy axis in Ca_2FeO_5. *Solid State Sci., 7*, 656-659.

6 LIST OF TABLES

7 LIST OF FIGURES

8 RESUME DE LA THESE EN FRANCAIS

8.1 INTRODUCTION

Les matériaux produits par l'industrie cimentière jouent un rôle important dans la vie quotidienne notamment le ciment et le béton représentant la base des constructions modernes des bâtiments des ponts et des monuments. Le ciment de Portland ou OPC (Ordinary Portland cement) est obtenu à partir d'un mélange de matières naturelles tel que le calcaire et l'argile broyés et cuit à haute température (~1450°C) afin de former le clinker qui possède des propriétés liantes fortes. Avec la hausse de la population mondiale, les demandes en production de ciment ont été multiplié de manière considérable poussant les industrielles à une production accrue. Cette croissance industrielle florissante n'est pas sans conséquence d'un point de vue environnementale. En effet, la production de clinker de Portland nécessite la décarbonatation du calcaire responsable de 50 % d'émissions de CO_2 issu processus de fabrication du ciment. De plus, les combustibles utilisés pour alimenter les fours proviennent des déchets émetteurs également de gaz polluants à hauteur de 40 % du processus industriel cimentier.

Une des solutions envisagées par les industrielles est de produire des ciments moins riches en clinker par ajout d'élément, mineurs. L'optimisation de ce procédé nécessite la contribution thermodynamique enfin de comprendre les processus chimiques et les énergies qui en découlent. Durant ces trois dernières années de thèse, l'objectif que l'on s'est fixé est une contribution purement thermodynamique à travers l'étude des propriétés thermodynamique des oxydes constituant les OPC. Ce travail est basé sur deux approches ; la première étant expérimentale, consiste à étudier en laboratoire les enthalpies relatives, les enthalpies de formations et les températures de transition de phase des silicates de calcium tel que la Belite et Rankinite ($Ca_3Si_2O_7$ et Ca_2SiO_4), les aluminates ($Ca_5Al_6O_{14}$; $CaAl_{12}O_{19}$) et la Brownmillerite ($Ca_2Fe_{2-x}Al_xO_5$). La seconde est une approche consiste en une modélisation du diagramme de phase de la section $CaO\text{-}Al_2O_3$.

La synthèse des phases et solutions solides est réalisée par méthode solide-solide, c'est-à-dire mélange de poudre recuit à haute température dans un four sous air pour les silicates et sous argon pour les aluminates. Les analyses de phase se font par diffraction de rayons X, les propriétés thermodynamiques telles que les enthalpies relatives et enthalpies de formation sont mesurées respectivement par calorimétrie de drop directe et calorimétrie en solution (avec un solvant solide de type CAS). En ce qui

concerne les températures de fusion et de transition polymorphique, la DSC a été principalement utilisée. La modélisation des énergies de Gibbs des aluminates solide est basée sur la fonction d'Einstein de troisième génération combinée à des termes polynomiaux correctifs dites anharmoniques, pour ce faire le module PARROT (data Optimisation Module) a été utilisé puis le diagramme de phase a été optimisées sur le logiciel PANDAT.

Ce travail entre dans le cadre d'un projet commun nommé Nanocem CP17 regroupant un consortium d'industrielle et d'universitaire. Dans le cadre de ce travail, une étroite collaboration avec l'université d'Aberdeen a été mis en place, notre contribution expérimentale à participer à l'évaluation du diagramme de phase du système CaO-SiO2 dont un article a été récemment soumis. L'une des particularités de cette étude est qu'elle apporte des données thermodynamiques expérimentales qui n'ont jamais été mesurées sur les oxydes étudiés. De fait, cela constitue une contribution intéressante pour la communauté scientifique.

8.2 CHAPITRE 1 : TECHNIQUES EXPERIMENTALES ET METHODE DE MODELISATION

8.2.1 MÉTHODES EXPÉRIMENTALES

Ce chapitre traite des méthodes expérimentales utilisées pour l'élaboration des oxydes de silices, les oxydes d'aluminium ainsi que les oxydes de fer ainsi que les techniques d'analyse structurelle et les méthodes de mesures de propriétés thermodynamiques.

8.2.1.1Synthèse et caractérisation

Tous les composés solides sont synthétisés par voie solide. Les précurseurs ($CaCO_3$, SiO_2, Al_2O_3, Fe_2O_3) de pureté ≥99.0% sont pesés sur une balance de précision (±0.01 g) puis séché durant 24 heures à 500 °C dans un four sous air afin d'éliminer toute trace d'humidité. Les traitements thermiques s'effectuent à haute température (C2S/1380°C; C3S2/1450°C; 1200-1250°C C4AF et C5A3) sur une durée minimum de 12 H. Les produits de synthèse sont analysés par diffraction de rayons X afin d'identifier la formation des phases attendues.

8.2.1.2Mesures des propriétés thermodynamiques Calorimétrie de chute

La calorimétrie de chute directe est une méthode de mesure de variation de l'enthalpie des phases condensées avec la température. Un échantillon de masse connue à une température T_0 est chuté dans un calorimètre maintenu à une température de mesure T. A pression constante la variation de l'enthalpie ΔH est égale à la variation de chaleur ΔQ. Cette relation (ΔH= ΔQ) permet de déterminer l'enthalpie d'échauffement entre T_0 et T et d'en dériver par intégration la capacité thermique (Cp). Cette méthode a été appliquée afin de déterminer les enthalpies relatives des oxydes étudiées. Nous avons également mesuré les enthalpies de formation des oxydes par calorimétrie dans un solvant solide type CAS (CaO-Al_2O_3-SiO_2).

8.2.1.3Calorimétrie différentielle à balayage

La calorimétrie différentielle à balayage est une technique d'analyse thermique qui permet de caractériser la température et l'enthalpie des transitions de phase dans le matériau étudié. Cette technique peut être utilisée pour mesurer la température de transition, les enthalpies des réactions de transition et la capacité thermique (Cp). Dans ce manuscrit, nous avons mesuré les enthalpies de transition de phase des polymorphes du C2S et de la solution solide C4AF.

8.2.2 MODELISATION

La modélisation des phases solides réalisées sur C3A, C12A7, CA et CA2 est basé sur la fonction d'Einstein à trois températures pour les capacités calorifiques basse température. Afin d'éviter les divergences du modèle à haute température, nous avons ajouté une fonction polynomiale pour une description plus ajuster comme décrit dans l'équation ci-dessous.

$$Cp = 3R\left(\sum_{i}^{n} \alpha^i \left(\frac{\Theta_E^i}{T}\right)^2 \frac{\exp\left(\frac{\Theta_E^i}{T}\right)}{\left(exp\left(\frac{\Theta_E^i}{T}\right)-1\right)^2}\right) + a_1 T + a_2 T^2$$

La description thermodynamique de la phase liquide se fait à l'aide du modèle associé. Ce modèle est particulièrement utilisé lorsqu'un ordre à courte portée est observé dans

la phase liquide, ce qui est le cas dans le système métal-oxygène mais aussi dans certains systèmes oxyde-oxyde à forte interaction.

$$G_m^{liq} = \sum_k x_k G_k^{liq} + RT \sum_k x_k ln(x_k) + \sum_i x_i \sum_j x_j \sum_v (x_i - x_j)^v L_{i,j}^{liq}$$

8.3 CHAPITRE 2 : ETUDE THERMODYNAMIQUE DE LA BELITE ET DE LA RANKINITE.

Dans ce chapitre, nous nous sommes focalisé sur l'étude expérimentale de la belite (C2S) et de la rankinite (C3S2). La revue de la littérature a mis en évidence un manque de donnée thermodynamique à haute température de ces deux phases solides. Après avoir synthétisé puis identifier les phases par diffractions de rayons X, les températures de transitions polymorphiques de C2S ont été mesuré et sont en accord avec la littérature. Par la suite, les enthalpies relatives ont été mesurées puis comparer aux valeurs fournies par la base de données commerciale FTPs ainsi que les résultats issus des calculs de Haas et al (1981). Nous avons ainsi confirmé la validité du modèle de Haas d'une part pour les polymorphes γ, α'-C2S et d'autre part la validité des valeurs provenant de FTPs pour γ-C2S. Toutefois, les enthalpies relatives des polymorphes α', α-C2S ont été surévalué. Ces données ont été utilisées dans le cadre d'un travail collaboratif avec l'université d'Aberdeen pour la réévaluation du diagramme de phase du système C-S (CaO-SiO_2).

8.4 CHAPITRE 3 : ETUDE DE LA PHASE C4AF

La solution solide de C4AF a été étudiée expérimentalement dans ce chapitre. De même comme dans le chapitre précèdent, les températures de transition (fusion) ont été mesuré pour chaque composition, tandis que les enthalpies relatives à haute température ont été mesuré sur deux compositions distinctes : x=1 et x=1.4. En ce qui concerne la première composition, les valeurs expérimentales valident les données calculées de la base FTOxid tandis que celle de la seconde composition, la base donnée rapporte des valeurs plus exothermiques. L'enthalpie de formation de C4AF (x=1) a également été mesurée par calorimétrie de dissolution.

8.5 CHAPITRE 4 : ETUDE THERMODYNAMIQUE DU SYSTEME C-A

Une revue de la littérature complète a été effectuée sur les phases solides du système C-A (CaO-Al_2O_3). Les composées solides C5A3 et CA6 ont été synthétisés ainsi que des diagrammes de phase de la section quasi-binaire. Il semblerait qu'une atmosphère inerte nécessaire pour l'obtention de C5A3. Due à la faible enthalpie de réaction, la synthèse de ce dernier est thermodynamiquement lente. Néanmoins, 93.9 % de pureté a été obtenue. Ce travail s'est conclu par la réévaluation du diagramme de phase basé sur les fonctions d'Einstein de 3^e génération.

8.6 CONCLUSION

L'étude thermodynamique des oxydes contenue dans le clinker de Portland permet de mieux comprendre les processus physico-chimiques des constituants majeurs du ciment de Portland. L'approche CALPHAD permet de modéliser le processus complexe de formation des clinkers et d'optimiser le procédé. Pour ce faire, il est nécessaire de constituer une base de donnée solide basée sur des mesures expérimentales des différents oxydes constituant du clinker (matière brute utilisée pour la fabrication de ciment). Dans cette thèse, nous nous sommes concentré sur l'étude thermodynamique de la Belite (C2S), Rankinite (C3S2), des Alumino-ferrite (C4AF) et des aluminates (CA6, C5A3). Les mesures d'enthalpie de formation, d'enthalpie relative et de point de fusion de ces oxydes apportent des données nouvelles qui pourront être utilisées afin de prédire les formations et les propriétés des clinkers.

Concernant la Belite, les données d'enthalpies relatives des variétés γ, α' α, -Ca_2SiO_4 viennent compléter celles de β- Ca_2SiO_4 mesuré par Coughlin. De même que les températures de transitions constituent des données consistant en accord avec reporté dans la littérature. Par l'étude de la Rankinite, on a pu d'une part mesurer les enthalpies relatives non reportées dans la littérature et d'autre part confirmer le point de fusion de ce composé. Pour le CAF, les enthalpies de formation et enthalpies relatives de la solution solide ont été mesurées pour la première fois et feront l'objet d'un prochain article. La synthèse de C5A3 a abouti à un composé pur à 93.9 %, il est difficile d'aller au-delà de ce pourcentage étant donné la cinétique lente liée à la faible enthalpie de réaction, de plus les conditions de synthèse exige un milieu sous gaz inerte pour éviter toute formation de C12A7. Néanmoins, nous avons pu mesurer les premières enthalpies relatives sur ce composé. À travers l'étude de CA6, nous avons

mesuré les enthalpies relatives à haute température, ce qui contribue également à enrichir la base de données des oxydes du système C-A. Nous avons pu également modéliser les capacités calorifiques des aluminates CA, CA2, C3A et C12A7 à partir des Cp basses températures ainsi que la dépendance d'énergie de Gibbs en fonction de la température.

L'une de problématique majeurs rencontré lors de cette thèse a été la contrainte liée au temps. En effet, le confinement lié au Covid-19 a impacté l'avancement des travaux. Des formations pratiques sur l'utilisation du MEB par exemple ont été annulé. Nous avons également commencé l'étude des limites de solubilités d'élément, mineurs tels que le MgO dans C3A, mais par contrainte de temps ces résultats n'ont pas pu être exploité totalement. De même, il était prévu de mesurer les capacités calorifiques de C5A3 et CA6, mais cela n'a pas pu également pu être réalisé suite à des délais de livraison de l'appareillage prévu pour cette expérimentation. Dans la continuité de ces travaux, il serait intéressant de compléter les données thermodynamiques manquantes et de réaliser un diagramme de phase complémentaire du système C-A. L'introduction de C5A3 dans la section quasi-binaire C-A serait une première, car dans tous les modèles de diagramme de phase reporté dans la littérature, cette phase a toujours été exclue. Il serait également intéressant d'étudier les effets de pré-fusion de C3S2 sur les capacités calorifiques et d'en mesurer l'enthalpie.

Concernant la phase C12A7, on aurait pu étudier la stabilité de cette phase en fonction de la quantité d'oxygène et d'en mesurer la quantité d'OH^- en cas de synthèse dans un milieu humide puis de réévaluer la température de fusion de ce composé. Les travaux présentés dans ce manuscrit apportent néanmoins des données nouvelles primordiale dans l'étude des constituants majeur de Clinker de Portland. Il est toutefois prévu de rédiger des articles notamment sur les résultats obtenus sur C4AF et le système C-A. Malgré ces contraintes indépendantes de notre volonté, à travers ces trois années de travail, nous avons su contribuer de manière non-négligeable à la conception d'une base de données solide et aussi ouvert des perspectives nouvelles sur des futurs travaux qui seront menés au laboratoire afin de compléter ce travail préliminaire.